SCAN-ACT: ADOPTIVE T CELL THERAPY TARGET DISCOVERY THROUGH SINGLE-CELL TRANSCRIPTOMICS

Stefano Testa[1,2], Aastha Pal[3], Ajay Subramanian[3], Sushama Varma[4], Jack Pengfei Tang[5], Danielle Graham[6], Sara Arfan[7], Minggui Pan[8], Nam Q. Bui[8], Kristen N. Ganjoo[8], Sarah Dry[9], Paul Huang[7], Matt van de Rijn[4], Wei Jiang[10], Anusha Kalbasi[3,11*], Everett J. Moding[3,11*]

[1]Department of Medicine, Stanford University, Stanford, CA, USA

[2]Current affiliation: Division of Hematology and Oncology, Beth Israel Deaconess Medical Center, Harvard Medical School, Boston, MA, USA

[3]Department of Radiation Oncology, Stanford University, Stanford, CA, USA

[4]Department of Pathology, Stanford University, Stanford, CA, USA

[5]Department of Pediatrics, Boston Children's Hospital, Boston, MA, USA

[6]Department of Surgery, Cedars-Sinai Medical Center, Los Angeles, CA, USA

[7]Division of Molecular Pathology, The Institute of Cancer Research, London, UK

[8]Division of Oncology, Department of Medicine, Stanford University, Stanford, CA, USA

[9]Department of Pathology, University of California, Los Angeles, CA, USA

[10]JWE Science Technology, Inc., Bejing, China

[11]Stanford Cancer Institute, Stanford University, Stanford, CA, USA

*Corresponding Authors

Contact Information

Everett J. Moding, M.D., Ph.D., Assistant Professor, Department of Radiation Oncology, Stanford Cancer Institute, 875 Blake Wilbur Drive, Stanford, CA 94305-5847. Email: emoding@stanford.edu. Tel: 650-498-1625.

and

27 Anusha Kalbasi, M.D., Associate Professor, Department of Radiation Oncology, Stanford
28 Cancer Institute, 875 Blake Wilbur Drive, Stanford, CA. Email: akalbasi@stanford.edu. Tel: 650-
29 498-4796.

Summary

The FDA approval of T cell receptor-engineered T cells (TCR-T) for synovial sarcoma demonstrates the potential for adoptive T cell therapies (ACTs) in solid tumors. However, the paucity of tumor-specific targets without expression in normal tissues remains a major bottleneck, especially in rare cancer subtypes. Here, we present a comprehensive computational pipeline called SCAN-ACT that leverages single cell RNA sequencing and multi-omics data from tumor and normal tissues to nominate and prioritize targets for both chimeric antigen receptor (CAR)- and TCR-T cells. For surface membrane targets, SCAN-ACT proposes target pairs for bispecific Boolean logic-gated CAR T cells. For peptide-MHC targets, SCAN-ACT proposes intracellular peptides bound to a diverse set of human leukocyte antigens. We applied the SCAN-ACT pipeline to soft tissue sarcoma (STS), analyzing 986,749 single cells to identify and prioritize 395 monospecific CAR-T targets, 14,192 bispecific CAR-T targets, and 5,020 peptide-MHC targets for TCR-T cells. Selected targets were validated experimentally by protein expression and for peptide-MHC binding. Proposed targets and target pairs reflected the mesenchymal, neuronal, and hematopoietic ontogeny of STS. This work provides a robust data repository along with a web-based and user-friendly set of analysis tools to accelerate ACT development for solid tumors.

Keywords

Cellular therapy, CAR-T cells, TCR-T cells, Peptide-centric CAR-T, logic-gated CAR-T, Single cell RNA sequencing, Soft tissue sarcoma, Immunotherapy

Introduction

Despite profound success in the treatment of hematologic malignancies, engineered adoptive T cell therapies (ACT) have had limited success in solid tumors[1–3]. While novel engineering strategies can address the major hurdles related to T cell function[4], including poor tumor

56 infiltration[5], terminal differentiation, effector dysfunction, and persistence or memory formation[6–
57 9], a lack of tumor-specific targets with uniformly high expression and low risk of on-target off-
58 tumor toxicity remains a challenge[10,11]. Advances in bispecific antigen targeting, synthetic gene
59 circuits, and Boolean logic-gating in engineered T cells have opened new opportunities to
60 improve antigen-discrimination between normal and tumor cells and increase the targetable
61 antigen pool[4,12,13]. However, there are no repositories of suitable target pairs for Boolean logic
62 CAR-T cells in solid tumors.
63
64 Prior ACT target discovery has focused on bulk RNA-sequencing and protein expression from
65 tumor and normal samples[3,14,15], which is confounded by non-malignant cells in the tumor
66 microenvironment. Similarly, analysis of cancer cell lines[16] may not reflect gene expression in
67 vivo or the heterogeneity of expression between individual cancer cells and across patients.
68 Furthermore, robust bulk transcriptomic and proteomic datasets are not available for many less
69 common human cancers. Compared to bulk RNA-seq and proteomics, scRNA-seq more
70 accurately represents the transcriptomic profile and heterogeneity of individual tumor cells
71 enabling the precise identification of tumor-specific genes[17,18].
72
73 Soft tissue sarcomas (STS) are rare and heterogeneous mesenchymal cancers with high rates
74 of metastatic disease and limited therapeutic options[19]. Although chemotherapy remains the
75 primary treatment for metastatic STS, most patients do not respond and the median overall
76 survival is less than two years[20,21]. Immune checkpoint blockers (ICBs) targeting programmed
77 cell death protein 1 (PD-1) and cytotoxic T-lymphocyte antigen-4 (CTLA-4) have shown promise
78 in specific STS histotypes[22–24], but are ineffective for most patients[25,26]. Recent studies have
79 shown promising efficacy for TCR-T cells in STS. Afamitresgene autoleucel (afami-cel) targeting
80 the cancer-testis antigen MAGE-A4 in patients with an HLA*02:01 allele achieved a 37% overall
81 response rate in heavily treated patients with synovial sarcoma (SS) and myxoid round cell

liposarcoma (MRCLS)[27,28], leading to the first FDA approval of a genetically engineered ACT in solid tumors. Likewise, the most promising results for TCR-T cell products targeting NY-ESO-1[29,30] have been reported in patients with STS[31]. However, additional targets will be critical to expand the availability of ACTs to patients with STS that do not express MAGE-A4 and NY-ESO-1. Furthermore, most patients lack the HLA-A*02:01 allele, which is most frequently expressed in Europeans, raising concerns about the equity of current ACTs[32]. Taken together, STS represent a challenging disease model with known effective ACT targets that can be used to benchmark target identification pipelines.

Here, we leveraged single cell RNA sequencing (scRNA-seq) from patient tumors and collated normal tissue and tumor genetic, transcriptomic, and proteomic data across public databases to develop a comprehensive computational pipeline for discovery of ACT targets in solid tumors, called SCAN-ACT (Single Cell Analysis Network for Adoptive Cellular therapy Targets). We applied SCAN-ACT in STS to build CellSARCTx (Cellular SARComa Therapy), a database describing and prioritizing over 20,000 TCR-T and CAR-T cell targets, including those for Boolean logic-gated and peptide-centric CAR-T cells (PC-CAR-T). Proposed targets captured the shared mesenchymal, neuronal and hematopoietic gene expression signatures of STS, reflecting the intertwined developmental ontogeny of these three lineages from the mesoderm and neural crest. We validated protein expression of select targets by IHC and binding of peptides derived from intracellular proteins to HLA molecules with a novel yeast display technology. We present two interactive web interfaces to explore and evaluate the identified STS ACT targets (CellSARCTx) and to apply SCAN-ACT to new scRNA-Seq samples (SCAN-ACT Custom). SCAN-ACT can be applied to individual patient samples to aid in therapy selection or broader panels of patients to identify conserved targets and accelerate ACT development. SCAN-ACT is freely accessible for academic use at scanact.stanford.edu.

Results

Overview of the SCAN-ACT pipeline

SCAN-ACT identifies tumor up-regulated and down-regulated genes through differential gene expression (DGE) analysis using scRNA-seq (**Figure 1A**). Tumor up-regulated genes are then compared against clinically tested CAR-T targets to identify novel targets with predicted low risk of on-target off-tumor toxicity. SCAN-ACT then defines Boolean logic-gated CAR-T target pairs by measuring tumor and normal cell/tissue co-expression patterns. Tumor-specific MHC-restricted peptides ($pMHCs$) targetable by TCR-T or PC-CAR-T cells are identified by integrating peptide immunogenicity and HLA presentation predictions with $pMHC$ cross-reactivity assessment. Lastly, SCAN-ACT prioritizes targets by integrating target homogeneity with normal tissue/cell expression, and functional, genomic, and proteomics tumor data.

scRNA-seq for cellular therapy target identification in STS

To identify ACT targets across STS histologies, we applied SCAN-ACT to newly sequenced and publicly available scRNA-seq data[17,33] from both translocation-driven and non-translocation-driven STS (**Table S1**). Our scRNA-seq dataset included 32 samples from 25 patients, totaling 128,122 cells after quality control (**Figure 1B, Figure S1A**, **S1B**, **S1C**, **S1E, S1G, S1I**). We included visceral (31%) and extremity/trunk (69%) tumor samples from male (72%) and female (28%) patients aged 22 to 77 years old. Samples included both primary (75%) and metastatic tumors (25%) collected before (84%) or after treatment (16%). Sarcoma cells were identified among the $CD45^{-}$ cells (PTPRC count = 0), using inferred copy number abnormalities[34,35] and transcriptional similarity to bulk samples of the same histology from The Cancer Genome Atlas (TCGA)[36] (Similarity Score)[33] (**Figure S1D, S1F**, **S1H**, **S1H**, **S1J**). Within the tumor microenvironment (TME), endothelial cells (ECs), myeloid cells (MCs), lymphoid cells (LCs), and cancer-associated fibroblasts (CAFs) were defined using canonical markers from the literature (**Table S2**).

134

135 **Identification of genes differentially expressed by malignant cells within the STS TME**

136 To identify tumor-specific genes, SCAN-ACT performs DGE analysis between sarcoma cells
137 and non-tumoral cells from the TME using Limma-voom[37], a pseudo-bulk method, and distinct[38],
138 a differential distribution method (**Figure 1C**). We also compared sarcoma cells with normal cell
139 clusters from 30 scRNA-seq datasets from the Human Protein Atlas (HPA)[39,40], Tabula Sapiens
140 (TS)[41], and the Human Cell Atlas (HCA)[42] covering the major normal human tissues (858,627
141 cells and 164 samples, **Figure 1D**). Unsupervised hierarchical clustering demonstrated that
142 STS were most similar to CAFs and ECs within the TME (**Figure S2A**, **S2C**) and mesenchymal
143 cells in normal tissues (**Figure S2B**, **S2D**), consistent with their putative mesenchymal origin. In
144 total, we identified 29,322 up-regulated genes and 15,812 down-regulated genes in STS cells
145 (**Table S3, S4**). SS and LMS had the most unique up-regulated and down-regulated genes,
146 respectively, while UPS, LPS, and MFS shared the most up-regulated and down-regulated
147 genes consistent with their biological similarity[36] (**Figure 1E**, **Figure S2E**).

148

149 There was concordance between Limma-voom and distinct for DGE analysis in the TME
150 (**Figure 1F**), with distinct identifying more unique differentially expressed genes. By measuring
151 differences in gene expression distribution between cell types, distinct identifies subtle
152 differences in expression[38], which can be advantageous when comparing transcriptionally
153 similar cells like STS and other mesenchymal cells in the TME. This approach identified a pool
154 of sarcoma-specific genes, including many like *FAP* or *MMP14* in UPS which are up-regulated
155 in STS compared to almost all normal cell types (**Figure 1G**). Notably, *FAP* has been targeted in
156 solid tumors due to its TME expression[43], though we found that *FAP* has intrinsic expression in
157 STS cells, particularly LPS, MFS, and UPS, consistent with IHC data from UPS patient samples
158 (**Figure 1H**), where 31/57 (54%) patients had *FAP* expression in ≥ 75% of cells (**Figure S2F,**

159 **S2G, S2H**). Other targets classically associated with the stroma that were upregulated in
160 malignant cells within the STS TME include *MRC2*, *CD248*, and *PDGFRB*.
161
162 **Monospecific CAR-T cell targets in STS**
163 The ideal monospecific CAR-T cell target would have homogeneously high expression on
164 cancer cells with low to no expression on normal cells to avoid on-target off-tumor toxicity[44].
165 However, development of CAR-T cells for solid tumors has been hampered by the scarcity of
166 antigens that meet these conditions with few targets tested in humans[10]. To address this, we
167 filtered the STS up-regulated genes to eliminate genes frequently expressed more highly in
168 normal cells than STS cells. We then selected genes coding for surface proteins with high
169 expression in STS by cross-referencing our scRNA-seq data with the TCGA STS bulk RNA-seq
170 data (TCGA SARC) and the HPA transcriptomics data in STS cell lines. Finally, we removed
171 targets with high RNA and protein expression in normal cells and tissues using CAR-T targets
172 tested in humans as references for maximum tolerable on-target off-tumor toxicity risk (**Figure**
173 **2A**, **Table S4**, **Table S5**, **Table S6**, **Table S7**)[45].
174
175 We identified targets with RNA and protein expression profiles in normal tissues that mimic the
176 normal tissue profiles of clinically tested CAR-T targets (**Figure 2B, Figure S3A**). Our approach
177 reassuringly identified several targets currently in clinical trials for sarcomas, including *IGF1R*[46],
178 *CD163*, *EPHB4*, *FGFR1, KDR*, *NCAM1*, *SMO*, *PSEN1* and *PSEN2*[47], and *NT5E*/CD73[48].
179 Overall, we found 395 unique targets, with 87 common to all sarcomas and 41 common to LPS,
180 MFS, and UPS (**Figure S3B**, **Table S8, Figure S3C**, **S3D**). LPS and SS were the histotypes
181 with the highest number of unique targets with 30 and 21, respectively.
182
183 In each sarcoma, transmembrane enzymes were the most common class (**Figure 2C**, **Table**
184 **S9**), including metalloproteases of the ADAM family[49] (*ADAM10*, *ADAM33*), metallopeptidases

185 (*MME*), serine proteases (*PRSS21*, *FAP*), and protein tyrosine phosphatases (*PTPRJ*, *PTPRB*).
186 Other common target classes were glypicans[50] (*GPC3*, *GPC6*), immune checkpoint molecules[51]
187 (*CD276*, *NECTIN2*, *BTN2A2*), protein tyrosine kinases[52] (*FGFR1*, *ERBB4*, *EFNA4*), NOTCH
188 family receptors[53] (*NOTCH2*, *NOTCH4*), G-protein coupled receptors – GPCRs[54] (*ADGRL2*,
189 *GPR107*), cell adhesion molecules of the Immunoglobulin superfamily – Ig-like CAMs (*CLMP*,
190 *NEO1*), semaphorins[55] (*SEMA4A*, *SEMA6D*), cytokine receptors (*IL1R1*, *IFNAR2*), c-type
191 lectins[56] (*MRC1*, *MRC2*), and solute transporters (*ABCA1*, *MMGT1*). Gene set over-
192 representation analysis (ORA) of the 395 targets revealed enrichment in gene sets associated
193 with cell–matrix interaction, axon and neural projections growth, cell mobility and migration, and
194 solute transport across the plasma membrane (**Figure 2D**, **Figure S4A–E, Table S10, S11**). We
195 observed moderate correlation between bulk RNA-seq expression of CAR-T targets in TCGA
196 SARC and scRNA-seq expression (**Figure S3E**). For many targets like *CLMP, PDGFRB,*
197 *NOTCH2,* and *GPC6*, TCGA SARC samples had the highest median expression compared with
198 other cancer types in the TCGA Pan-Cancer Atlas (**Figure 2E**, **Figure S4F**).
199
200 To prioritize targets, we identified those essential for sarcoma cell line growth in vitro by
201 analyzing publicly available CRISPR KO screening data from DepMap[57] (**Figure 2F**, **Table**
202 **S12**). Twenty-two genes were essential for at least one sarcoma cell line, with some being more
203 selective for specific STS, like *TSPAN31* for LPS. Other genes were essential for multiple
204 sarcoma cell lines, like *PTK2*, *VPS28*, and *UBE2D3*. We then studied the frequency of CNAs,
205 gene fusions, and SNVs and small insertions/deletions (indels) involving each target, using
206 publicly available DNA sequencing data (TCGA SARC[36] and MSK-IMPACT, **Table S13, S14,**
207 **S15, S16**)[58]. We found targets that were frequently amplified in specific STS histotypes in TCGA
208 with high correlation between their CNA level and RNA expression, indicating that these events
209 could have a driver effect[59,60] (**Figure 2G**). For example, *TSPAN31* (r = 0.89) was amplified in
210 72.4% of DDLPS, and *FGFR1* (r = 0.68) was amplified in 12.5% of UPS. Integrating data from

211 TCGA and MSK-IMPACT with the results of a search in the public Mitelman Database[61],
212 encompassing 52 STS types and 3283 unique fusions (**Figure 2H**, **Table S15**), we found 213
213 fusions across 20 STS histologies that involved at least one target. The CAR-T targets most
214 altered by SNVs or indels included *MACF1* and *AXL* in UPS/MFH (10.2% and 6.1% in TCGA,
215 **Figure 2I**, **Table S16**).
216
217 **Bispecific CAR-T targets in STS: 'AND' and 'AND–NOT' logic-gated CARs**
218 To increase the surface antigen pool targetable by CAR-T cells in solid tumors, new bispecific
219 CAR-T designs have been developed. Specifically, Boolean-logic 'AND'-gated CAR-T cells[62] like
220 the logic-gated intracellular network (LINK) CAR-T[12], and the synthetic NOTCH receptor
221 (synNOTCH) CAR-T[63] cause T-cell activation only when two separate antigens are recognized
222 on target cells. Conversely, inhibitory CAR-T cells (iCARs)[64] are an example of Boolean-logic
223 'AND-NOT'-gated CAR-T cells, where an inhibitory domain prevents T-cell activation upon
224 recognition of an antigen selectively expressed on normal but not on tumoral cells.
225
226 To discover targets for 'AND' CAR-T cells in STS, we sought to identify genes with high co-
227 expression in STS cells and low to no co-expression in normal cells and tissues. (**Figure 3A,**
228 **Figure S5A**). To this end, we measured co-expression of STS up-regulated genes in tumor cells
229 at the single cell level using CS-CORE[65] (**Figure S5B**), and in normal cells and tissues using
230 the Genotype-Tissue Expression (GTEx)[66] bulk RNA-seq and proteomics datasets, the Human
231 Proteome Map (HMP)[67] proteomics dataset, and the HPA scRNA-seq, bulk RNA-seq, and IHC
232 datasets. We then compared tumor co-expression to normal tissue co-expression and
233 calculated the $TS_{'AND'}$ score as a measure of targetability for each 'AND' logic-gated CAR-T
234 gene pair, where pairs with $TS_{'AND'} \geq 1$ were those with better targetability. Although we found
235 3608 unique 'AND' CAR-T pairs (**Figure 3B, Table S17**), only 4 (0.1%) were common to all

236 sarcoma histotypes, highlighting the histotype specificity of gene pairs as well as the challenge
237 of identifying broadly applicable target pairs for 'AND' logic-gated CAR T cells.
238
239 Most 'AND' CAR-T pairs consisted of genes with restricted expression in orthogonal normal cell
240 types but shared expression in STS. Consistent with the mesenchymal cell origin of STS[68],
241 gene pairs from "Blood & Immune Cells" and "Neuronal Cells" were the most frequent in all STS
242 histotypes reflecting the shared development of mesenchymal, hematopoietic, and neuronal
243 cells from the embryonic mesoderm and neural crest[69] (**Figure 3C, Figure S5C–F**). We
244 previously observed expression of epithelial markers in malignant STS cells[17], and gene pairs
245 from both epithelial and mesenchymal cells were identified as targets for 'AND' CAR-T cells.
246 These results highlight the potential for bispecific CAR-T cells to leverage the dysregulated
247 differentiation of malignancies as a therapeutic target[70].
248
249 For 'AND-NOT' CAR-T target pairs, the ideal combination would include an activator highly
250 expressed on cancer cells, and an inhibitor with no expression on cancer cells but always co-
251 expressed with the activator on normal cells (**Figure 3D, Figure S5A**). To find activator-inhibitor
252 target pairs for 'AND-NOT' CAR-T cells, we used highly expressed STS up-regulated genes as
253 activators and STS down-regulated genes with average scRNA-seq tumor expression $\leq 50^{th}$
254 percentile as inhibitors and measured their expression in normal cells and tissues. We
255 combined the results of the co-expression analysis in each dataset to obtain a summative
256 targetability measure, the $TS_{'AND\text{-}NOT'}$ score, with values raging from -1 to 1, where higher values
257 indicate higher co-expression in normal tissues/cells. Overall, we found a total of 10,584 'AND-
258 NOT' CAR-T pairs across all sarcomas (**Figure 3E**, **Table S18**). Of these, 79 (0.7%) pairs were
259 shared across all five STS, including *TSPAN6–CLDN17*, *PDGFC–GPR33*, and *IL17RD–ZNRF4.*
260 Pairs with genes belonging to the same HPA single cell gene signatures were the most frequent,
261 reflecting similar patterns of expression in normal cells (**Figure 3F**).

262

263 Considering the ‘AND’ and ‘AND-NOT’ CAR-T target pairs with high *TS* scores, again we found
264 that most ‘AND’ pairs tend to have similar expression profiles in the same cells and tissues,
265 while ‘AND-NOT’ pairs show opposite expression in the same tissues and cells, which was true
266 both at the protein and RNA level (**Figure 3G-H**). Examples of ‘AND’ pairs include *NCSTN*–
267 *BCAN* (“Blood & Immune Cells” – “Glial Cells”), *TM9SF1–CD81* (“Blood & Immune Cells” –
268 “Glandular Epithelial Cells”), and *NTRK2–CD99* (“Neuronal Cells” – “Mesenchymal Cells”).
269 Examples of ‘AND–NOT’ CAR-T target pairs include *PTPRC–ITGAM* (“Blood & Immune Cells”),
270 *PTPRZ1–NRXN3* (“Glial Cells” – “Neuronal Cells”), and *ADAM2–LY6K* (“Germ Cells”). Many of
271 the bispecific CAR-T targets were essential for STS cell line growth (**Figure S6A**) and/or were
272 genetically altered in human STS (**Figure S6B-H**, **Table S19-S21**), suggesting their importance
273 in STS oncogenesis.

274

275 **Targeting intracellular antigens in STS: TCR-T and PC-CAR-T cells**

276 CAR-T cells target cell surface antigens but cannot directly recognize intra-cellular proteins,
277 which constitutes a large fraction of cancer antigens[71]. To address this issue, TCR-T and
278 peptide-centric CAR-T (PC-CAR-T)[72] cells have been developed targeting peptides presented
279 by the major histocompatibility complex (MHC) on tumor cells. Most peptides targeted by TCR-T
280 cells tested in humans so far derive from cancer germline antigens (CGAs)[73], which are highly
281 expressed in cancer and reproductive organs, such as *MAGEA4* or *CTAG1B,* coding for the NY-
282 ESO-1 protein[27,30]. SCAN-ACT uses DGE analysis to identify tumor cell up-regulated genes
283 coding for either intra- or extracellular proteins, with normal tissue expression similar to CGAs
284 targeted by TCR-T cells tested in humans to find tumor-specific genes with expression restricted
285 to immune-privileged sites thus minimizing on-target off-tumor toxicity (**Figure 4A**, **Table S22**).

286

287 SCAN-ACT identified 76 genes across five STS, with some showing uniformly high expression,
288 and others more specific to one or few histologies (**Figure 4B**, **Table S23**). UPS had the highest
289 number of targets (45), followed by LMS (35), LPS (28), SS and MFS (26), with 7 shared across
290 all histologies (*ACTRT3*, *ADAM12*, *ADAM32*, *CXCL16*, *MAP10*, *MSX1*, and *SUV39H2*, **Figure**
291 **S7A**). Overall, 34/76 antigens (44.7%) were known CGAs[73], and gene set ORA identified a roles
292 of the targets in gametogenesis and gonadal cells function (**Figure 4C**). Few of the targets were
293 essential for STS cell line growth in vitro (**Figure S7B**), amplified in human STS (**Figure S7C**,
294 **Table S24**), or involved in SNVs/Indels (**Figure S7E**, **Table S25**). However, 20 gene fusions in
295 STS involved at least one target (**Figure S7D**).
296
297 Next, we identified a pool of $pMHCs$ suitable as TCR-T or PC-CAR-T targets for each antigen.
298 Specifically, we assessed the HLA presentation and immunogenicity potential of all the 9-mer
299 and 10-mer peptides derived from each antigen, using HLAthena[74] and DeepImmuno[75],
300 respectively, focusing on 9-mers and 10-mers as these account for more than 97.5% of HLA
301 class I-bound peptides[76]. Also, we chose the top 10 most frequent HLA alleles in each major
302 geographical area as reported in the Allele Frequency Net Database (AFND)[77], accounting for
303 118 HLA alleles (**Table S26**). A major limitation of TCR-T cells is their ability to recognize
304 peptides presented on one or rarely two HLA alleles, making them accessible to a small fraction
305 of the population. To address this, we combined the HLAthena and DeepImmuno predictions
306 with the average global HLA allele frequency of each $pMHC$ to obtain a combined TCR-T/PC-
307 CAR-T targetability score, $TS_{TCR/PC}$. We retained the top 5,020 $pMHCs$ formed by 348 peptides
308 and 115 HLA alleles with 322 $pMHCs$ shared between ≥ 1 antigen (**Table S27**). *ADAM32* had
309 the highest number of targetable $pMHCs$ (*n* =136), covering 64 HLA alleles (**Figure S7F**). We
310 found a higher number of targetable $pMHCs$ for HLA-C (*n* = 2,041), compared to HLA-B (*n* =
311 1,540) and HLA-A (*n* = 1,439). The top three alleles by number of targetable $pMHCs$ were

312 C*07:01 (*n* =168), C*06:02 (*n* =145), and C*07:02 (*n* =131), while C*04:01 had $pMHCs$ with the
313 highest median $TS_{TCR/PC}$ (2.1) (**Figure S7G**).
314
315 Because TCR degeneracy allows T-cells to recognize different peptides presented on the same
316 MHC molecule[78], we designed a $pMHC$ cross-reactivity prediction algorithm called PS-TRACT
317 (Peptide Similarity and TCR Reactivity Analysis for Cellular Therapies). PS-TRACT measures
318 the similarity of each tumoral peptide to peptides of the same length in the normal MHC
319 ligandome (**Supplementary Data**) while considering the tissue-specific expression and
320 likelihood of presentation of each cross-reactive peptide. Peptide similarity was measured in
321 terms of amino acid physicochemical[79] and HLA binding energy covariance similarity[80], given
322 that peptide sequence identity alone cannot fully predict T-cell cross-reactivity[81–83]. Also,
323 because not all peptide residues bear the same importance in mediating TCR recognition[84], we
324 applied an entropy-based weighting, postulating that residues with higher entropy could be more
325 relevant for $pMHC$ TCR recognition[74].
326
327 We validated PS-TRACT on experimentally observed cross-reactive peptides, including tumoral
328 and microbial epitopes[85], and the *TTN* peptide ESDPIVAQY which was found to be the off-tumor
329 target in cases of fatal myocarditis in patients receiving TCR-T cells directed at the *MAGEA3*
330 epitope EVDPIGHLY[86] (**Figure S8A**). In each known cross-reactive pair, the target peptide was
331 scored for similarity both against its known cross-reactive peptide and against all the normal
332 peptides of same length binding to the same MHC molecule, used as controls. As expected,
333 known cross-reactive peptides had peptide similarity scores (S_{sim}) ≥ 99.9th percentile
334 (**Supplementary and Source Data**). We applied PS-TRACT to each STS $pMHC$ and quantified
335 cross-reactivity scores, S_{CR}, for each tissue in the HPA/GTEx consensus database
336 (**Supplementary Data**).

To test if PS-TRACT can predict tissue-specific TCR cross-reactivity, we applied it to $pMHC$ targets for which TCR-T cells have been tested in clinical trials with safety outcome data available[11] (**Figure S8B**, **Table S28**). We selected the S_{CR} score for the $pMHC$ target of afami-cel, GVYDGREHTV–HLA-A*02:01, as the upper limit for our analyses given afami-cel's promising safety profile in clinical trials[27,28]. We found that $pMHCs$ for which cross-reactivity was observed in clinical trials[11] had higher tissue-specific S_{CR} scores compared to GVYDGREHTV–HLA-A*02:01, as well as higher overall S_{CR} profile difference ($S_{CR}Diff$) with GVYDGREHTV–HLA-A*02:01 when considering all tissues (**Figure S8C**). For example, the *MAGEA3*-derived $pMHC$ KVAELVHFL–HLA-A*02:01, targeted by TCR-T cells causing two cases of fatal necrotizing leukoencephalopathy[87], had a S_{CR} in the cerebral cortex which was 2.4 standard deviations above the S_{CR} of GVYDGREHTV–HLA-A*02:01 with the cross-reactive peptide identified as AVADLVHIV from *MCHR2,* which is highly expressed on neurons. Similarly, we observed a high cardiac S_{CR} score for EVDPIGHLY–HLA-A*01:01 driven by the known cross-reactive *TTN* epitope ESDPIVAQY[86].

Using PS-TRACT, we found 1113 STS $pMHCs$ with $S_{CR}Diff \leq 0$ across 182 peptides, 69 antigens, and 113 HLA alleles, and of these 74 were shared between ≥ 2 antigens (**Table S27**). We found several peptides predicted to form $pMHCs$ with $S_{CR}Diff \leq 0$ with ≥ 10 different HLA alleles for either the class A, class B, or class C locus (**Figure 4D**). Such MHC-promiscuous peptides could be targetable with a PC-CAR-T recognizing the same peptide presented on different MHC molecules as long as the molecular surface of the resulting $pMHCs$ is similar. For example, YVVDGQIIIY derived from both *PSG8* and *PSG11* bound to 17 class C (total allele frequency: 70%), 10 class B (total allele frequency: 8%), and 4 class A alleles (total allele frequency: 6%). Lastly, we found peptides forming $pMHCs$ with very low risk of on-target off-

362 tumor toxicity ($S_{CR}Diff \leq 10^{th}$ percentile) with highly prevalent HLA alleles (**Figure 4E**). These
363 peptides could be ideal TCR-T targets, given the increased TCR dependency on HLA restriction,
364 and could be targeted in a larger fraction of the population due to the high prevalence of their
365 HLA alleles. For example, YFKDKRVHHF from *DAZL* and QFYDNKGITY from *SUV39H2* were
366 both targetable on C*07:01 (allele frequency: 14%).
367

368 **Validation of peptide-MHC binding for high-priority targets**

369 Most $pMHC$ binding prediction tools rely on datasets from mass spectrometric measurements of
370 eluted peptide ligands (EL method), which require further verifications using the actual binding
371 measurements (BA method) to eliminate false identifications[88]. Here, we adopted a recently
372 developed empirical system, IMMUNE (Identifying Massive MHC Utilized Novel Epitopes), to
373 validate the peptide-MHC binding of targets identified with PS-TRACT. IMMUNE employs a
374 yeast display system enabling fast cloning as well as mammal-like post-translational
375 modifications for the ex-vivo expression of complex HLA heterodimers[89,90]. Through anchorage
376 to agglutinin (formed by Aga1p and Aga2p), a peptide-receptive format of HLA-A, B, or C non-
377 covalent heterodimer can be assembled on the cell surface for antibody detection and peptide
378 accommodation (**Figure 5A**). Using A*02:01, A*11:01, B*35:01, and C*12:03 as examples, we
379 observed the entire heavy chain fusion protein represented by its C-terminal HA staining, the
380 soluble form of β2m in association with the heavy chain, and the correctly folded heavy
381 chain/β2m heterodimer represented by the HLA-A, B, C conformation-specific antibody staining,
382 on the surface of correspondingly transformed yeast strains (**Figure S9A**). The successful
383 detection of each component of the separately expressed heavy chain and β2m without any
384 covalent linkers allowed further development of on-yeast peptide binding assays. Without the
385 necessity to purify HLA proteins, the IMMUNE system substantially expedited BA evaluation and
386 synergized with our computational prediction for rapid TCR-T or PC-CAR-T target discovery.
387

388 By comprehensively analyzing the epitope repertoire of each HLA in the immune epitope
389 database (IEDB), we designed indicator peptides that could be biotinylated without affecting
390 HLA binding. Co-staining of HLA molecules and the exogenously loaded biotinylated indicators
391 confirmed specific binding on the surface of each yeast strain (**Figure S9B**). The capability of
392 IMMUNE to display peptide-receptive HLA mono-alleles represents an ideal system for
393 competitive binding analysis against the indicator. Based on overall S_{CR} profile and $TS_{TCR/PC}$, we
394 selected 9 peptides forming 14 $pMHC$ targets for testing. All test peptides bound A*02:01,
395 including RLHRIIPKI from SSX (**Figure 5B**, **5C**). However, other than AVLDGLDVLL and
396 VLYPVPLESY from PRAME, most peptides showed low to moderately competitive binding for
397 B*35:01 and C*12:03. These results suggest that IMMUNE can be utilized to prioritize pMHCs
398 for targeting.
399
400 **Target expression in STS Proteomics Datasets**
401 Next, we analyzed target expression in STS clinical proteomics databases[91,92], sarcoma cell
402 lines[93,94], and STS tissue micro-arrays (TMAs). Since none of the TCR-T/PC-CAR-T target
403 antigens were measured in the clinical STS proteomics datasets, we analyzed their expression
404 in STS cell lines, as reported in the Cancer Cell Line Encyclopedia (CCLE)[93] and in the ProCan-
405 DepMapSanger[94] repositories. Overall, 33/76 (43.4%) targets were expressed in 21 cell lines
406 spanning 13 STS histotypes (**Figure 5D, Figure S9C**). Of all the targets assessable for
407 expression, *SSX2*/*SSX2B*, *LIN28B*, and *MAGEA4* had the most cell lines with medium-high
408 expression in ProCan-DepMapSanger at 32%, 18% and 14%, respectively. In the Tang et al.
409 STS clinical proteomics dataset[91], we found overall good correlation between scRNA-seq and
410 protein expression for the STS up-regulated surfaceome genes (**Figure S9D**, **S9E**). This
411 correlation was consistent across histotypes when considering the monospecific CAR-T targets,
412 particularly only those with protein expression ≥ 50th percentile (**Figure 5E**, **Figure S9F**). We

413 found that many targets had high expression in a large fraction of samples (**Figure 5F, Figure**
414 **S10A, S10C**). Similar results were observed in the Burns et al. dataset (**Figure S10B**).
415
416 For the 'AND' CAR-T targets with measurable expression of both genes in the Tang et al.
417 dataset, we measured co-expression across all the STS samples (**Table S29**). Of the 1207
418 'AND' pairs, 274 showed positive correlation in protein expression between the two targets
419 across all STS samples (**Figure 5G**). Of the 438 'AND' CAR-T pairs found in the Burns et al.
420 dataset, 79 had positive correlation in expression across all samples (**Table S29**). Notably, we
421 were unable to distinguish tumor and normal cell protein expression from the bulk analysis,
422 which may confound the correlation.
423
424 Lastly, we measured expression of selected targets using in-house TMAs of LMS, SS, MFS,
425 UPS, and MPNST samples (**Figure 5H**). *GPC6* was expressed in 100% (*n* = 10) of SS, 81.4%
426 (*n* = 59) of UPS, and 95% (*n* = 537) of LMS samples, similarly to *MRC2* which was expressed in
427 all SS samples, 84.6% LMS, 79.7% UPS, and 76.1% LPS (*n* = 21) samples. LMS had the
428 highest proportion of positive samples for *KITLG* (91.0%), while SS had the highest number of
429 samples positive for *CLMP* (90.0%), followed by LMS (89.4%). These antigens were selected
430 for IHC assessment due to their overall high STS expression and low normal expression profile.
431
432 **Target Prioritization**
433 We calculated a Target Priority Index (TPI) for each cell therapy target class, integrating normal
434 cell/tissue expression with functional, genomics, and proteomics STS data, while considering
435 single-cell tumor expression homogeneity and existing immunotherapeutic agents (**Table S30-**
436 **S33**). We defined scRNA-seq expression homogeneity as the product of average expression
437 and fraction of cells with non-zero expression (H_{RNA} score). For monospecific and bispecific
438 CAR-T targets, we used the average H_{RNA} score of *CD276* across all histotypes as the

439 homogeneity reference, and the average fraction of samples in the Tang et al. proteomics
440 dataset with *CD276* z-score ≥ 0 as the protein expression reference because *CD276* has been
441 tested as a CAR-T target in STS[95]. Using LPS as an example (**Figure 6A**, **6B**), notable
442 monospecific CAR-T targets in the top 100 TPI_{CAR} included *GPC6* (high protein expression and
443 H_{RNA}), *FGFR1* (essential in LPS cell lines and with ADCs in clinical development[96]), and
444 *TSPAN31* (essential for LPS cell lines and involved by gene fusions and amplifications in LPS).
445
446 For bispecific CAR-T targets, we integrated the average $TS_{,AND,}$ and $TS_{,AND-NOT,}$ for all the
447 targetable pairs in which each gene appears into the TPI, prioritizing genes suitable both as
448 'AND' CAR-T targets and 'AND-NOT' CAR-T activators. In LMS as an example (**Figure 6C**, **6D**,
449 **6E**), notable targets with antibodies developed clinically or pre-clinically include *GPNMB*[97],
450 *RTN4*[98] and *CD46*[99]. Considering all the monospecific and bi-specific CAR-T targets identified,
451 69 had a clinically developed monoclonal antibody (mAb), antibody-drug conjugate (ADC),
452 single-chain variable fragments (scFv), fusion protein, nanobody, or fragment antigen binding
453 region (Fab), while 36 had at least a mAb or ADC in pre-clinical development. Also, of all the
454 CAR-T targets described, 26 and 32 have been previously tested as CAR-T targets either
455 clinically or pre-clinically, respectively.
456
457 Finally, we calculated a TPI for TCR-T and PC-CAR-T target antigens, using *MAGEA4* H_{RNA} in
458 SS as the homogeneity reference, given afami-cel's efficacy in SS. In addition, we considered
459 protein expression in STS cell lines, the total number of target $pMHCs$, and the HLA allele
460 frequency per antigen (**Table S33**). Top targets included *PRAME* and *LY6K*, which have more
461 homogenous expression than *MAGEA4* in SS and a higher total HLA allele frequency. In
462 addition, *SSX1* is recurrently involved in pathogenic fusions in SS and has a higher predicted
463 number of targetable $pMHCs$ than *MAGEA4* (**Figure 6F**, **6G**). Given the large number of targets

464 predicted by SCAN-ACT, the TPI will be helpful to identify the most promising tumor-specific
465 antigens for further testing.
466
467 **Discussion**
468 The major bottleneck for development of ACTs in solid tumors continues to be the lack of tumor-
469 specific antigens with low expression on normal cells[100,101]. Differently from hematological
470 malignancies, solid tumors lack lineage-specific antigens with homogeneous high-density
471 expression. Also, it remains challenging to ascertain an acceptable level of target expression in
472 normal tissues. To address this, we developed SCAN-ACT, a computational pipeline leveraging
473 scRNA-seq to discover targets for TCR-T cells, and monospecific, bispecific, and peptide-centric
474 CAR-T cells, targeting both intracellular and surface proteins.
475
476 We utilized SCAN-ACT to screen for targets in STS, a disease with limited therapeutic options
477 where ACT has proven potential. The characteristic heterogeneity of STS is also an ideal small-
478 scale representation of solid tumor heterogeneity, thus providing a high-bar test case for SCAN-
479 ACT. We screened sarcoma-specific antigens using single-cell DGE analysis between STS
480 cells, non-tumoral cells in the TME, and normal cells across 30 human tissues. scRNA-seq can
481 identify genes that are more selectively expressed in tumoral cells compared to non-tumoral
482 cells in the TME, as opposed to bulk transcriptomics and proteomics[17,18]. Additionally, scRNA-
483 seq allows measurement of target expression heterogeneity, a crucial barrier to ACT efficacy in
484 solid tumors[1], and the availability of normal tissue scRNA-seq data allows for better estimation
485 of the on-target off-tumor toxicity risk[41,42]. Previous studies demonstrated that target expression
486 even on rare cellular populations in vital organs can mediate CAR-T cell toxicity[102], and scRNA-
487 seq may better predict such off-tumor effects than bulk RNA-seq[103].
488

489 We extensively validated the off-tumor toxicity risk of the identified targets using publicly
490 available multiomics data in normal cells and tissues, including scRNA-seq, bulk RNA-seq, IHC,
491 and proteomics, with targets already tested in humans as reference. Through this approach, we
492 identified targets with lower predicted risk of on-target off-tumor toxicity than those currently
493 available. We assessed the relevance of the identified targets to STS biology at the
494 transcriptomic, genomic, and proteomic level, as well as functionally, through CRISPR KO
495 screens. This highlighted *TSPAN31* on chromosome 12, which is frequently involved by CNAs in
496 DDLPS and co-amplified with *MDM2* in both WDLPS and DDLPS[104], indicating a potential
497 oncogenic driver role in LPS.
498
499 We found targets not previously studied in STS like *GPC6,* a member of the glypican family
500 which is pathogenic in sarcomas[105], or *CLMP,* described as tumor suppressor in colon cancer[106].
501 We show targetable pathways and protein families in STS, including semaphorins and plexins
502 that are physiologically involved in neural development[107] and poorly studied in STS[108]; the
503 NOTCH pathway, previously targeted in STS[109,110]; the EPH/Ephrin system, described as
504 pathogenic in sarcomas[111] and physiologically involved in neuron migration, axon guidance, and
505 vascular remodeling[112]; and the WNT/β-Catenin pathway, implicated in sarcomagenesis and
506 previously targeted in STS[113]. Also, we identify stromal antigens, previously targeted to
507 manipulate the TME, as tumor cell intrinsic in STS like *FAP*[43], *FOLR2*[114], or *CD248*[115].
508
509 Here we also provide a tool for screening safe and effective $pMHC$ targets for ACT in solid
510 tumors. We expand the pool of known CGAs targetable in STS[116], identifying antigens not
511 previously described such as *SUV39H2* or *MEIOC*, while confirming the role of known CGAs
512 like *PRAME*, *SSX1*, and those of the MAGE and GAGE families[116]. Targetable $pMHCs$ were
513 identified using computational tools measuring peptide HLA presentation and immunogenicity.
514 Despite being an in silico analysis, this approach prioritizes peptides likely to trigger cytotoxic T-

515 cell responses while maximizing the number of patients who could benefit from targeting a
516 specific $pMHC$. Almost all TCR-T cells tested in humans so far recognize peptides presented on
517 HLA-A*02:01[11], which is highly prevalent in Caucasians, and less so in African Americans and
518 Asians and Pacific Islanders[77]. This creates equity and generalizability issues for HLA-restricted
519 ACTs[32]. To address this, we integrated allele frequency into $pMHC$ target prioritization, including
520 the most frequent HLA alleles from each major geographical area[77]. We curated a normal MHC
521 ligandome database of 46x10^6 $pMHCs$, including 630,022 experimentally validated peptides,
522 and developed PS-TRACT, a tool for $pMHC$ T-cell cross-reactivity assessment. PS-TRACT
523 overcomes limitations of current methods[72,117], allowing predictions for 9-mer and 10-mer
524 peptides over 223 HLA alleles and measuring peptide similarity through biophysical properties
525 while applying an entropy-based weighting that prioritizes amino acids critical for TCR
526 recognition. By using a large pool of experimentally observed and computationally predicted
527 normal $pMHCs$, PS-TRACT provides a multi-tissue cross-reactivity risk estimation for each
528 tumoral $pMHC$. Finally, we experimentally measured HLA binding of selected target peptides
529 using a novel yeast display technology, IMMUNE, especially critical for validation of peptide-
530 binding to less common HLA alleles where in silico predictions may be inaccurate.
531
532 Compared to prior CAR-T target discovery efforts that either performed DGE analysis between
533 tumoral and normal bulk RNA-seq samples[14,15] or analyzed patterns of protein expression in
534 tumor samples[45] or cancer cell lines[16], we leveraged single-cell DGE analysis with a large cohort
535 of non-tumoral reference cells, allowing a more precise screening for tumor-specific genes.
536 Unlike prior studies on bispecific CAR-T targets[14,16,45], we defined tumoral target co-expression
537 at the single cell level and directly measured co-expression in normal cells and tissues using
538 correlation analyses, including normal tissue scRNA-seq and proteomics data. Lastly, compared
539 to prior scRNA-seq studies for CAR-T target discovery[18], we analyzed a larger number of tumor

540 samples, included more normal reference cells, applied robust single-cell DGE analyses less
541 prone to false discovery[118], validated the identified targets with genomics, proteomics,
542 transcriptomics, and functional assays in STS, and identified TCR-T/PC-CAR-T and Boolean-
543 logic gated CAR-T cell targets.
544
545 In summary, we developed a comprehensive tool for the identification of ACT targets in solid
546 tumors enabling the targeting of both intracellular and membrane proteins. By applying the tool
547 for STS, we nominate and prioritize novel putative targets to expand and accelerate the early
548 success of ACT in this disease. Our pipeline and sarcoma ACT target database are freely
549 accessible for academic use at scanact.stanford.edu.
550

551 **Acknowledgments**
552 We thank the patients and families who participated in this study. This work was supported by
553 the My Blue Dots organization (E.J.M.) and the Tad and Diane Taube Family Foundation
554 (M.v.R., E.J.M.). This work used the UCLA Technology Center for Genomics and Bioinformatics
555 and the UCLA Translational Pathology Core Lab. The schematics in Figure 1, 2, 3, 4, and Figure
556 S5 were created with BioRender.com.
557

558 **Author contributions**
559 S.T., A.K., and E.J.M. were responsible for conceptualization. S.T., A.K., and E.J.M. were
560 responsible for the methodology. S.T. and E.J.M. were responsible for software. S.T., A.P., A.K.,
561 and E.J.M were responsible for formal analysis. S.T., A.S., A.K., and E.J.M. were responsible for
562 data curation. S.T., A.K., and E.J.M. were responsible for writing the original draft. W.J. and A.K.
563 were responsible for the IMMUNE validation and related methods and results. S.T., A.P., A.S.,
564 S.V., M.P., N.Q.B, K.N.G., M.v.R., P.H., D.G., S.D., W.J., A.K., and E.J.M. were responsible for
565 review and editing. S.T. A.P., S.A., P.T., S.A., D.G. and E.J.M. were responsible for visualization.

P.H., M.v.R., A.K., and E.J.M. were responsible for supervision. A.K. and E.J.M. were responsible for funding acquisition.

Declaration of Interests

E.J.M. has served as a consultant for GLG and Guidepoint. A.K. serves on the advisory board and holds stock for Dispatch Therapeutics, and Certis Oncology and consults for Sastra Cell Therapy. W.J. serves as CSO for JWE Science Technology, Inc. who owns the intellectual property of the IMMUNE technology. The other authors declare no financial interests.

Data and Code Availability

The processed scRNA-seq data new to this paper have been deposited to GEO with accession code GSE279852 (reviewer token: qbejwckcjnkvbgv). The raw scRNA-seq data new to this project is available on SRA with project code PRJNA117421. The previously published scRNA-seq datasets reanalyzed in this project are available in GEO with accession codes GSE212527 and GSE131309. The SCAN-ACT pipeline and code used to create the images in the manuscript are available on Github at https://github.com/StefTesta/SCAN_ACT and as supplementary material. The SCAN-ACT pipeline and the CellSARCTx interactive interface are fully accessible for academic use at https://scanact.stanford.edu.

Supplemental Information

Document S1. Figures S1-S10.

Document S2. Excel File containing Supplementary Tables S1-S34.

Methods

Human subjects

All samples analyzed in this study were collected with informed consent from subjects enrolled

592 on protocols approved by the Institutional Review Boards at Stanford University and University
593 of California Los Angeles.
594
595 **Single cell RNA sequencing of STS samples**
596 STS belonging to the following STS histotypes were included in the study: LMS, MFS, UPS,
597 DDLPS, WDLPS, and SS. Pathological diagnosis was confirmed through intuitional pathologist
598 review for the samples analyzed at Stanford University and University of California Los Angeles,
599 and as reported in the original study for the SS samples[33]. For the MFS2 sample, initial tumor
600 biopsy was diagnosed as MFS, while final surgical specimen was classified as UPS. Due to the
601 ambiguity of diagnosis, and the lower representation of MFS samples in our cohort, we decided
602 to analyze this sample as MFS. Also, the UPS6 sample was classified as Spindle Cell Sarcoma
603 versus UPS and was hence analyzed with the other UPS samples in the study.
604
605 For samples processed at Stanford University, fresh tumors were minced and enzymatically
606 dissociated using the Human Tumor Dissociation Kit (Miltenyi Biotec) using a GentleMACS Octo
607 Dissociator with heaters (Miltenyi Biotec) following the manufacturer's instructions. The
608 dissociated cell suspension was then applied to a 70 um MACS SmartStrainer (130-098-462;
609 Miltenyi Biotec). The quality of the suspension was checked by generating a hematoxylin and
610 eosin (H&E) smear and analyzed using a TC10 automated cell counter (BioRad). Samples were
611 further processed by the Stanford Genomics Shared Resource or the using the Chromium 3'
612 Gene Expression Solution v3.1 (10x Genomics) per the manufacturer's instructions and
613 sequenced on a NovaSeq 6000 (Illumina). For samples processed at the University of California
614 Los Angeles (MFS1/BO112_sarc04, UPS1/BO112_sarc10, UPS2/BO112_sarc11,
615 UPS3/BO112_sarc13, UPS4/BO112_sarc15, UPS5/BO112_sarc17, LPS1/BO112_sarc07,
616 LPS2/BO112_sarc09, LPS2sx/BO112_sarc09_sx, LPS3sx/BO112_sarc16_sx), these were
617 dissociated by treatment with collagenase D (100mg/mL) and DNase I (100mg/mL) using a 100

618 μm cell strainer, following the manufacturer's instructions. After digestion, RBC lysis was
619 performed by adding 1mL of BD lysing buffer (BD Biosciences) and incubating for 5 mins. Then,
620 dead cells were eliminated using a dead cell removal kit (Miltenyi Biotec). Cells were counted
621 using a Countess II cell counter (Thermo Scientific). Samples were then further processed by
622 the UCLA Technology Center for Genomics & Bioinformatics (TCGB) using the Chromium 3'
623 Gene Expression Solution v3.1 (10x Genomics) per the manufacturer's instructions and
624 sequenced on a NexSeq500 High Output instrument (Illumina).
625
626 **Pre-processing of scRNA-seq STS samples**
627 Sample demultiplexing, read alignment to the GRCh38 human reference genome, and
628 generation of feature-barcode matrices were performed using CellRanger v6.0.0 (10x
629 Genomics). Raw data was pre-processed in R (version 4.2.2.)[119] using the Seurat package
630 (version 4.3.0)[120]. Quality control was performed separately for each sample and consisted of
631 excluding cells with number of expressed genes < 200 and percentage of mitochondrial genes >
632 15%. We then identified and excluded doublets using the R package DoubletFinder[121] (version
633 2.0.3) applying the standard workflow as described by the developer.
634
635 **Sample Integration and cell annotation**
636 Log-normalization was performed independently for each sample using the Seurat function
637 NormalizeData. After this step, the Seurat objects for each independent sample were merged
638 preserving the individual normalization of the data. Sample integration and clustering were
639 performed separately for each histotype, accounting for batch effects and differences in
640 sequencing technologies. The top 2000 highly variable genes of the merged and normalized
641 expression matrices were identified using the function FindVariableFeatures, and then centered
642 and scaled using the ScaleData function. Principal component analysis was then run using the
643 top 2000 highly variable genes previously identified. To integrate multiple samples, the harmony

644 R package[122] (version 0.1.0) was employed for batch correction. Harmony was ran using both
645 the sample of origin and the sequencing technology variables as arguments of “group.by.vars”,
646 and based on the first 25 PCA dimensions previously identified. UMAP embeddings were then
647 obtained using the first 25 Harmony dimensions, and clusters were obtained by calculating the
648 k-nearest neighbors (k-NN) and a shared nearest-neighbor graph using the Louvain algorithm
649 implemented in the FindClusters function of the Seurat package with a resolution of 1.0. For the
650 LPS, MFS, UPS, and LMS samples, endothelial cells, myeloid cells, lymphoid cells, and CAFs
651 were annotated using the differentially expressed genes discovered with the FindMarkers
652 function in Seurat, which was run with the default parameters except for only.pos = T and
653 min.pct = 0.25. Canonical cell identity markers obtained from the literature were used for cell
654 type annotations. A list of the marker genes for each cell type in our samples is provided in
655 **Table S2**. A small number of cells could not be uniquely assigned to a specific cell identity and
656 were removed from further downstream analysis. UMAP plots were generated with Seurat and
657 scCustomize[123]. Density plots were generated with the R package Nebulosa[124].
658
659 **Public scRNA-seq Datasets**
660 *Synovial Sarcoma Samples*
661 Previously published synovial sarcoma 10x Genomics and SMART-seq2 scRNA-seq data from
662 Jerby-Arnon et al.[33] were downloaded from GEO (GSE131309). After applying quality control
663 filtering as described above, the Seurat objects for each sample were integrated using the
664 harmony[122] pipeline as previously described. Author-provided annotations were used to classify
665 cells as sarcoma cells, endothelial cells, lymphoid cells, myeloid cells, and CAFs.
666
667 *Normal Tissue scRNA-seq Datasets*
668 A list of normal tissue scRNA-seq samples of reference used for differential gene expression
669 was obtained from the HPA website

670 (https://www.proteinatlas.org/about/assays+annotation#singlecell_rna). If for any of the
671 reference datasets listed on the HPA dataset, only one sample was available, additional data
672 was obtained from either Tabula Sapiens[41] or from the Human Cell Atlas[42]. For each dataset, the
673 raw count matrices were downloaded from the publication-specific repositories as follows:
674 Adipose Tissue (GEO: accession code GSE155960); Bone Marrow (GEO: accession codes
675 GSE159929-GSM4850584, and Tabula Sapiens: https://cellxgene.cziscience.com/e/4f1555bc-
676 4664-46c3-a606-78d34dd10d92.cxg/); Brain (The Allen Brain Map: https://portal.brain-
677 map.org/atlases-and-data/rnaseq/human-m1-10x); Breast (GEO: accession code GSE164898,
678 except for D6-D10 samples); bronchus (figshare: accession code fig11981034); Colon (GEO:
679 accession code GSE116222); Endometrium (GEO: accession code GSE111976); Esophagus
680 (GEO: accession codes GSE159929-GSM4850580 and HCA:
681 https://cellxgene.cziscience.com/e/b07fb54c-d7ad-4995-8bb0-8f3d8611cabe.cxg/); Eye (GEO:
682 accession code GSE137537); Fallopian Tube (GEO: accession code GSE178101, excluding
683 hydrosalpinx samples); Heart Muscle (GEO: accession code GSE109816 and Tabula Sapiens:
684 https://cellxgene.cziscience.com/e/e6a11140-2545-46bc-929e-da243eed2cae.cxg/); Kidney
685 (GEO: accession code GSE131685); Liver (GEO: accession code GSE115469); Lung (Tabula
686 Sapiens: https://cellxgene.cziscience.com/e/0d2ee4ac-05ee-40b2-afb6-ebb584caa867.cxg/);
687 Lymph Node (GEO: accession codes GSE159929-GSM4850583 and Tabula Sapiens:
688 https://cellxgene.cziscience.com/e/18eb630b-a754-4111-8cd4-c24ec80aa5ec.cxg/); Ovary
689 (EMBL-EBI: accession code E-MTAB-8381); Pancreas (GEO: accession code GSE131886);
690 PBMC (GEO: accession code GSE112845 and Tabula Sapiens:
691 https://cellxgene.cziscience.com/e/983d5ec9-40e8-4512-9e65-a572a9c486cb.cxg/); Placenta
692 (EMBL-EBI: accession code E-MTAB-6701); Prostate (Tabula Sapiens:
693 https://cellxgene.cziscience.com/e/d77ec7d6-ef2e-49d6-9e79-05b7f8881484.cxg/); Rectum
694 (GEO: accession code GSE125970); Salivary Gland (Tabula Sapiens:
695 https://cellxgene.cziscience.com/e/f01bdd17-4902-40f5-86e3-240d66dd2587.cxg/); Skeletal

696 Muscle (GEO: accession code GSE143704); Skin (GEO: accession code GSE130973); Small
697 Intestine (GEO: accession code GSE125970); Spleen (GEO: accession codes GSE159929-
698 GSM4850589 and Tabula Sapiens: https://cellxgene.cziscience.com/e/cee11228-9f0b-4e57-
699 afe2-cfe15ee56312.cxg/); Thymus (Tabula Sapiens:
700 https://cellxgene.cziscience.com/e/0ced5e76-6040-47ff-8a72-93847965afc0.cxg/); Testis (GEO:
701 accession code GSE120508); Tongue (Tabula Sapiens:
702 https://cellxgene.cziscience.com/e/55cf0ea3-9d2b-4294-871e-bb4b49a79fc7.cxg/); Vascular
703 (Tabula Sapiens: https://cellxgene.cziscience.com/e/a2d4d33e-4c62-4361-b80a-
704 9be53d2e50e8.cxg/). After download, each dataset was pre-processed in a similar fashion as
705 our own STS samples. The pre-processed samples for a given tissue were then integrated with
706 the harmony pipeline[122] using the sample variable, and for the SS samples the sequency
707 technology variable as well, for batch correction, as previously described. Then, unsupervised
708 clustering using the Louvain algorithm with a resolution of 1 was applied for all datasets.
709 Exceptions to this workflow include the brain dataset where the dimensionality reduction and
710 clustering from HPA were used, as well as the endometrium and the bronchus datasets where
711 the author-provided clusters and annotations were used. Author-provided annotations were
712 used whenever possible, and if these were not available, the package SingleR[125] and common
713 gene markers were used for cluster cell-type annotation, where each cluster was assigned to its
714 most frequent cell type. In SingleR[125], the Encode[126] and Blueprint epigenomics[127] datasets
715 were used for annotation of all datasets except for the pancreas for which the scRNA-seq
716 reference data from Baron et al.[128] was used instead.
717
718 **Identification of tumor cells based on InferCNV**
719 CNVs were calculated using the R package inferCNV[35]. Each sample was independently
720 analyzed using as reference cells the previously annotated CAFs, endothelial cells, myeloid
721 cells, and lymphoid cells from the TME. These were identified based on expression of known

722 marker genes available from the literature as described above. The following parameters were
723 used to run the inferCNV function: analysis_mode="subclusters";
724 tumor_subcluster_partition_method="qnorm"; cluster_by_groups= FALSE; k_obs_groups = 3,
725 denoise=T, HMM=TRUE. All the other parameters were set as default. Only for UPS
726 k_obs_groups was set to 2 since this resulted in better overlap with the classification based on
727 comparison to bulk sarcoma tumors (see below). To define a cell as potentially malignant, we
728 used the CNA states across all genes calculated using a hidden Markov model (HMM) as
729 implemented in the inferCNV package. To reduce the number of false positive CNVs identified,
730 a Bayesian latent mixture model was applied with a default p-value threshold of 0.1 for all
731 samples. For each gene, inferCNV reports a CNA state as one of the following: state 1
732 corresponding to a complete allele loss, state 2 corresponding to loss of one allele, state 3
733 corresponding to the neutral state with both allelic copies intact, state 4 corresponding to gain of
734 one allele, state 5 corresponding to gain of 2 alleles, and state 6 corresponding to gain of more
735 than two alleles. For each sample, CNA states of 6 in the output data matrix obtained in the 19th
736 step of the inferCNV workflow were first converted to a state of 5, and then the CNA states were
737 normalized to values ranging from -1 to +1 and centered on 0 using the following formula:
738 $(\text{CNA State} - 3) / 2$. The matrix values were then squared to give the same weight in the
739 analysis to copy gains and copy losses. Then we calculated the overall CNA level of each cell.
740 For each sample, we identified, the CD45^{-} cells with the top 10% CNA level. Cells with
741 normalized PTPRC RNA count $= 0$ were defined as CD45^{-}. The average CNA level for these
742 cells was defined as the CNA profile of the tumor. A spearman correlation coefficient was then
743 calculated for each cell between its overall CNA level and the CNA profile of the tumor. Cells
744 whose spearman correlation coefficient was above the 25th percentile of all the cells in each
745 sample were considered to have detected CNAs and labeled as potentially malignant. The
746 output of the inferCNV analysis used to identify tumor cells is provided in the supplementary
747 data.

748

749 **Bulk sarcoma similarity score**

750 Bulk RNA-seq of STS samples from TCGA were downloaded (Tatlow and Piccolo, 2016) and
751 scaled to transcripts per million (TPM) as previously described and used as the bulk tumor
752 references. Cells from scRNA-seq data available from Jerby-Arnon et al.[33] that were annotated
753 as normal fibroblasts, macrophages, and endothelial cells were used as the normal reference
754 cells. First, the sarcoma histotypes of reference were extracted from TCGA, then the expression
755 matrices for both the bulk RNA-seq sarcoma samples (TPM) and the scRNA-seq samples (raw
756 UMI counts) were subsampled to include only genes in common between each dataset to
757 compare. Then, two spearman correlation coefficients were calculated for a given cell of a
758 scRNA-seq sample, respectively comparing its gene expression profile to the average
759 expression profile of all the bulk RNA-seq tumor samples of reference (ρ Tumor) and to the
760 average gene expression profile of all the normal cells in the scRNA-seq dataset used as
761 normal control (ρ Normal). Based on these, we defined the similarity score as
762 $\rho\ \mathrm{Tumor} - \rho\ \mathrm{Normal}$. Cells with similarity score > 0 were classified as potentially malignant. The
763 InferCNV and similarity to bulk analyses were combined so that a cell was labeled as malignant
764 if it was $CD45^{-}$ (PTPRC RNA count = 0) and had either detected CNV or a similarity score > 0.
765 Cells that could not be classified into a specific cell type based on any of the above methods
766 were labeled as “unknown” and excluded from further downstream analysis.

767

768 **Differential Expression Analysis**

769 To limit false discovery of differentially expressed genes in STS using scRNA-seq[118], we used a
770 pseudobulk DGE method, limma-voom[37], which has been shown to be statistically more robust
771 and less prone to false discovery than other methods when applied to single cell
772 transcriptomics. Also, for the STS cells versus non-tumoral cells in TME, we complemented the

773 limma-voom results with a new differential distribution testing method, distinct[38], which was
774 specifically designed for DGE using scRNA-seq.
775
776 *Pseudobulk Limma-Voom*
777 Sarcoma cells and normal cells were identified as above. For each STS histotype, the tumor
778 cells were compared to endothelial cells, myeloid cells, lymphoid cells, and CAFs in the TME, as
779 well as with each normal cell cluster of the normal tissues scRNA-seq samples of reference. For
780 each comparison, first a single integrated Seurat object was created and from this, the raw non-
781 normalized mRNA count matrix was extracted. To minimize variability in DE analysis and reduce
782 false discoveries, the synovial sarcoma samples analyzed with plate sequencing technology
783 and those analyzed with droplet-based technology were tested separately. Also, when
784 comparing tumor samples to normal samples from HPA-TS-HCA, only genes that were present
785 in both gene expression matrices were included in the differential expression test, to avoid
786 identification of falsely up-regulated or down-regulated genes. Based on the information in the
787 Seurat object metadata, the total mRNA counts for each gene were calculated by summing
788 across all the cells of a certain cell type belonging to a specific sample, obtaining a unique
789 pseudobulk for each cell type belonging to a given sample in the analysis. The pseudobulk gene
790 expression matrix was then converted to a DGEList object using the DGEList function in the
791 edgeR[129] package (version 3.99.4), and subsequently normalized using the calcNormFactors
792 function. Before voom transformation using the voom function from the R package limma[37]
793 (version 3.57.11), lowly expressed genes were filtered from the expression matrix, using a cutoff
794 of 1 CPM. Counts data was then voom-transformed and a limma workflow was implemented
795 using the sample variable as the blocking variable to control for batch effect. The limma model
796 was then fitted using the patient sex as a covariate. Contrasts were then compared between
797 each normal cell cluster and each sarcoma cluster separately (UPS, MFS, LMS, LPS, and SS).
798 Genes with a Benjamini-Hochberg (BH) corrected p-value < 0.25 and $\log_2(FC) \neq 0$ were

799 considered as significantly differentially expressed. We used a more lenient BH-corrected p-
800 value cutoff given the screening and exploratory nature of this part of our analysis.
801
802 *Differential Distribution Testing with distinct*
803 The R package distinct[38] (version 1.10.2) was used to perform differential gene distribution
804 testing between sarcoma cells and non-tumoral cells of the TME. Since distinct compares
805 empirical cumulative distribution functions for a given gene across cell types, it allows
806 identification of subtle differences in expression that are not captured by other methods which
807 might consider only measures of central tendency in the expression distribution. We
808 hypothesized that this could be particularly useful in comparing transcriptionally similar cells, as
809 STS and non-tumoral mesenchymal cells in TME. Due to its computational load, it resulted
810 unfeasible to use distinct for the HPA-TS-HCA normal cells comparisons. The raw gene
811 expression matrices of sarcoma cells and non-tumoral cells were first processed in Seurat as
812 described above to create a merged Seurat object. Afterwards, a single cell experiment object
813 specific to each tumor versus normal comparison was created using the SingleCellExperiment
814 R package[130] (version 1.20.1). The expression data was then log normalized using the
815 logNormCounts function from the R package Scuttle[131] (version 1.8.4). A “batch” variable
816 indicating the sex of the patient was included in the design matrix as a covariate, unless patients
817 were of the same sex. The distinct_test function was then used to run differential distribution
818 testing using default parameters. To obtain the $\log_2$ FC of the gene expression between
819 sarcoma and normal cells, counts were first converted to CPM using the calculateCPM function
820 from Scuttle[131], and these were used as input for the log2_FC function in distinct[38]. Then the
821 $\log_2$FC was then calculated as $\log_2 \frac{(\text{average sarcoma cells CPM} + 0.01)}{(\text{average normal cells CPM} + 0.01)}$, where the average RNA
822 expression in the normal and sarcoma cells were calculated through the distinct function

823 log2_FC. Genes with a $\log_2$FC $\neq 0$ and a “p_adj.glb” value < 0.25 were considered as
824 significantly differentially expressed between sarcoma and normal cells.
825
826 *Identification of differentially expressed genes in STS*
827 For each STS histotype, we defined a gene as up-regulated, if it resulted as differentially up-
828 regulated ($\log_2$FC > 0, FDR < 0.25) in sarcoma cells in at least one of the comparisons made,
829 either against reference cells in the TME (limma-voom or distinct), or in the HPA-TS-HCA
830 datasets (limma-voom). STS down-regulated genes were instead defined as those that resulted
831 as down-regulated in sarcoma cells ($\log_2$FC < 0, FDR < 0.25) in at least one of the comparisons
832 made, and that were never up-regulated in sarcoma cells, separately considering the TME and
833 the HPA-TS-HCA tests. For genes with more than one alternative transcript, these were tested
834 separately.
835
836 **Hierarchical Clustering of STS versus non-tumoral cells in the TME and normal tissues**
837 To perform hierarchical clustering between STS and non-tumoral cells in the TME as well as
838 normal cells in the HPA-TS-HCA datasets, we used the R package factoextra (version 1.0.7)
839 and base R functions. First, we filtered the CPM normalized scRNA count matrices to retain only
840 genes defined as differentially expressed in STS (either up- or down-regulated), considering the
841 TME and HPA-TS-HCA comparisons separately. Then we merged the count matrices from
842 different samples/tissues, averaged gene expression per cell type and $\log_2$(+1) transformed the
843 expression values. Pearson correlation was then used to obtain pairwise distances between cell
844 types, separately analyzing STS cells versus non-tumoral cells in the TME, and STS cells
845 versus normal cells in HPA-TS-HCA (supplementary data). The Pearson distance matrices were
846 used to create a dendrogram with the hclust base R function, setting the agglomeration method
847 to “ward.D2”, and this was then visualized using the fviz_dend function from factoextra. The
848 optimal number of clusters, k, was obtained by calculating the silhouette score to estimate how

849 similar cells within the same cluster are to each other and how different they are from cells in
850 other clusters, for $k \in \{2, \ldots, n-1\}$, where n is the number of cells considered. The silhouette
851 score peaked at $k = 3$ for the TME comparisons, and around $k = 5$ and $k = 6$, for the HPA-TS-
852 HCA comparisons. We chose $k = 6$ for the latter as it provided a more biologically relevant
853 separation of the different cell types.
854
855 **List of Surface Proteins**
856 To obtain a comprehensive list of genes coding for proteins that are known to or predicted to be
857 expressed on the plasma membrane, we combined The Cancer Surfaceome Atlas[14] with the in
858 silico human surfaceome (SURFY)[132] after conversion of gene names to standard HGNC
859 symbols (**Table S4**).
860
861 **Normal Tissue Expression Datasets**
862 To assess the suitability of a given gene as a cellular therapy target, we used several normal
863 tissue and cell datasets to measure RNA and protein expression.
864 Normal tissue RNA expression was assessed using the bulk RNA-seq dataset from the Human
865 Protein Atlas[39] (version 22.0, Ensembl version 103.38) accessed at
866 https://www.proteinatlas.org/about/download (file name: rna_tissue_hpa.tsv.zip), and the bulk
867 RNA-seq dataset from the GTEx[66] accessed at https://gtexportal.org/home/datasets
868 (expression file: GTEx_Analysis_2017-06-05_v8_RNASeQCv1.1.9_gene_tpm.gct; annotation
869 file: GTEx_Analysis_v8_Annotations_SampleAttributesDS.txt).
870 RNA expression in normal cells was evaluated through the HPA single cell RNA-seq dataset
871 (version 22.0, Ensembl version 103.38), accessed at
872 https://www.proteinatlas.org/about/download (file name: rna_single_cell_type.tsv.zip).
873
874 Protein expression in normal tissues was evaluated using three separate datasets:

875 1. The HPA dataset (version 22.0, Ensembl version 103.38) obtained at (file name:
876 normal_tissue.tsv.zip), which contains protein expression data across 44 normal human
877 tissues obtained through immunohistochemistry.
878 2. The Human Proteome Map[67] (HPM) dataset obtained at
879 http://www.humanproteomemap.org/download.php , which reports protein expression
880 data in 30 normal human tissues obtained through LC-MS/MS proteomics.
881 3. The GTEx Proteomics dataset[133] which reports protein expression data in 32 normal
882 human tissues, obtained through tandem mass tag (TMT) proteomics. Data was
883 obtained from the Supplemental data (Table S2D) of the corresponding manuscript.
884 Specifically, we used the $\log_2$ transformed protein abundances relative to the average of
885 the reference in the same run.
886
887 *Dataset pre-processing*
888 Gene names across datasets were standardized using the R package mygene[134] (version
889 1.38.0) by converting the gene name aliases to the corresponding standardized HGNC symbol.
890 For the bulk RNA-seq datasets (GTEx and HPA), TPM expression values were converted to
891 $\log_2$(TPM +1). Then, the expression data was processed differently based on the target
892 discovery pipeline considered. For the permissive on-target off-tumor toxicity filter of the
893 monospecific CAR target discovery pipeline, RNA expression from the GTEx dataset was first
894 averaged across all samples belonging to a given tissue type. Then tissues were organized in
895 tissue groups in a similar fashion as done by MacKay et al.[45], and the average gene expression
896 per tissue group was calculated (**Tables S5**, **S6**). Similarly, for the HPA dataset, the RNA
897 expression was averaged across tissues belonging to same tissue group. Then, tissue
898 expression in both the GTEx and HPA dataset was categorized as “Medium–High” (M-H) for
899 $\log_2(\text{TPM}+1) \geq 4$, and “Not Detected–Low” (ND-L) for $\log_2(\text{TPM}+1) < 4$. In all the other
900 pipelines, the expression matrices of the bulk RNA-seq GTEx and HPA dataset were median-

901 centered across tissues (HPA) or samples (GTEx), and then z-scored within genes, before use
902 for downstream analysis.
903
904 In the HPA IHC protein expression dataset, the protein expression is reported for each cell type
905 in each tissue as either “Not Detected”, “Low”, “Medium”, or “High”. For use in the permissive
906 on-target off-tumor toxicity filter of the monospecific CAR target discovery pipeline, protein
907 expression for each tissue was classified as follows: “ND-L” if all the cells in a tissue had only
908 “Not Detected” or “Low” expression; “M-H” if all the cells in a tissue had “Medium” or “High”
909 expression, or only “High” expression; “Medium” if all the cells in a tissue had “Medium”
910 expression; “Variable” if the cells in a tissue had either “Not Detected”, “Low”, “Medium” or
911 “High” expression. Tissue group expression was then calculated as the highest tissue
912 expression within a tissue group using the following hierarchy: M-H > Variable > Medium > ND-
913 L. Again, tissue groups were defined as above. For use in all the other pipelines, we first
914 converted the cell type protein expression level from a categorical to a numerical score, where
915 “Not Detected” = 1, “Low” = 2, “Medium” = 3, and “High” = 4. Then, we calculated the average
916 expression value per tissue group for each gene, and then obtained a gene per tissue group
917 expression matrix that was median-centered across tissue groups and z-scored within genes for
918 downstream analysis.
919
920 In the HPA single cell RNA-seq dataset, gene expression is reported as normalized TPM
921 (nTPM) for each normal cell cluster in 31 tissues. We first, converted the nTPM values to
922 $\log_2$(nTPM+1) and then obtained a gene per cell cluster matrix, where columns represented cell
923 clusters in each normal tissue in the dataset. The $\log_2$(nTPM+1) expression values were then
924 median-centered across cell clusters and z-scored within genes, and this matrix was used for
925 downstream analysis.
926

927 The LC-MS/MS proteomics expression data from the HPM was $\log_2(+1)$ transformed and then
928 median-centered across tissues and z-scored within genes, before further analysis. Lastly, in
929 the GTEx TMT proteomics dataset the relative $\log_2$ transformed protein abundance data
930 provided by the authors was median-centered across tissue samples and z-scored within
931 genes, similarly to the other datasets. All the processed normal tissue and cell expression
932 datasets used in the study are provided in the supplementary data.
933
934 **Sarcoma Cell Lines RNA Expression**
935 The HPA cancer cell line expression was downloaded from HPA (version 22.0, Ensembl version
936 103.38) at https://www.proteinatlas.org/about/download (file: rna_celline_cancer.tsv.zip). The
937 dataset was subsetted to retain only data corresponding to sarcoma cell lines including: GCT,
938 HT-1080, MES-SA, RD, Rh18, Rh30, Rh41, RKN, S-117, SK-LMS-1, SK-UT-1, TE 441.T, TE
939 617.T, and U-2197. For each gene, HPA reports the average expression as nTPM for all the cell
940 lines of a given cancer type. The nTPM values were averaged for those genes with alternative
941 transcripts, and then converted to $\log_2(\text{nTPM}+1)$ before use for downstream analyses. The
942 processed data is provided in the supplementary data.
943
944 **Monospecific CAR-T Cell Discovery Pipeline**
945 To define genes suitable for a monospecific CAR-T cell design, first we removed from our initial
946 pool of STS up-regulated genes any genes that were up-regulated more often in normal cells
947 than in sarcoma cells, considering all the comparisons in which that gene appeared. Then this
948 gene pool was filtered to retain only those present in the surfaceome. HLA class I and II genes
949 were also removed from the pool.
950
951 To increase tumor-specificity of our candidate targets, we filtered the gene pool to retain only
952 those with high tumor expression in both our scRNA-seq data, in TCGA SARC, and in the HPA

953 sarcoma cell lines (bulk RNA-seq). Tumor expression in our scRNA-seq data was calculated as
954 the average $\log_2$(CPM+1) across the sarcoma cells of a given STS histotype, where CPM
955 indicates RNA expression in counts per million, while RNA expression in TCGA SARC was
956 calculated as the average $\log_2$(TPM+1) across all the samples of a given STS histotype. Then,
957 we filtered our candidate pool to retain any gene that had above-median expression in both the
958 SARC TCGA data and in the scRNA-seq data, or above-median expression in the scRNA-seq
959 data and in the HPA sarcoma cell lines. Genes without expression data in SARC TCGA or
960 sarcoma HPA cell lines but with scRNA-seq expression $\geq$ the 50th percentile were also retained.
961
962 Then we assessed the potential for on-target off-tumor toxicity of each candidate target by
963 measuring its RNA and protein expression in normal tissues and cells and comparing it to that of
964 targets for which CAR-T cells are currently available for clinical use or in clinical development.
965 The list of tested CAR-T targets was obtained from the previous work from MacKay et al[45]
966 (**Table S7**). Specifically, we identified genes at risk for on-target off-tumor toxicity by applying
967 both a *permissive* and a *stringent filter*.
968
969 For our *permissive filter*, we used the HPA IHC protein database, as well as the GTEx and HPA
970 bulk RNA-seq databases. Specifically, protein and RNA expression were categorized as
971 described above, and then the number of tissue groups (TGs) with medium-high (M-H)
972 expression was measured for the tested CAR-T targets. We used the 90th percentile of the
973 number of TGs with M-H expression for the tested CAR-T targets in each of the three datasets
974 as cutoffs. A gene was considered to have passed the filter in a dataset if it had number of TGs
975 with M-H expression below the respective cutoff.
976
977 For our *stringent filter*, we assessed the risk of on-target off-tumor toxicity both at the single cell
978 level, using the HPA scRNA-seq dataset, and by measuring protein expression at the tissue

979 level, using the HPA, HPM, and the GTEx protein expression datasets. For this analysis, we
980 used the HPA protein numerical scoring classification obtained as described above. Also, for the
981 HPA scRNA-seq dataset we used the average cell type expression across all tissues. Again, we
982 used the normal cell/tissue expression of tested CAR-T targets as a reference to score our
983 candidate genes against.
984
985 For a gene to have an acceptable on-target off-tumor toxicity risk based on its expression in the
986 HPA scRNA-seq dataset, it had to meet two conditions. First, we categorized gene expression
987 as "high" for z-score> 1, and "low" for z-score ≤ 1. Based on this, genes from our pool that had
988 "high" expression in $\leq$14 cell types, which corresponds to the 75th percentile of the number of
989 cell types with "high" expression for the tested CAR-T targets, were initially retained. Then, we
990 calculated the maximum expression value per cell type for the tested CAR-T targets and
991 retained only those genes that had RNA expression below this threshold in each cell type. The
992 following cell types were not considered: lymphoid immune cells (T-cells, NK-cells, B-cells,
993 plasma cells), due to the potentially higher tolerability of their depletion; fibroblasts, adipocytes,
994 and endometrial stromal cells due to potential high transcriptional similarity to the STS in the
995 study; and cells in the gonads and placenta (ovarian stromal cells, granulosa cells, oocytes,
996 peritubular cells (testis), cytotrophoblasts, extravillous trophoblasts, Hofbauer cells,
997 syncytiotrophoblasts, Leydig cells, spermatocytes, late spermatids, spermatogonia, early
998 spermatids, and Sertoli cells) being sites of immune privilege. Only those genes that met both
999 criteria were retained based on their single cell RNA expression in normal cells.
1000
1001 For each of the 3 protein expression datasets, we calculated the maximum expression values
1002 per tissue (GTEx and HPM) or tissue group (HPA) for the tested CAR-T targets and used these
1003 as thresholds so that only the candidate targets with protein expression below the threshold in
1004 each of the tissues or tissue groups studied were retained. The following tissues and tissue

1005 groups were not considered: fetal tissues, male or female reproductive tissues, placenta, CD4
1006 T-cells, CD8 T-cells, NK-cells, B-cells, spleen, immune cells and immune tissue. Notably, for the
1007 GTEx proteomics dataset, we used the average z-scored protein expression across all samples
1008 belonging to a given tissue.
1009
1010 For each candidate gene (*g*), we then combined the results of both filters by calculating a
1011 monospecific CAR Targetability Score, TS_{CAR}, as follows:

1012 $$TS_{CAR}(g) = \sum_{i=1}^{2} m_i + \sum_{j=1}^{4} m_j + m_k$$

1013 Where:

1014 - m_i represents the score from the 2 bulk RNA-seq datasets (HPA and GTEx categorical)
1015 and is calculated as +1 if the gene passes the filter, –1 if it does not, and 0 if the gene is
1016 not present in the dataset.
1017 - m_j represents the score from any of the 4 protein expression datasets (HPA categorical,
1018 GTEx proteomics, HPM, and HPA numeric) and is calculated as +2 if the gene passes
1019 the filter, –2 if it does not, and 0 if it is not present in the dataset.
1020 - m_k represents the score from the HPA scRNA-seq dataset and is calculated as +1.5 if
1021 the gene passes the filter, –1.5 if it does not, and 0 if it is not present in the dataset.

1022 Any gene with $TS_{CAR} \geq 5$ which corresponds to the 25th percentile of the TS_{CAR} for the tested
1023 CAR-T targets was considered as a suitable target for a monospecific CAR-T cell. The results of
1024 the pipeline are reported in **Table S8**.
1025
1026 **Gene set over-representation analyses**
1027 Gene set over-representation analysis (ORA) was performed using the R packages,
1028 clusterProfiler[135] (version 4.10.0), ReactomePA[136,137] (version 1.46.0), and org.Hs.eg.db[138]

1029 (version 3.18.0). Before analysis, the gene symbols were converted to Entrez gene IDs. Then,
1030 we analyzed all the candidate targets for monospecific CAR-T cells for each STS, using the
1031 function enrichGO for Gene Ontology (GO) term enrichment, the function enrichKEGG for Kyoto
1032 Encyclopedia of Genes and Genomes (KEGG) pathways enrichment, the function
1033 enrichPathway for enrichment of Reactome pathways, and the function enrichWP for
1034 enrichment of WikiPathways terms. The p-value cutoff for significance was set to 0.05 and the
1035 Bonferroni-Hochberg method was used for FDR correction, while minimum and maximum gene
1036 sets sizes were set respectively to 10 and 500. We then performed a clustered ORA on the
1037 monospecific CAR-T targets by STS histotype. In this case we used the compareCluster
1038 function from clusterProfiler and within this we used the same enrichment functions as
1039 described above, depending on the reference database used, again setting FDR cutoff to 0.05
1040 and minimum and maximum gene sets sizes to 10 and 500. When performing the cluster ORA
1041 analysis on the TCR-T and PC-CAR targets, the FDR cutoff was instead set to 0.1 due to
1042 smaller gene pool to test, while the minimum and maximum gene sets sizes were set to 2 and
1043 500, respectively.
1044
1045 **TCGA Pan-Cancer Atlas**
1046 RNA expression data for the Pan-Cancer Atlas TCGA[139] samples (batch normalized RSEM
1047 values) was obtained from cBioPortal[140,141] for the genes of interest. The downloaded data is
1048 available in the Source Data. Data for the following cancer types was analyzed: KICH: Kidney
1049 Chromophobe; ACC: Adrenocortical carcinoma; LIHC: Liver hepatocellular carcinoma; UVM:
1050 Uveal Melanoma; PCPG: Pheochromocytoma and Paraganglioma; KIRP: Kidney renal papillary
1051 cell carcinoma; LAML: Acute Myeloid Leukemia; THYM: Thymoma; SKCM: Skin Cutaneous
1052 Melanoma; KIRC: Kidney renal clear cell carcinoma; READ: Rectum Adenocarcinoma; LGG:
1053 Brain Lower Grade Glioma; CHOL: Cholangiocarcinoma; COAD: Colon Adenocarcinoma;
1054 PRAD: Prostate Adenocarcinoma; STAD: Stomach Adenocarcinoma; UCEC: Uterine Corpus

1055 Endometrial Carcinoma; CESC: Cervical squamous cell carcinoma and endocervical
1056 adenocarcinoma; BLCA: Bladder Urothelial Carcinoma; ESCA: Esophageal Carcinoma; DLBC:
1057 Diffuse Large B-Cell Lymphoma; TGCT: Testicular Germ Cell Tumors; OV: Ovarian serous
1058 cystadenocarcinoma; LUSC: Lung Squamous Cell Carcinoma; LUAD: Lung Adenocarcinoma;
1059 HNSC: Head and Neck Squamous Cell Carcinoma; BRCA: Breast Invasive Carcinoma; PAAD:
1060 Pancreatic Adenocarcinoma; GBM: Glioblastoma Multiforme; THCA: Thyroid Carcinoma; UCS:
1061 Uterine Carcinosarcoma; SARC: Sarcoma; MESO: Mesothelioma.
1062
1063 **Cell Line Gene Dependency**
1064 The DepMap project[57,71] reports the results of CRISPR KO experiments on 1100 human cell
1065 lines. To assess the essentiality of our candidate targets for sarcoma cell lines (including both
1066 soft tissue sarcomas as well as chondrosarcoma, osteosarcoma and Ewing's sarcoma), we
1067 used the "CRISPRGeneEffect.csv" file obtained from the DepMap website, containing data
1068 regarding the effect of the KO of each gene in each cell line. Gene effects less than –1 indicate
1069 a significant reduction in cell growth and proliferation, as this was the median gene effect
1070 estimate of genes known to be essential for cell growth and survival.
1071
1072 **Soft Tissue Sarcoma Genomics Data**
1073 Data on copy number alterations (CNAs) and mutations in soft tissue sarcomas were obtained
1074 from the TCGA SARC firehose database[36] and from the MSK-IMPACT[58] sarcoma study. Both
1075 datasets were downloaded from cBioPortal[140,141]. The file named "data_linear_cna.txt" was used
1076 to analyze linear CNA data from TCGA firehose, while the file named "data_cna.txt" was used to
1077 determine amplification status of a given gene in each sample for both the TCGA and MSK-
1078 IMPACT databases. For the Pearson correlation analysis between linear CNA and RNA
1079 expression, the TCGA SARC bulk RNA-seq expression data obtained as above, was used.

1080 Correction for multiple hypothesis was obtained using the BH method setting the threshold for
1081 significance to 0.01.
1082
1083 Data regarding single nucleotide variants (SNVs) and small insertions/deletions (Indels) was
1084 retrieved from the "data_mutations.txt" files for both the TCGA and the MSK-IMPACT cohorts.
1085 Lastly, data on gene fusions in soft tissue sarcomas was obtained by integrating data in the
1086 "data_sv.txt" file obtained from cBioPortal for the MSK-IMPACT cohort, data from the study from
1087 Gao et al.[142] on recurrent gene fusions in TCGA tumor samples, and from a search through the
1088 Mitelman Database[61,143] (https://mitelmandatabase.isb-cgc.org/mb_search) that included the
1089 following sarcoma types: Ewing sarcoma; Atypical lipomatous tumor/atypical lipoma/well-
1090 differentiated liposarcoma; Alveolar rhabdomyosarcoma; Myxoinflammatory fibroblastic
1091 sarcoma; Undifferentiated pleomorphic sarcoma; Liposarcoma, dedifferentiated; Inflammatory
1092 myofibroblastic tumor/myofibroblastic sarcoma; Soft tissue tumor, NOS; Clear cell sarcoma;
1093 Undifferentiated round cell sarcoma; Undifferentiated sarcoma; Mesenchymal tumor, NOS;
1094 Fibrosarcoma; Embryonal rhabdomyosarcoma; Spindle cell/sclerosing rhabdomyosarcoma;
1095 Myxofibrosarcoma; Endometrial stromal sarcoma; Pleomorphic rhabdomyosarcoma;
1096 Liposarcoma, NOS; Alveolar soft part sarcoma; Leiomyosarcoma; Sclerosing epithelioid
1097 fibrosarcoma; Malignant soft tissue tumor, NOS; Angiosarcoma; Rhabdomyosarcoma, NOS;
1098 Epithelioid sarcoma; Dermatofibrosarcoma protuberans/Bednar tumor/giant cell fibroblastoma;
1099 Low-grade fibromyxoid sarcoma; Synovial sarcoma; Histiocytic sarcoma/malignant histiocytosis;
1100 Liposarcoma, myxoid/round cell; Liposarcoma, pleomorphic. The combined fusion data in STS
1101 is available from **Table S15**.
1102
1103 **Logic-gated 'AND' CAR Targets Discovery Pipeline**
1104 To discover gene pairs suitable for a bispecific logic-gated 'AND' CAR design, first we selected
1105 genes up-regulated in sarcoma cells, separately for each STS, as described above. Next, we

1106 removed from this pool of STS up-regulated genes any genes that were up-regulated more
1107 often in normal cells than in sarcoma cells, considering all the comparisons in which that gene
1108 appeared. Then, we filtered this gene pool to include only highly expressed genes, as defined in
1109 the monospecific CAR-T cell target discovery pipeline. Then, for the selected genes we
1110 computed all possible pairs and measured gene co-expression at the single cell level by running
1111 the CS-CORE algorithm from the R package CSCORE[65] (version 0.0.0.9). Specifically, we ran
1112 CS-CORE on all the tumor cells of a given sarcoma histotype and corrected p-values for
1113 multiple hypothesis testing using the BH method. Any non-significant correlations were
1114 converted to a score of 0, using an adjusted p-value significance threshold of 0.05. For a given
1115 gene pair (g_i, g_j), CS-CORE computes a correlation score, which we will refer to as
1116 $\rho_{Tumor}(g_i, g_j)$, and which can assume values between –1 (lowest likelihood of co-expression)
1117 and +1 (highest likelihood of co-expression).
1118
1119 Then, for each gene pair we assessed co-expression in normal cells and tissues, with the
1120 caveat that genes for an ideal target pair of an 'AND' logic-gated CAR would have mutually
1121 exclusive expression across all normal cells and tissues. To assess this, we used, the GTEx and
1122 HPA bulk RNA-seq databases, the HPA scRNA-seq database, the HPA IHC protein expression
1123 database, as well as the TMT GTEx proteomics and the HPM LC-MS/MS proteomics datasets.
1124 For the bulk RNA-seq datasets (GTEx and HPA), the median-centered, z-scored numerical
1125 gene expression matrices were used, where expression per each tissue (HPA), or tissue sample
1126 (GTEx) was measured. In this case, we used Pearson correlation to assess gene co-expression
1127 across normal tissues. Correction for multiple hypothesis testing was performed using the BH
1128 method, and for pairs with a corrected p-value ≥ 0.05 the correlation coefficient ρ was set to 0.
1129 Similarly, for the scRNA-seq HPA database, we used Pearson correlation to measure gene co-
1130 expression across normal cell clusters, with non-significant correlations set to $\rho = 0$, using a

BH-corrected p-value threshold of 0.05. For the GTEx TMT proteomics database, we first removed any genes with more than 25% missing values across all tissue samples analyzed. Then, we applied the Pearson correlation as above to assess protein co-expression across normal tissue samples, again using a BH-corrected p-value threshold of 0.05 for significance and setting $\rho = 0$ for any non-significant correlations.

For the HPA IHC database (numerical score data) and for the HPM proteomics database, given the low number of comparisons, we did not use Pearson correlation but instead calculated a modified odds ratio (OR) for each gene pair (g_i, g_j) as follows:

$$OR_{mod(g_i,g_j)} = \frac{d}{b \times c}$$

Where:

- *d* is the number of tissues/cells where both g_i and g_j have z-score > 1
- *b* is the number of tissues/cells where g_i has z-score > 1 and g_j has z-score ≤ 1
- *c* is the number of tissues/cells where g_j has z-score > 1 and g_i has z-score ≤ 1

In this case, pairs with mutually exclusive protein expression were considered those where $OR_{mod} = 0$. Of note, if both *d* and $b \times c$ were 0, the OR was set to 0.

Then, for each gene pair (g_i, g_j) we combined results from each normal tissue/cell database to obtain a score that estimates gene co-expression across normal tissues and cells, $N(g_i, g_j)$, as follows:

$$N(g_i, g_j) = \sum_{k=1}^{2} r_{g_i,g_j}^{k} + \sum_{l=1}^{2} r_{g_i,g_j}^{l} + r_{g_i,g_j}^{m} + r_{g_i,g_j}^{n}$$

Where:

- $r^k_{g_i,g_j}$ represents the score from the 2 bulk RNA-seq datasets and is calculated as:

$$\begin{cases} +1 \ \ if \ \rho_{g_i,g_j} < 0 \text{ and } p_{g_i,g_j} < 0.05 \\ -1 \times \ if \ \rho_{g_i,g_j} > 0 \text{ and } p_{g_i,g_j} < 0.05 \\ 0 \ if \ p_{g_i,g_j} \geq 0.05 \text{ or } if \text{ either } g_i \ or \ g_j \ is \ not \ in \ the \ dataset \ or \ if \ g_i \ or \ g_j \ SD = 0 \end{cases}$$

- $r^l_{g_i,g_j}$ represents the score from the HPA IHC and the HPM proteomics datasets and is calculated as:

$$\begin{cases} +2 \ \ if \ OR_{mod(g_i,g_j)} = 0 \\ -2 \times if \ OR_{mod(g_i,g_j)} \neq 0 \\ 0 \ if \text{ either } g_i \ or \ g_j \ is \ not \ in \ the \ dataset \end{cases}$$

- $r^m_{g_i,g_j}$ represents the score from the HPA scRNA-seq dataset and is calculated as:

$$\begin{cases} +1.5 \ \ if \ \rho_{g_i,g_j} < 0 \text{ and } p_{g_i,g_j} < 0.05 \\ -1.5 \times \ if \ \rho_{g_i,g_j} > 0 \text{ and } p_{g_i,g_j} < 0.05 \\ 0 \ if \ p_{g_i,g_j} \geq 0.05 \text{ or } if \text{ either } g_i \ or \ g_j \ is \ not \ in \ the \ dataset \ or \ if \ g_i \ or \ g_j \ SD = 0 \end{cases}$$

- $r^n_{g_i,g_j}$ represents the score from the GTEx proteomics dataset and is calculated as:

$$\begin{cases} +2 \ \ if \ \rho_{g_i,g_j} < 0 \text{ and } p_{g_i,g_j} < 0.05 \\ -2 \times \ if \ \rho_{g_i,g_j} > 0 \text{ and } p_{g_i,g_j} < 0.05 \\ 0 \ if \ p_{g_i,g_j} \geq 0.05 \text{ or } if \text{ either } g_i \ or \ g_j \ is \ not \ in \ the \ dataset \ or \ if \ g_i \ or \ g_j \ SD = 0 \end{cases}$$

- ρ_{g_i,g_j} is the Pearson correlation coefficient in a dataset between the two genes in a pair and p_{g_i,g_j} is the respective BH-corrected p-value.

The raw score $N(g_i, g_j)$ was then normalized and scaled as follows:

$$N_{norm}(g_i, g_j) = -\left\{\left(\frac{N(g_i, g_j) \ - min(N)}{max(N) \ - min(N)} \times \ 2\right) - 1\right\}$$

Where:

- $N(g_i, g_j)$ is the raw score for a given gene pair (g_i, g_j)

- min(N) and max(N) are the maximum and minimum raw scores across all gene pairs for a given STS histotype, respectively.

This normalization ensures that a score between 0 and 1 indicates higher likelihood of gene co-expression across normal tissues/cells and conversely a score between -1 and 0 indicates a lower likelihood of co-expression.

Finally, for each gene pair (g_i, g_j) we calculated an 'AND' logic-gated Targetability Score, called $TS_{'\mathrm{AND}'}$ score, as follows:

$$TS_{'\mathrm{AND}'}(g_i, g_j) = \rho_{Tumor}(g_i, g_j) - N_{norm}(g_i, g_j)$$

Gene pairs with $TS_{'\mathrm{AND}'}$ score ≥ 1 were considered to have higher fitness as targets for an 'AND'-gated CAR design. The results of the pipeline by STS histotype are reported in **Table S17**.

Logic-gated 'AND–NOT' CAR Targets Discovery Pipeline

To discover gene pairs for an 'AND–NOT' bispecific CAR design, we applied a similar logic to that used for discovery of gene pairs for an 'AND'-gated CAR. In this case, we looked for genes with high expression in sarcoma cells that would function as activators, and for genes with low to no expression in sarcoma cells but high co-expression with the paired activator in normal cells/tissues that would function as inhibitors, thus preventing on-target off-tumor toxicity.

To do this, first we obtained a list of highly expressed sarcoma up-regulated genes for each STS histotype, removing any genes up-regulated in normal cells more often than STS cells, as described above, and considered these as candidate activators. Then, to define a list of possible inhibitors with little to no expression in sarcoma cells, for each STS histotype we

selected surfaceome genes with scRNA-seq expression below the 50th percentile among the sarcoma down-regulated genes as defined in our differential gene expression pipeline. Single cell RNA expression was again measured as the average $\log_2$(CPM+1) across all the tumor cells in a sarcoma histotype.

We then calculated all the possible unique pairs between the candidate activators and inhibitors and measured their co-expression in normal cells/tissues using the same datasets used for the 'AND'-gated CAR targets discovery pipeline. Specifically, for the GTEx and HPA bulk RNA-seq datasets, as well as for the scRNA-seq HPA and the GTEx TMT proteomics datasets we used Pearson correlation to measure co-expression of the two genes in each pair, and applied BH multiple hypothesis testing correction setting the threshold for significance to a p-value < 0.05. For non-significant correlations, we then set $\rho = 0$. For the GTEx TMT proteomics dataset, again we first removed any genes with more than 25% missing values across all tissue samples analyzed before performing correlation testing.

For the HPA IHC and the HPM proteomics databases, instead of performing Pearson correlation analysis we calculated a modified odds ratio (OR) for each gene pair (g_a, g_i) between an activator, g_a, and an inhibitor, g_i as follows:

$$OR_{mod(g_a,g_i)} = \frac{d}{b}$$

Where:

- *d* is the number of tissues where both the activator g_a and the inhibitor g_i have z-score > 1
- *b* is the number of tissues where the activator g_a has z-score > 1 and the inhibitor g_i has z-score ≤ 1

Pairs where $OR_{mod} = Inf$ were considered as suitable for an 'AND–NOT' CAR design. In cases where both *d* and *b* were 0, we set OR_{mod} to Inf.

Then, for each gene pair (g_a, g_i) we combined results from each normal tissue/cell database to calculate an 'AND–NOT' logic-gated Targetability Score, $TS_{'AND-NOT'}$, as follows:

$$TS_{'AND-NOT'}(g_a, g_i) = \sum_{k=1}^{2} S^k_{g_a,g_i} + \sum_{l=1}^{2} S^l_{g_a,g_i} + S^m_{g_a,g_i} + S^n_{g_a,g_i}$$

Where:

- $S^k_{g_a,g_i}$ represents the score from the 2 bulk RNA-seq datasets and is calculated as:

$$\begin{cases} +1 \times \left(1 + I_{g_a,g_i}\right) \; if \; \rho_{g_a,g_i} > 0 \text{ and } p_{g_a,g_i} < 0.05 \\ -1 \times \left(1 + A_{g_a,g_i}\right) \; if \; \rho_{g_a,g_i} < 0 \text{ and } p_{g_a,g_i} < 0.05 \\ 0 \; if \; p_{g_a,g_i} \geq 0.05 \text{ or } if \text{ either } g_a \; or \; g_i \; is \; not \; in \; the \; dataset \; or \; if \; g_a \; or \; g_i \; SD = 0 \end{cases}$$

- $S^l_{g_a,g_i}$ represents the score from the HPA IHC and the HPM proteomics datasets and is calculated as:

$$\begin{cases} +2 \times \left(1 + I_{g_a,g_i}\right) \; if \; OR_{mod(g_a,g_i)} = Inf \\ -2 \times \left(1 + A_{g_a,g_i}\right) \; if \; OR_{mod(g_a,g_i)} \neq Inf \\ 0 \; if \text{ either } g_a \; or \; g_i \; is \; not \; in \; the \; dataset \end{cases}$$

- $S^m_{g_a,g_i}$ represents the score from the HPA scRNA-seq dataset and is calculated as:

$$\begin{cases} +1.5 \times \left(1 + I_{g_a,g_i}\right) \; if \; \rho_{g_a,g_i} > 0 \text{ and } p_{g_a,g_i} < 0.05 \\ -1.5 \times \left(1 + A_{g_a,g_i}\right) \; if \; \rho_{g_a,g_i} < 0 \text{ and } p_{g_a,g_i} < 0.05 \\ 0 \; if \; p_{g_a,g_i} \geq 0.05 \text{ or } if \text{ either } g_a \; or \; g_i \; is \; not \; in \; the \; dataset \; or \; if \; g_a \; or \; g_i \; SD = 0 \end{cases}$$

- $S^n_{g_a,g_i}$ represents the score from the GTEx proteomics dataset and is calculated as:

$$\begin{cases} +2 \times \left(1 + I_{g_a,g_i}\right) \; if \; \rho_{g_a,g_i} > 0 \text{ and } p_{g_a,g_i} < 0.05 \\ -2 \times \left(1 + A_{g_a,g_i}\right) \; if \; \rho_{g_a,g_i} < 0 \text{ and } p_{g_a,g_i} < 0.05 \\ 0 \; if \; p_{g_a,g_i} \geq 0.05 \text{ or } if \text{ either } g_a \; or \; g_i \; is \; not \; in \; the \; dataset \; or \; if \; g_a \; or \; g_i \; SD = 0 \end{cases}$$

- I_{g_a,g_i} is the proportion of comparisons in a dataset where the expression of the inhibitor is equal or above that of the activator ($z - score_{g_i} \geq z - score_{g_a}$)

1239 • A_{g_a,g_i} is the proportion of comparisons in a dataset where the expression of the activator

1240 is above that of the activator ($z - score_{g_a} > z - score_{g_i}$)

1241 • ρ_{g_a,g_i} is the Pearson correlation coefficient in a dataset between the activator and the

1242 inhibitor and p_{g_a,g_i} is the respective BH-corrected p-value.

1243

1244 The $TS_{'AND-NOT'}$ scores were then normalized as follows:

1245 $$TS_{'AND-NOT'}(g_a, g_i) = \left\{\left(\frac{TS_{'AND-NOT'}(g_a, g_i) - min(TS_{'AND-NOT'})}{max(TS_{'AND-NOT'}) - min(TS_{'AND-NOT'})} \times 2\right) - 1\right\}$$

1246 Where:

1247 • $TS_{'AND-NOT'}(g_a, g_i)$ is the raw score for a given gene pair (g_a, g_i)

1248 • $min(TS_{'AND-NOT'})$ and $max(TS_{'AND-NOT'})$ are the maximum and minimum raw scores

1249 across all gene pairs for a given STS histotype, respectively.

1250 In each sarcoma histotype, gene pairs with values above the 99th percentile of the normalized

1251 $TS_{'AND-NOT'}$ score were considered as those suitable for an 'AND-NOT'-gated CAR design. The

1252 results of the pipeline by STS histotype are reported in **Table S18**.

1253

1254 **HPA Single Cell Gene Clusters and Signatures**

1255 HPA categorizes genes based on their expression profile across different normal cell types in

1256 their scRNA-seq dataset[144]. Specifically, genes are categorized into 80 clusters, with one or

1257 more clusters corresponding to a specific cell type. We downloaded the gene cluster

1258 assignments directly from the HPA website and grouped gene clusters specific to a given cell

1259 type together to obtain cell type-specific gene signatures that were used to annotate genes in

1260 each bispecific CAR target pair. Also, the expression of these gene signatures in our STS

1261 scRNA-seq data was measured using the Seurat function AddModuleScore and shown in

1262 **Figure S7**. The HPA single cell gene clusters and signatures are provided in the Supplementary
1263 Data.
1264
1265 **T cell receptor-engineered T cell and Peptide-Centric CAR Target Discovery Pipeline**
1266 To identify targets for TCR-T or PC-CAR-T cells in STS, we obtained a list of up-regulated
1267 genes for each of the STS histotype studied. This was defined as any gene, either coding for
1268 intracellular or surface proteins, that was up-regulated in at least one of the DET comparisons
1269 made. Within this gene pool we then identified genes with high STS expression, defined in this
1270 case as those with expression $\geq 25^{th}$ percentile in both our scRNA-seq data and in the SARC
1271 TCGA samples, or those genes with expression $\geq 25^{th}$ percentile in both the sarcoma HPA cell
1272 lines and our scRNA-seq data. Genes without expression data in SARC TCGA or sarcoma HPA
1273 cell lines but with scRNA-seq expression $\geq$ the 25th percentile were also considered to have
1274 high STS expression.
1275
1276 Then we compared the expression in normal cells and tissues of each of the up-regulated
1277 genes to that of known TCR-T cell therapy targets that are currently in clinical development
1278 identified through a search on clinicaltrials.gov with the term “solid tumor” for the
1279 Condition/disease field, and “TCR-T cells” or “cellular therapy” for the Intervention/treatment
1280 field (**Table S22**). Specifically, only genes belonging to the cancer germline antigen (CGA) class
1281 were chosen as reference due to their preferential expression in immune-privileged sites like the
1282 gonads.
1283
1284 Normal cell and tissue expression was measured again using the HPA scRNA-seq dataset
1285 (average cell type expression), the HPA and GTEx bulk RNA-seq datasets (average tissue
1286 group expression), the GTEx TMT proteomics dataset (average tissue expression), the HPM
1287 LC-MS/MS proteomics dataset, or the HPM IHC data, obtained as previously described.

1288

1289 For each gene (g) we calculated a summative score $N(g)$, representing its normal cell/tissue
1290 RNA and protein expression as compared to that of the CGAs used as TCR-T cell targets, and
1291 calculated as follows:

1292 $$N(g) = \sum_{i=1}^{2} t_i + \sum_{j=1}^{3} t_j + t_k$$

1293 Where:

1294 • t_i is the score calculated by comparing the candidate target expression to that of the
1295 reference targets in the HPA and GTEx bulk RNA-seq datasets and is calculated as $+1$ if
1296 the candidate has expression below the maximum expression value for the reference
1297 targets in each tissue group, 0 if the candidate has expression above the maximum
1298 value for the reference targets in at least one of the tissue groups or if the gene is not
1299 present in the parent dataset;

1300 • t_j is the score calculated by comparing the candidate target expression to that of the
1301 reference targets in the HPA IHC, GTEx, and HPM proteomics datasets and is
1302 calculated as $+2$ if the candidate has expression below the maximum expression value
1303 for the reference targets in each tissue or tissue group, 0 if the candidate has expression
1304 above the maximum value for the reference targets in at least one of the tissues or
1305 tissue groups or if the gene is not present in the parent dataset;

1306 • t_k is the score calculated by comparing the candidate target expression to that of the
1307 reference targets in the HPA scRNA-seq dataset and is calculated as $+1.5$ if the
1308 candidate has expression below the maximum expression value for the reference targets
1309 in each cell type and 0 if the candidate has expression above the maximum value for the
1310 reference targets in at least one of the cell types or if the gene is not present in the
1311 parent dataset.

1312

1313 Genes with a $N(g)$ score ≥ 3.5 and with high STS expression as defined above were retained
1314 for further analysis. Due to the low number of genes with $N(g) \geq 3.5$ meeting the combined high
1315 expression criteria, possibly related to RNA expression dilution in bulk tissue analysis (TCGA
1316 SARC) and differences between in vivo and in vitro analysis (HPA cell lines), genes that had
1317 $N(g)$ score ≥ 3.5 and scRNA-seq expression ≥ the 25th percentile, regardless of TCGA SARC
1318 or HPA cell line expression, were also considered for further analysis as below (**Table S23**).

1319

1320 *Global HLA Allele Frequency Estimation*

1321 To estimate the global HLA allele frequencies at the HLA-B, HLA-C, and HLA-A loci, we
1322 downloaded allele frequencies for all the population studies available in the Allele Frequency
1323 Net Database (AFND)[77]. Then, we used the python package HLAfreq[145] to combine allele
1324 frequencies across populations, first within countries and then across countries to obtain an
1325 average world allele frequency. Analyses were ran using default parameters. The population
1326 size of each country was use as weight in the global allele frequency calculation, as described
1327 by the developer. Population sizes by country updated to 2022 were downloaded from the World
1328 Bank (https://data.worldbank.org/indicator/SP.POP.TOTL?most_recent_year_desc=false), or
1329 from the United Nations Populations Division (Martinique, Turkey, Taiwan), or from the European
1330 Union Commission (Madeira, Azores).

1331

1332 *Peptide-MHC targetability assessment*

1333 Next for each candidate target antigen, we used the MSiC model from HLAthena[74] to infer
1334 presentation and binding to HLA class I molecules of all the possible 9-mer and 10-mer peptides
1335 derived from each target. The amino acid sequence of each candidate target in FASTA format
1336 was obtained from UniProt[146]. For our analysis, we chose the top 10 most frequent HLA class I
1337 alleles by geographical region worldwide as reported in the Allele Frequency Net Database

1338 (AFND)[77] https://www.allelefrequencies.net/top10freqs.asp, and then applied DeepImmuno[75] to
1339 measure the predicted immunogenicity, the ability to elicit a $CD8^+$ immune response, of each
1340 peptide-MHC pair ($pMHC$). Then, for each HLA allele we calculated the average worldwide
1341 allele frequency across all the populations in which that allele was detected in the AFND (**Table**
1342 **S26**). Finally, for each $pMHC$ of each candidate target gene *g*, a targetability score, $TS_{TCR/PC}$,
1343 was calculated to assess its suitability as a target for either TCR-T or PC-CAR-T cells as
1344 follows:
1345

1346 $$TS_{TCR/PC}(pMHC_i) = \left(S_{HLAthena} + S_{DeepImmuno}\right) \times (1 + F_{allele})$$

1347

1348 Where $pMHC_i$ represents the ith $pMHC$ pair of a target gene *g*, $S_{HLAthena}$ is the score from the
1349 MSiC HLAthena model for $pMHC_i$, $S_{DeepImmuno}$ is the immunogenicity score assigned by
1350 DeepImmuno for $pMHC_i$, and F_{allele} is the average worldwide frequency for the HLA allele in
1351 $pMHC_i$. For each target antigen, we then ranked peptides based on their cumulative HLA allele
1352 frequency calculated as the sum of the allele frequencies of the HLA alleles in all of the $pMHCs$
1353 formed by each peptide, and then retained for cross-reactivity assessment only those $pMHCs$
1354 originating from peptides with the top five highest cumulative HLA allele frequency, and with
1355 $TS_{TCR/PC} \geq$ the 99th percentile, and $S_{HLAthena} \geq 0.85$. The results for HLAthena and
1356 DeepImmuno for all the target antigens, as well as the $TS_{TCR/PC}$ scores, are available in the
1357 supplementary data.
1358

1359 *Peptide-MHC cross-reactivity assessment*

1360 For the $pMHCs$ of each target antigen selected as described above, we assessed the likelihood
1361 of cross-reactivity with $pMHCs$ derived from other proteins expressed in normal cells and
1362 tissues. To do this, we developed an algorithm called PS-TRACT (Peptide Similarity and TCR

1363 Reactivity Analysis for Cellular Therapies), that considers the similarity of each tumoral $pMHC$ to
1364 a pool of normal $pMHCs$ of reference while accounting for the likelihood of presentation of the
1365 cross-reactive $pMHCs$ in normal tissues. Specifically, first we obtained a list of $pMHCs$
1366 experimentally detected in normal tissues/cells (*observed normal ligandome*) by integrating data
1367 from IEDB[147], systeMHC[148], and the HLA Ligand Atlas[149]. For IEDB, the full dataset was
1368 downloaded from https://iedb.org/database_export_v3.php (file: "mhc_ligand_full.csv.csv"), and
1369 epitopes were filtered to retain only linear peptides derived from human proteins and binding to
1370 MHC class I, with any qualitative binding measurement other than "Negative", and of either 9 or
1371 10 amino acids in length. Epitopes where MHC binding was measured with any of the following
1372 methods were also removed: half maximal effective concentration (EC50), dissociation constant
1373 KD (~EC50), and dissociation constant KD (~IC50). Lastly, only epitope binding data for alleles
1374 in standard four-digit typing HLA allele nomenclature were retained. For the HLA Ligand Atlas,
1375 the 2020.12 data release was obtained from https://hla-ligand-atlas.org/downloads. Epitope data
1376 was filtered to retain only 9-mer and 10-mer peptides binding to HLA class I or HLA class I and
1377 II, categorized as either strong or weak binders, and only those binding to HLA alleles reported
1378 in standard four-digit typing nomenclature. For systeMHC, data for the following SYSMHCIDs
1379 were obtained from https://systemhc.sjtu.edu.cn/datasets: SYSMHC00002, SYSMHC00003,
1380 SYSMHC00004, SYSMHC00007, SYSMHC00026, SYSMHC00028, SYSMHC00029,
1381 SYSMHC00031, SYSMHC00037, SYSMHC00039, SYSMHC00040, SYSMHC00044,
1382 SYSMHC00047, SYSMHC00052, SYSMHC00053, SYSMHC00055, SYSMHC00057,
1383 SYSMHC00064, SYSMHC00073, SYSMHC00088, and SYSMHC00089. In this case, only 9-
1384 mer and 10-mer peptides binding HLA class I and derived from human proteins were retained.
1385 To expand the pool of $pMHCs$ presented in normal tissues, we ran MHCflurry[150] for all the
1386 possible 9-mer and 10-mer peptides derived from the whole human proteome (*predicted normal*
1387 *ligandome*), using all the HLA alleles tested in our $pMHC$ targetability pipeline as described
1388 above. Protein FASTA sequences for 20,409 proteins total were obtained from UniProt and

1389 mhcflurry-predict-scan was used to obtain binding, processing, and presentation predictions,
1390 with results filtered for affinity percentile < 2.0. Data from the observed and predicted normal
1391 ligandomes were combined to obtain a unified non-redundant reference dataset of unique
1392 $pMHC$/protein combinations (*unified normal ligandome*, supplementary data). Those $pMHCs$
1393 with MHCflurry presentation score ≤ 0.5 were removed from the unified normal ligandome
1394 unless they were listed in the observed ligandome. Then for each selected tumoral peptide we
1395 measured its similarity with normal peptides accounting for both their physicochemical and HLA
1396 binding properties. Specifically, given a tumoral peptide p_t and a normal reference peptide p_n
1397 both binding to an HLA allele A, peptide similarity S_{sim} was calculated as:
1398

1399 $$S_{sim}(A, p_t, p_n) = \frac{simPMBEC - min(simPMBEC)}{max(simPMBEC) - min(simPMBEC)} + \frac{simAAindex - min(simAAindex)}{max(simAAindex) - min(simAAindex)}$$

1400

1401 Where $simPMBEC$ is a similarity score based on the peptide:MHC binding energy covariance
1402 (PMBEC) matrix[80] which measures amino acid similarity based on their effect on peptide HLA
1403 binding. Specifically, $simPMBEC$ was calculated as:
1404

1405 $$\frac{\sum_{i=1}^{L}\left(\frac{1}{1 + distPMBEC(p_{ti}, p_{ni})} \times (1 + H_{Ai})\right)}{L}$$

1406 Where $distPMBEC = max(PMBEC) - PMBEC$, $PMBEC$ is the value in the PMBEC matrix for the
1407 pair of amino acids at the ith position of p_t and p_n, L is the peptide length (9 or 10 amino acids),
1408 and H_{Ai} is the entropy at the i^{th}peptide residue calculated for all the peptides of same length as
1409 p_t binding to the HLA allele A in both the observed and predicted ligandome. This was obtained
1410 using the MolecularEntropy function from the R package HDMD[151] (version 1.2), with values
1411 ranging from 0 to 1, indicating respectively no amino acid sequence variability and maximum
1412 sequence variability at the ith peptide residue.

1413

1414 On the other end, $simAAindex$ was calculated as follows:

1415
$$\frac{\sum_{i=1}^{L}\left(\frac{1}{1+distAAindex(p_{ti},p_{ni})}\times(1+H_{Ai})\right)}{L}$$

1416 Where $distAAindex$ is the Euclidean distance calculated between the pair of amino acids at the
1417 i^{th} position of p_t and p_n, considering the first nine principal components of a PCA dimensionality
1418 reduction of 554 physicochemical amino acid properties available from AAindex[79] and obtained
1419 through the R package ftrCOOL[152] (version 2.0.0), L is the peptide length, and H_{Ai} is the residue
1420 entropy calculated as above. The results of the peptide similarity analysis for the candidate
1421 $pMHCs$ for each target antigen are available in the supplementary data.

1422

1423 To define a significant threshold for S_{sim}, we tested PS-TRACT on known cross-reactive peptide
1424 pairs[85] and found that a similarity score of 0.95 was the lowest observed for cross-reactive
1425 peptides. Also, we ran PS-TRACT between the *MAGEA3*-derived peptide EVDPIGHLY and the
1426 *TTN*-derived peptide ESDPIVAQY, which was found to be the off-tumor target leading to cases
1427 of fatal myocarditis in patients that received EVDPIGHLY-targeted TCR-T cells[86], obtaining a
1428 peptide similarity score of 1.19. Based on these results, we chose a threshold of $S_{sim} > 1.15$ as
1429 this provided the highest specificity in identifying known cross-reactive peptides (**Figure S11A**).
1430 Thus, after running PS-TRACT on each candidate tumoral $pMHC$, we selected only the
1431 corresponding normal $pMHCs$ with $S_{sim} > 1.15$ for further cross-reactivity assessment.
1432 Specifically, for each of these highly similar normal $pMHCs$ we calculated a tissue-specific
1433 cross-reactivity score, S_{CR}, that considers the tissue abundance of the antigen from which the
1434 cross-reactive peptide originates, the likelihood of presentation based on MHCflurry, and the
1435 presence of the peptide in the observed ligandome:

1436

1437 $S_{CR}(pMHC_y, pMHC_i)$

1438 $$= (P_{MHCflurry} + 0.5) \times (E_{HPA/GTEx}) \times \begin{cases} 1.25 \; if \; pMHC_y \in observed \; ligandome \\ 1 \; if \; pMHC_y \notin observed \; ligandome \end{cases}$$

1439

1440 Where $pMHC_y$ is the yth cross-reactive $pMHC$ for a given tumoral $pMHC_i$, $P_{MHCflurry}$ is the
1441 MHCflurry presentation score for $pMHC_y$, and $E_{HPA/GTEx}$ is the median-centered, z-scored RNA
1442 expression for the parent antigen of the $pMHC_y$ peptide in the HPA and GTEx bulk RNA-seq
1443 consensus datasets (source: https://www.proteinatlas.org/about/download, file:
1444 rna_tissue_consensus.tsv.zip). Then for each tumoral $pMHC$ in each of the 50 normal tissues,
1445 we selected the maximum S_{CR} score among all the filtered cross-reactive normal $pMHCs$, and
1446 this vector of S_{CR} scores was used to define the cross-reactivity profile of the tumoral target
1447 $pMHC$ considered.

1448

1449 Finally, we benchmarked the cross-reactivity profile of each candidate tumoral $pMHC$ pair
1450 against that of the $pMHC$ targeted by afami-cel (GVYDGREHTV–HLA-A*02:01) which was used
1451 as reference given afami-cel's promising safety and tolerability profile observed in clinical
1452 trials[27,28]. Specifically, for each candidate tumoral peptide-MHC pair $pMHC_i$, we calculated the
1453 difference $S_{CR}Diff(i)$ between its S_{CR} cross-reactivity profile and that of GVYDGREHTV–HLA-
1454 A*02:01, as follows:

1455

1456 $$S_{CR}Diff(i) = \frac{1}{n}\sum_{j=1}^{n} \begin{cases} \left(\left(S_{CR}^{ij} - S_{CR}^{refj}\right) / \sigma_j\right) \times \alpha \; if \; S_{CR}^{ij} > S_{CR}^{refj} \\ \left(S_{CR}^{ij} - S_{CR}^{refj}\right) / \sigma_j \qquad otherwise \end{cases}$$

1457

1458 Where S_{CR}^{ij} is the S_{CR} score in the jth tissue of $pMHC_i$, while S_{CR}^{refj} is the S_{CR} score in the jth
1459 tissue of the reference $pMHC$ (GVYDGREHTV–HLA-A*02:01), n is the number of tissues

1460 considered, σ_j is the standard deviation of the S_{CR} scores for all the $pMHC$ pairs in the jth tissue,
1461 and $\alpha = 2$. Target tumoral $pMHCs$ with differential S_{CR} profile compared to GVYDGREHTV–HLA-
1462 A*02:01 ($S_{CR}Diff$) ≤ 0 were considered to have acceptable risk of cross-reactivity.
1463

1464 **Clinical STS proteomics datasets**

1465 Two clinical STS MS proteomics datasets were used to validate the expression of the identified
1466 cell therapy targets at the protein level, one from Tang et al.[91] and one from Burns et al.[92] The
1467 dataset from Tang et al. was obtained from the supplementary material of the relative paper
1468 ("Proteomic_matrix(tumor)" and "Clinical_information" tables). The relative fraction of total (Fot)
1469 protein intensities for the Tang et al. dataset were $\log_2(+1)$ transformed and then median
1470 centered across samples and z-scored across all proteins for standardization. Protein symbols
1471 were standardized to the current HGNC symbols before analysis. The proteomics dataset from
1472 Burns et al. was obtained from the supplementary material (Supplementary Data 2). The
1473 expression matrix in this case was used as is given that protein expression values were already
1474 log-transformed, and median centered across samples and z-scored across proteins. Protein
1475 symbols were standardized to the current HGNC symbols before analysis. For SCAN-ACT
1476 implementation in other cancers, we obtained pre-processed mass spectrometry-based
1477 proteomics data from either LinkedOmicsKB[153], the Proteomic Data Commons (PDC)[154], or from
1478 a literature search (**Table S34**). Most of the data was derived from studies conducted by Clinical
1479 Proteomic Tumor Analysis Consortium (CPTAC) or the International Cancer Proteogenome
1480 Consortium (ICPC). For data obtained from LinkedOmicsKB, which was provided as $\log_2$
1481 reference-normalized protein abundance, we applied median-centering across samples and z-
1482 scoring across proteins. In contrast, for data from the PDC, where the $\log_2$ reference-normalized
1483 protein abundance was already standardized across proteins, we performed only median-
1484 centering across samples. For the gastric adenocarcinoma dataset, expression data from

1485 different technical replicates of the same patient was averaged before analysis. For other
1486 cancers, expression data provided in the supplementary materials of the related publications
1487 was used[155–158]. For the prostate cancer dataset, which was provided as log2 reference-
1488 normalized protein abundance, we applied median-centering across samples and z-scoring
1489 across proteins. For the melanoma and esophageal cancer datasets, only median-centering
1490 across samples was necessary, as the data was already standardized across proteins. The
1491 bladder cancer expression data was used as provided by the authors, as it was already
1492 standardized across both samples and proteins. Prior to analysis, gene symbols across all
1493 datasets were updated to the current HGNC version. Proteins with missing values in 50% or
1494 more samples were removed, and the remaining missing values were imputed with a value of
1495 1e-6. For genes with multiple protein isoforms, the isoform with the highest expression was
1496 used.
1497
1498 **STS cell line proteomics data**
1499 Protein expression data in soft tissue sarcoma cell lines was obtained from the Cancer Cell Line
1500 Encyclopedia[93] (CCLE) and the ProCan-DepMapSanger repository. For CCLE, the normalized
1501 $\log_2$ transformed relative protein intensities were obtained from
1502 https://gygi.hms.harvard.edu/publica Shtions/ccle.html (file:
1503 protein_quant_current_normalized.csv). Gene symbols were standardized to the current HGNC
1504 symbols, and for different protein isoforms for a given gene symbol we retained the isoform with
1505 maximum expression (supplementary data). Then, data was median-centered across all cell
1506 lines and z-scored within genes before use for downstream analysis. The following “soft tissue”
1507 cell lines were considered in the CCLE dataset for further analysis: "A-204", "RD", "RH-41", "HT-
1508 1080", "RH-30", and "KYM-1". The ProCan-DepMapSanger dataset was obtained from the
1509 figshare repository associated with the corresponding publication:
1510 https://doi.org/10.6084/m9.figshare.19345397 (file: ProCan-

1511 DepMapSanger_protein_matrix_8498_averaged.txt). Similarly to the CCLE dataset, first we
1512 standardized gene symbols to the current HGNC nomenclature, then for genes with more than
1513 one protein isoform we retained the isoform with highest expression (supplementary data).
1514 Since the data was already provided as $\log_2$ transformed relative protein intensities, the protein
1515 per cell line expression matrix was median-centered across cell lines and z-scored within genes
1516 before further analysis. The following soft tissue sarcoma cell lines were considered for
1517 downstream analysis: "A204" , "ESS-1", "G-402", "GCT", "Hs-633T", "HT-1080" , "KYM-1",
1518 "MES-SA", "MFH-ino", "RD", "RH-18", "RH-41", "RKN", "SJRH30", "SK-LMS-1", "SK-UT-1" ,
1519 "SKN", "SW684", "SW872", "SW982", "TE-441-T", and "VA-ES-BJ".
1520
1521 **IHC of Selected CAR-T Targets**
1522 IHC was performed by the Stanford Human Pathology/Histology Service Center for ACVR1,
1523 AXL, CLMP, GPC6, KITLG, and MRC2. Previously obtained tissue microarrays constructed
1524 using one to seven 1-mm FFPE cores per patient were used for the analysis, including UPS,
1525 LPS, LMS, SS, and MPNST samples. The following antibodies were used for the analysis:
1526 ACVR1 Rabbit IgG (cat. HPA007505, Sigma Aldrich, MO, USA), AXL Rabbitt IgG (cat.
1527 HPA037422, Sigma Aldrich, MO, USA), GPC6 (cat. HPA017671, Sigma Aldrich, MO, USA),
1528 KITLG (cat. HPA070395, HPA017671), CLMP (cat. 16127-1-AP, Thermo Fisher Scientific, MA,
1529 USA), and MRC2 (cat. HPA041991, Sigma Aldrich, MO, USA). All the antibodies were used at a
1530 dilution titer of 1:50 except for the CLMP antibody (1:400), and the KITLG antibody which was
1531 used at a 1:100, 1:200, or 1:50 dilution depending on the TMA analyzed. Tumor cell staining
1532 intensity was scored using a three-point scale (0, negative; 1, weakly positive; and 2, strongly
1533 positive). Staining for FAP was performed at the UCLA pathology department on a tissue
1534 microarray of 60 undifferentiated pleomorphic sarcomas in triplicate (no previous treatment), of
1535 which 57 samples were evaluable. FAP immunostaining was performed on Leica Bond platform
1536 using a polyclonal rabbit anti-FAP alpha antibody (Abcam, ab207178). All slides were scanned

1537 at 20X magnification. The percentage of FAP expressing cells was quantified using the HALO®
1538 image analysis platform based on automatic cell segmentation (Indica Labs). Missing or folded
1539 tissue cores were excluded. Replicate cores were averaged.
1540
1541 **Measurement of peptide-MHC binding through IMMUNE**
1542 *Plasmid construction*
1543 To construct plasmids driving the expression of non-covalent HLA-I heterodimers, the
1544 commercially available backbone vector pRS315 was modified[89]. Briefly, the entire expression
1545 cassette containing genes encoding the Aga2 leader sequence, the ectodomain of a particular
1546 HLA-I heavy chain allele (A*02:01 or A*11:01 or B*35:01 or C*12:03), the Aga2p yeast native
1547 protein subunit, an HA epitope tag, and the MFα terminator was cloned to the downstream of
1548 the GAL10 promoter in pRS315, so that the expressed HLA-I heavy chain ectodomain was
1549 fused to the N-terminus of Aga2p for yeast surface display. Subsequently, a second expression
1550 cassette containing genes encoding the Aga2 leader sequence, β2m, a C-myc epitope tag and
1551 the MFα terminator was cloned to the downstream of the GAL1 promoter in the same pRS315-
1552 based vector, allowing the secretion of the β2m domain for HLA heavy chain/β2m dimerization
1553 and surface detection. In addition, the Aga2p subunit was further removed from the above
1554 plasmids, which resulted in control plasmids yielding no HLA detection on the surface of yeast.
1555 Gene synthesis and subcloning services were provided by GenScript (Jiangsu, China).
1556
1557 *Electrotransformation of yeast cells and expression of HLA*
1558 The *Saccharomyces cerevisiae* yeast parent strain, EBY100[159] was used for generation of
1559 daughter strains displaying each of the aforementioned HLA alleles. The constructed plasmids
1560 were transformed into EBY100 one at a time by electroporation, following the MicroPulser
1561 electroporation mannual (BioRad). Transformed cells that received the corresponding plasmid
1562 were recovered on selected dextrose-based (SD) medium agar plates minus the nutrient

1563 corresponding to the selection marker gene within the plasmid. Single colonies on SD agar
1564 plates appeared after 2-3 days of incubation at 30°C. To induce yeast expression of target
1565 proteins, a single yeast colony was inoculated with liquid SD medium and cultured in a shaking
1566 tube at 30°C until it reached the exponential growth phase. A sufficient amount of yeast cells
1567 was then transferred from the SD medium to selected galactose-based (SG) medium for protein
1568 expression under the promotion of GAL1 or GAL10. Typically, an overnight shaking and
1569 induction at 30°C can promote effective expression of the protein of interest in yeast for surface
1570 detection by flow cytometry.
1571
1572 *Immunofluorescent labeling and flow cytometric analysis*
1573 A sufficient amount of galactose-induced yeast cells was collected by centrifugation and labeled
1574 by primary antibodies in PBS + 0.5% bovine serum albumin (BSA) for 1 h on ice. The primary
1575 antibody was rabbit anti-HA tag monoclonal antibody (mAb clone C29F4, Cell signaling), mouse
1576 anti-human β2m mAb (clone 2M2, Biolegend), or mouse anti-HLA-A, B, C conformation-specific
1577 mAb (clone W6/32, Biolegend). After the primary staining, the cells were washed at least twice
1578 with ice cold PBS + 0.5% BSA and labeled by secondary antibodies on ice for another 1 h. The
1579 secondary antibody was Alexa Fluor 488 conjugated goat anti-rabbit IgG (H+L) highly cross-
1580 adsorbed secondary antibody, Alexa Fluor 488 or Alexa Fluor 647 conjugated goat anti-mouse
1581 IgG (H+L) highly cross-adsorbed secondary antibody (Thermo Fisher Scientific). After the
1582 secondary staining, cells were washed with ice cold PBS + 0.5% BSA and resuspended in PBS
1583 + 0.5% BSA for flow cytometric analysis. A FACSCalibur flow cytometer (BD biosciences) was
1584 used to acquire flow data. At least 10000 cell events were collected for each sample and gated
1585 through forward and side scattering. FL1 and FL4 fluorescence channels were selected for
1586 Alexa Fluor 488 and Alexa Fluor 647, respectively, according to the fluorophore selected at the
1587 secondary labeling step as mentioned above. Flowjo (BD biosciences) was used for data
1588 analysis.

1589

1590 *Peptide design and synthesis*

1591 To design indicator peptides appropriate for evaluation of HLA peptide binding on the surface of
1592 yeast cells and for downstream competitive assay development, the reported epitope repertoire
1593 for each aforementioned HLA allele from the Immune Epitope Database (https://www.IEDB.org)
1594 was carefully analyzed. First, an epitope peptide was considered only if it contained a cysteine
1595 residue at P4 or P5 or P6 anchor position available for site-specific modification, i.e.,
1596 biotinylation or fluorophore conjugation. After that, the chosen peptide was further analyzed and
1597 validated 1) based on its predicted %Rank_EL (<2) and %Rank_BA scores (<2) from the
1598 NetMHCpan-4.1 webserver, and 2) based on its sequence similarity to the peptides with
1599 available X-ray structure in complex with the given HLA. For example, Bio-KLT (amino acids:
1600 KLTPL{Cys-Biotin}VTL), Bio-AIF (aa: AIFQ{Cys-Biotin}SMTK), Bio-RYP (aa: RYPV{Cys-
1601 Biotin}KFPSL), and Bio-FAF (aa: FAF{Cys-Biotin}RITSF) were designed as the indicator peptide
1602 for A*02:01, A*11:01, B*35:01, and C*12:03, respectively. All peptides were synthesized
1603 (GenScript) with over 95% purify.

1604 *On yeast peptide binding*

1605 About half a million yeast cells displaying a peptide-receptive HLA were collected by
1606 centrifugation, resuspended in 40 µl of PBS, and incubated with 0.5 uM biotinylated indicator
1607 peptides ([peptide]>>[HLA]) overnight prior to fluorescent labeling for flow cytometry. After
1608 peptide binding reached equilibrium, yeast cells were washed twice with ice-cold PBS + 0.5%
1609 BSA and then simultaneously stained for bound biotinylated indicator peptides and HLA
1610 molecules on the surface using Alexa Fluor 647 conjugated streptavidin and HLA conformation-
1611 specific mAb W6/32 followed by Alexa Fluor 488 conjugated goat anti-mouse IgG (H+L) highly
1612 cross-adsorbed secondary antibody (Thermo Fisher Scientific). Double stained cells were then
1613 washed and resuspended in ice-cold PBS + 0.5% BSA for analysis on a BD FACSCalibur. Flow
1614 cytometric data was analyzed using FlowJo.

1615

1616 *On yeast peptide competition*

1617 To evaluate the competitive binding of a test peptide against the indicator peptide to HLA on the
1618 surface of yeast cells, about half a million yeast cells were collected and incubated with the
1619 biotinylated peptide as mentioned above, but with addition of a 20-fold more concentrated test
1620 peptide in its non-biotinylated format. The peptide competition assay was also performed under
1621 a similar condition as mentioned above, allowing reaction to reach equilibrium. Yeast cells were
1622 then collected, washed, and co-stained for bound biotinylated indicator peptides and HLA
1623 molecules using the aforementioned fluorescent labeling method for flow cytometric analysis.
1624 The %Binding in the presence of competitors was quantified as $[(MFI_{with\ competitor}-BG)/(MFI_{no}$
1625 $_{competitor}-BG)]\times 100\%$, where $MFI_{with\ competitor}$ represents the average fluorescence intensity in the
1626 presence of test peptide (a competitor), $MFI_{no\ competitor}$ represents the average fluorescence
1627 intensity in the absence of competitors, and BG represents the background fluorescence
1628 intensity. The %Competition was calculated as 100%−%Binding to reveal binding of the test
1629 peptide competitor to HLA molecules displayed on yeast. MFI was determined using
1630 appropriately gated cell populations.

1631

1632 **Target Priority Index**

1633 For each target discovery pipeline, we calculated a final Target Priority Index (TPI) that
1634 integrates normal tissues/cells target expression, scRNA-seq tumor expression and
1635 homogeneity, STS protein expression, DepMap sarcoma cell line essentiality, incidence of
1636 SNVs/Indels, gene fusions and CNAs in STS involving the target considered, and the presence
1637 of clinically or pre-clinically developed immunotherapeutic agents against each target (for
1638 monospecific and bispecific CAR-T cells targets only).

1639

1640 Homogeneity of expression at the single-cell level in each STS was calculated as the product of
1641 the average tumor expression in $\log_2$(CPM+1) and the percentage of tumor cells with
1642 $\log_2$(CPM+1) > 0, which we defined as H_{RNA} score:

1643 $$H_{RNA} = \left(\overline{log_2(CPM+1)}\right) \times \left(\frac{n\ cells\ log_2(CPM+1) > 0}{total\ cells} \times 100\right)$$

1644 To assess if a gene has been previously studied as an immunotherapy target, we focused on
1645 therapeutic monoclonal antibodies (mAb), ADCs, single-chain variable fragments (scFv), fusion
1646 proteins, nanobodies, and fragment antigen binding regions (Fab), as well as CAR-T cells.
1647 Specifically, we downloaded a list of clinically developed mAbs, ADCs, scFvs, Fabs, nanobodies
1648 and fusion proteins from Thera-SAbDab[160] (https://opig.stats.ox.ac.uk/webapps/sabdab-
1649 sabpred/therasabdab, accessed on 07/16/2024, Supplementary Data), retaining only agents
1650 developed for human use, and removing all those agents with clinical development phase
1651 reported as "TBC", "Preregistration", or "Preregistration (w)". We complemented Thera-SAbDab
1652 with a PubMed search for pre-clinically developed therapeutic antibodies or ADCs against any
1653 genes in the surfaceome, using the following search query: "gene AND antibody, OR gene AND
1654 antibody drug conjugate, OR gene AND ADC OR gene AND antibody-drug conjugate" (**Table**
1655 **S30**). Targets with clinical development phase reported as "TBC", "Preregistration", or
1656 "Preregistration (w)" in Thera-SAbDab were included as pre-clinical targets, unless they were
1657 described as clinical targets. As far CAR-T cells, for clinically developed targets we used the
1658 previously defined list of targets as per MacKay et al[45], while for pre-clinically developed targets
1659 we performed a PubMed search for all the genes in the surfaceome using the following search
1660 query: "gene AND CAR-T OR gene AND chimeric antigen receptor T-cells OR gene AND
1661 chimeric antigen receptor", **Table S30**).
1662
1663 *Monospecific CAR-T Cell Target TPI Calculation*

To obtain the TPI for monospecific CAR-T targets, we used the list of targets defined based on the TS_{CAR} as described above. Then, for these targets we normalized the TS_{CAR} to assume values between 0 and 1 as follows:

$$TS_{CAR}(g)(norm) = \frac{TS_{CAR}(g) - \min(TS_{CAR})}{\max(TS_{CAR}) - \min(TS_{CAR})}$$

Where $TS_{CAR}(g)$ is the TS_{CAR} for a target g, and $\min(TS_{CAR})$ and $\max(TS_{CAR})$ represents the minimum and maximum TS_{CAR} values, respectively, for all the final targets being considered for the STS histotype analyzed.

Then, for each target g, we obtained a summative validation score, V_{CAR}, calculated as the sum of different scores assigned for each validation feature, defined as follows:

- If the H_{RNA} score for g is equal or greater than the average H_{RNA} for *CD276* across the five STS studied, g is assigned a score of 2, otherwise g is assigned a score of 0. *CD276* was used as reference as it has been clinically (NCT04433221) and pre-clinically[95] studied as a CAR-T target in STS.
- For each gene g and STS histotype we measured the percentage of samples in the STS proteomics Tang et al. dataset with medium-high (M-H) expression (z-score ≥ 0). DDLPS and WDLPS samples were considered as one group (LPS) for this analysis. If the percentage of samples of the STS analyzed with M-H expression for g was greater than or equal to the average percentage of samples with M-H expression for CD276 across SS, MFS, UPS, LMS and LPS, then we assigned a score of 2, otherwise we assigned a score of 0.
- If g was reported as target for clinically developed mAbs, ADCs, scFv, Fabs, nanobodies or fusion proteins, we assigned a score of 1. If instead g was only studied preclinically as target for therapeutic antibodies or ADCs, we assigned a score of 0.5. Otherwise, we assigned a score of 0.

1689 • If g was reported as target for clinically developed CAR-T cells, we assigned a score of
1690 1, while we assigned a score of 0.5 if g was only explored as a CAR-T target
1691 preclinically, and a score of 0 if it was never tested as a CAR-T target.
1692 • If g resulted as essential (Chronos DepMap score ≤ -1) in sarcoma cell lines derived
1693 from the STS histotype studied, we assigned a score of 1, otherwise we assigned a
1694 score of 0.5 if g was essential in any sarcoma cell line, or a score of 0 if g was not
1695 essential in any sarcoma cell lines.
1696 • If g was involved in at least one gene fusion in the STS histotype studied we assigned a
1697 score of 1, otherwise we assigned a score of 0.5 if g was involved in at least one gene
1698 fusion in any STS, or a score of 0 if g was never involved in gene fusions in STS.
1699 • If g was involved by at least one SNV or Indel in the STS histotype studied we assigned
1700 a score of 1, otherwise we assigned a score of 0.5 if g was involved by at least one
1701 SNV/Indel in any STS histotype, or a score of 0 if g was never involved by SNVs/Indels.
1702 • If g was involved by CNAs in the STS histotype studied and there was a positive
1703 correlation between its linear CNV level and RNA expression in TCGA, we assigned a
1704 score of 1, otherwise if it was involved by CNAs either in TCGA or MSK-IMPACT in the
1705 same STS histotype studied we assigned a score of 0.5. Instead, if g was never involved
1706 by CNAs in STS we assigned a score of 0.

1707 We then normalized V_{CAR} to assume values ranging from 0 to 1 as follows:

1708 $$V_{CAR}(g)(norm) = \frac{V_{CAR}(g) - \min(V_{CAR})}{\max(V_{CAR}) - \min(V_{CAR})}$$

1709 Finally, we calculated the TPI for each gene g as follows:

1710 $$TPI_{CAR} = TS_{CAR}(g)(norm) + V_{CAR}(g)(norm)$$

1711 The TPI for the monospecific CAR-T targets is reported in **Table S31**.

1712

1713 *Bispecific CAR-T Cells Targets TPI Calculation*

1714 For bispecific CAR-T cells targets we obtained a TPI for logic-gated 'AND' CAR-T cells

1715 ($TPI_{'AND'}$), and a separate TPI for 'AND-NOT' CAR-T cells ($TPI_{'AND-NOT'}$). Specifically, we

1716 defined suitable target pairs for both 'AND' and 'AND-NOT' CAR-T cells as described above,

1717 and then for each 'AND' CAR-T target and 'AND-NOT' CAR-T activator we calculated the

1718 average $TS_{'AND'}$ and $TS_{'AND-NOT'}$ scores considering all the target pairs in which that gene

1719 appears. We then normalized the average $TS_{'AND'}$ and $TS_{'AND-NOT'}$ for each gene g to assume

1720 values ranging from 0 to 1 as follows:

1721 $$TS_{'AND'}(g)(norm) = \frac{\overline{TS_{'AND'}}(g) - \min(\overline{TS_{'AND'}})}{\max(\overline{TS_{'AND'}}) - \min(\overline{TS_{'AND'}})}$$

1722

1723 $$TS_{'AND-NOT'}(g)(norm) = \frac{\overline{TS_{'AND-NOT'}}(g) - \min(\overline{TS_{'AND-NOT'}})}{\max(\overline{TS_{'AND-NOT'}}) - \min(\overline{TS_{'AND-NOT'}})}$$

1724 Then, for each target g we calculated $V_{CAR}(g)$ and $V_{CAR}(g)(norm)$ as described above, and

1725 finally obtained the TPIs as follows:

1726 $$TPI_{'AND'} = TS_{'AND'}(g)(norm) + V_{CAR}(g)(norm)$$

1727 $$TPI_{'AND-NOT'} = TS_{'AND-NOT'}(g)(norm) + V_{CAR}(g)(norm)$$

1728 The TPIs for the bispecific CAR-T targets are reported in **Table S32**.

1729

1730 *TCR and PC-CAR-T Cells Targets TPI Calculation*

1731 For each of the defined target antigens g for TCR-T and PC-CAR-T cells in each STS, we first

1732 normalized the $N(g)$ score, indicative of the normal tissue and cell expression of g as previously

1733 defined, to assume values between 0 and 1:

1734 $$N(g)_{norm} = \frac{N(g) - \min(N)}{\max(N) - \min(N)}$$

1735 Then, for each target g we obtained a summative validation score, $V_{TCR/PC}$, calculated as the

1736 sum of the following scores:

1737 • If the H_{RNA} score for g is equal or greater than the H_{RNA} for *MAGEA4* in SS, g is
1738 assigned a score of 2, otherwise is assigned a score of 0. *MAGEA4* was used as
1739 reference in this case since it is the source antigen for the target of afami-cel, the first
1740 TCR-T cell therapy to receive FDA approval in soft tissue sarcomas.
1741 • If g had a z-score ≥ 0 in at least two separate STS cell lines in either CCLE or in the
1742 ProCan-DepMapSanger datasets, we assigned a score of 1, otherwise we assigned a
1743 score of 0.
1744 • If g resulted as essential (Chronos DepMap score ≤ -1) in sarcoma cell lines derived
1745 from the STS histotype studied, we assigned a score of 1, otherwise we assigned a
1746 score of 0.5 if g was essential in any sarcoma cell line, or a score of 0 if g was not
1747 essential in any sarcoma cell lines.
1748 • If g was involved in at least one gene fusion in the STS histotype studied we assigned a
1749 score of 1, otherwise we assigned a score of 0.5 if g was involved in at least one gene
1750 fusion in any STS, or a score of 0 if g was never involved in gene fusions in STS.
1751 • If g was involved by at least one SNV or Indel in the STS histotype studied we assigned
1752 a score of 1, otherwise we assigned a score of 0.5 if g was involved by at least one
1753 SNV/Indel in any STS histotype, or a score of 0 if g was never involved by SNVs/Indels.
1754 • If g was involved by CNAs in the STS histotype studied and there was a positive
1755 correlation between its linear CNV level and RNA expression in TCGA, we assigned a
1756 score of 1, otherwise if it was involved by CNAs either in TCGA or MSK-IMPACT in the
1757 same STS histotype studied we assigned a score of 0.5. Instead, if g was never involved
1758 by CNAs in STS we assigned a score of 0.
1759 We then normalized $V_{TCR/PC}$ to assume values ranging from 0 to 1 as follows:

1760 $$V_{TCR/PC}(g)(norm) = \frac{V_{TCR/PC}(g) - \min(V_{TCR/PC})}{\max(V_{TCR/PC}) - \min(V_{TCR/PC})}$$

Next, for each target antigen we considered the target $pMHCs$ defined based on their $TS_{TCR/PC}$ as reported in **Table S27**. Specifically, for each target antigen g we calculated the average HLA allele frequency at each locus, by considering all the peptides derived from each antigen binding to HLA-A, HLA-B, or HLA-C class alleles, as follows:

$$HLA_A(f_{TOT}) = \frac{\sum_{i=1}^{pA} HLA_A(f)}{pA}$$

$$HLA_B(f_{TOT}) = \frac{\sum_{i=1}^{pB} HLA_B(f)}{pB}$$

$$HLA_C(f_{TOT}) = \frac{\sum_{i=1}^{pC} HLA_C(f)}{pC}$$

Where pA, pB, pC are respectively the number of $pMHC$ pairs including class A, class B and class C alleles for the target g, while $HLA_A(f), HLA_B(f)$, and $HLA_C(f)$ represent the HLA allele frequencies of the $i^{th} pMHC$ considered. We then obtained the total HLA allele frequency, $HLA_{TOT}(g)$ for each target g by adding $HLA_A(f_{TOT})$, $HLA_B(f_{TOT})$, and $HLA_C(f_{TOT})$, and normalized this to obtain values ranging from 0 to 1, as follows:

$$HLA_{TOT}(g)(norm) = \frac{HLA_{TOT}(g) - \min(HLA_{TOT})}{\max(HLA_{TOT}) - \min(HLA_{TOT})}$$

Next, for each target g we calculated the total number of $pMHC$ targets ($pMHC_{TOT}$) and the number of $pMHC$ targets with $S_{CR}Diff \leq 0$ ($pMHC_{SCR}$). We divided these by the target antigen total number of amino acids (L_{AA}) to account for differences in protein size, and then normalized them to obtain values ranging from 0 to 1, as follows:

$$pMHC_{TOT} = \frac{n(pMHC_{TOT})}{L_{AA}}$$

$$pMHC_{TOT}(g)(norm) = \frac{pMHC_{TOT}(g) - \min(pMHC_{TOT})}{\max(pMHC_{TOT}) - \min(pMHC_{TOT})}$$

$$pMHC_{SCR} = \frac{n(pMHC_{SCR})}{L_{AA}}$$

1782 $$pMHC_{SCR}(g)(norm) = \frac{pMHC_{SCR}(g) - \min(pMHC_{SCR})}{\max(pMHC_{SCR}) - \min(pMHC_{SCR})}$$

1783 Finally, we calculated the TPI for each target g as follows:

1784 $$TPI_{TCR/PC} = N(g)_{norm} + V_{TCR/PC}(g)(norm) + HLA_{TOT}(g)(norm) + pMHC_{TOT}(g)(norm)$$

1785 $$+ pMHC_{SCR}(g)(norm)$$

1786 The TPIs for the TCR-T and PC-CAR-T cells targets are reported in **Table S33**.

1787

1788 **References**

1789 1. Wagner, J., Wickman, E., DeRenzo, C., and Gottschalk, S. (2020). CAR T Cell Therapy for

1790 Solid Tumors: Bright Future or Dark Reality? Mol. Ther. J. Am. Soc. Gene Ther. *28*, 2320–

1791 2339. https://doi.org/10.1016/j.ymthe.2020.09.015.

1792 2. Neelapu, S.S., Locke, F.L., Bartlett, N.L., Lekakis, L.J., Miklos, D.B., Jacobson, C.A.,

1793 Braunschweig, I., Oluwole, O.O., Siddiqi, T., Lin, Y., et al. (2017). Axicabtagene Ciloleucel

1794 CAR T-Cell Therapy in Refractory Large B-Cell Lymphoma. N. Engl. J. Med. *377*, 2531–

1795 2544. https://doi.org/10.1056/NEJMoa1707447.

1796 3. Maude, S.L., Laetsch, T.W., Buechner, J., Rives, S., Boyer, M., Bittencourt, H., Bader, P.,

1797 Verneris, M.R., Stefanski, H.E., Myers, G.D., et al. (2018). Tisagenlecleucel in Children

1798 and Young Adults with B-Cell Lymphoblastic Leukemia. N. Engl. J. Med. *378*, 439–448.

1799 https://doi.org/10.1056/NEJMoa1709866.

1800 4. Labanieh, L., and Mackall, C.L. (2023). CAR immune cells: design principles, resistance

1801 and the next generation. Nature *614*, 635–648. https://doi.org/10.1038/s41586-023-

1802 05707-3.

1803 5. Adachi, K., Kano, Y., Nagai, T., Okuyama, N., Sakoda, Y., and Tamada, K. (2018). IL-7 and
1804 CCL19 expression in CAR-T cells improves immune cell infiltration and CAR-T cell
1805 survival in the tumor. Nat. Biotechnol. *36*, 346–351. https://doi.org/10.1038/nbt.4086.
1806 6. Lynn, R.C., Weber, E.W., Sotillo, E., Gennert, D., Xu, P., Good, Z., Anbunathan, H., Lattin,
1807 J., Jones, R., Tieu, V., et al. (2019). c-Jun overexpression in CAR T cells induces
1808 exhaustion resistance. Nature *576*, 293–300. https://doi.org/10.1038/s41586-019-1805-
1809 z.
1810 7. Rafiq, S., Yeku, O.O., Jackson, H.J., Purdon, T.J., van Leeuwen, D.G., Drakes, D.J., Song,
1811 M., Miele, M.M., Li, Z., Wang, P., et al. (2018). Targeted delivery of a PD-1-blocking scFv by
1812 CAR-T cells enhances anti-tumor efficacy in vivo. Nat. Biotechnol. *36*, 847–856.
1813 https://doi.org/10.1038/nbt.4195.
1814 8. Narayan, V., Barber-Rotenberg, J.S., Jung, I.-Y., Lacey, S.F., Rech, A.J., Davis, M.M.,
1815 Hwang, W.-T., Lal, P., Carpenter, E.L., Maude, S.L., et al. (2022). PSMA-targeting TGFβ-
1816 insensitive armored CAR T cells in metastatic castration-resistant prostate cancer: a
1817 phase 1 trial. Nat. Med. *28*, 724–734. https://doi.org/10.1038/s41591-022-01726-1.
1818 9. Doan, A.E., Mueller, K.P., Chen, A.Y., Rouin, G.T., Chen, Y., Daniel, B., Lattin, J.,
1819 Markovska, M., Mozarsky, B., Arias-Umana, J., et al. (2024). FOXO1 is a master regulator
1820 of memory programming in CAR T cells. Nature *629*, 211–218.
1821 https://doi.org/10.1038/s41586-024-07300-8.
1822 10. Larson, R.C., and Maus, M.V. (2021). Recent advances and discoveries in the
1823 mechanisms and functions of CAR T cells. Nat. Rev. Cancer *21*, 145–161.
1824 https://doi.org/10.1038/s41568-020-00323-z.

1825 11. Baulu, E., Gardet, C., Chuvin, N., and Depil, S. (2023). TCR-engineered T cell therapy
1826 in solid tumors: State of the art and perspectives. Sci. Adv. *9*, eadf3700.
1827 https://doi.org/10.1126/sciadv.adf3700.
1828 12. Tousley, A.M., Rotiroti, M.C., Labanieh, L., Rysavy, L.W., Kim, W.-J., Lareau, C.,
1829 Sotillo, E., Weber, E.W., Rietberg, S.P., Dalton, G.N., et al. (2023). Co-opting signalling
1830 molecules enables logic-gated control of CAR T cells. Nature *615*, 507–516.
1831 https://doi.org/10.1038/s41586-023-05778-2.
1832 13. Choe, J.H., Watchmaker, P.B., Simic, M.S., Gilbert, R.D., Li, A.W., Krasnow, N.A.,
1833 Downey, K.M., Yu, W., Carrera, D.A., Celli, A., et al. (2021). SynNotch-CAR T cells
1834 overcome challenges of specificity, heterogeneity, and persistence in treating
1835 glioblastoma. Sci. Transl. Med. *13*, eabe7378.
1836 https://doi.org/10.1126/scitranslmed.abe7378.
1837 14. Hu, Z., Yuan, J., Long, M., Jiang, J., Zhang, Y., Zhang, T., Xu, M., Fan, Y., Tanyi, J.L.,
1838 Montone, K.T., et al. (2021). The Cancer Surfaceome Atlas integrates genomic, functional
1839 and drug response data to identify actionable targets. Nat. Cancer *2*, 1406–1422.
1840 https://doi.org/10.1038/s43018-021-00282-w.
1841 15. Shaw, T.I., Wagner, J., Tian, L., Wickman, E., Poudel, S., Wang, J., Paul, R., Koo, S.C.,
1842 Lu, M., Sheppard, H., et al. (2024). Discovery of immunotherapy targets for pediatric
1843 solid and brain tumors by exon-level expression. Nat. Commun. *15*, 3732.
1844 https://doi.org/10.1038/s41467-024-47649-y.
1845 16. Perna, F., Berman, S.H., Soni, R.K., Mansilla-Soto, J., Eyquem, J., Hamieh, M.,
1846 Hendrickson, R.C., Brennan, C.W., and Sadelain, M. (2017). Integrating Proteomics and

Transcriptomics for Systematic Combinatorial Chimeric Antigen Receptor Therapy of AML. Cancer Cell *32*, 506-519.e5. https://doi.org/10.1016/j.ccell.2017.09.004.

17. Subramanian, A., Nemat-Gorgani, N., Ellis-Caleo, T.J., Van IJzendoorn, D.G.P., Sears, T.J., Somani, A., Luca, B.A., Zhou, M.Y., Bradic, M., Torres, I.A., et al. (2024). Sarcoma microenvironment cell states and ecosystems are associated with prognosis and predict response to immunotherapy. Nat. Cancer *5*, 642–658. https://doi.org/10.1038/s43018-024-00743-y.

18. Gottschlich, A., Thomas, M., Grünmeier, R., Lesch, S., Rohrbacher, L., Igl, V., Briukhovetska, D., Benmebarek, M.-R., Vick, B., Dede, S., et al. (2023). Single-cell transcriptomic atlas-guided development of CAR-T cells for the treatment of acute myeloid leukemia. Nat. Biotechnol. *41*, 1618–1632. https://doi.org/10.1038/s41587-023-01684-0.

19. Lochner, J., Menge, F., Vassos, N., Hohenberger, P., and Kasper, B. (2020). Prognosis of Patients with Metastatic Soft Tissue Sarcoma: Advances in Recent Years. Oncol. Res. Treat. *43*, 613–619. https://doi.org/10.1159/000509519.

20. Judson, I., Verweij, J., Gelderblom, H., Hartmann, J.T., Schöffski, P., Blay, J.-Y., Kerst, J.M., Sufliarsky, J., Whelan, J., Hohenberger, P., et al. (2014). Doxorubicin alone versus intensified doxorubicin plus ifosfamide for first-line treatment of advanced or metastatic soft-tissue sarcoma: a randomised controlled phase 3 trial. Lancet Oncol. *15*, 415–423. https://doi.org/10.1016/S1470-2045(14)70063-4.

21. Tap, W.D., Papai, Z., Van Tine, B.A., Attia, S., Ganjoo, K.N., Jones, R.L., Schuetze, S., Reed, D., Chawla, S.P., Riedel, R.F., et al. (2017). Doxorubicin plus evofosfamide versus

1869 doxorubicin alone in locally advanced, unresectable or metastatic soft-tissue sarcoma
1870 (TH CR-406/SARC021): an international, multicentre, open-label, randomised phase 3
1871 trial. Lancet Oncol. *18*, 1089–1103. https://doi.org/10.1016/S1470-2045(17)30381-9.
1872 22. Tawbi, H.A., Burgess, M., Bolejack, V., Van Tine, B.A., Schuetze, S.M., Hu, J.,
1873 D'Angelo, S., Attia, S., Riedel, R.F., Priebat, D.A., et al. (2017). Pembrolizumab in
1874 advanced soft-tissue sarcoma and bone sarcoma (SARC028): a multicentre, two-cohort,
1875 single-arm, open-label, phase 2 trial. Lancet Oncol. *18*, 1493–1501.
1876 https://doi.org/10.1016/S1470-2045(17)30624-1.
1877 23. Burgess, M.A., Bolejack, V., Schuetze, S., Van Tine, B.A., Attia, S., Riedel, R.F., Hu,
1878 J.S., Davis, L.E., Okuno, S.H., Priebat, D.A., et al. (2019). Clinical activity of
1879 pembrolizumab (P) in undifferentiated pleomorphic sarcoma (UPS) and
1880 dedifferentiated/pleomorphic liposarcoma (LPS): Final results of SARC028 expansion
1881 cohorts. J. Clin. Oncol. *37*, 11015–11015.
1882 https://doi.org/10.1200/JCO.2019.37.15_suppl.11015.
1883 24. Somaiah, N., Conley, A.P., Parra, E.R., Lin, H., Amini, B., Solis Soto, L., Salazar, R.,
1884 Barreto, C., Chen, H., Gite, S., et al. (2022). Durvalumab plus tremelimumab in
1885 advanced or metastatic soft tissue and bone sarcomas: a single-centre phase 2 trial.
1886 Lancet Oncol. *23*, 1156–1166. https://doi.org/10.1016/S1470-2045(22)00392-8.
1887 25. Keung, E.Z., Burgess, M., Salazar, R., Parra, E.R., Rodrigues-Canales, J., Bolejack, V.,
1888 Van Tine, B.A., Schuetze, S.M., Attia, S., Riedel, R.F., et al. (2020). Correlative Analyses of
1889 the SARC028 Trial Reveal an Association Between Sarcoma-Associated Immune

1890 Infiltrate and Response to Pembrolizumab. Clin. Cancer Res. Off. J. Am. Assoc. Cancer
1891 Res. *26*, 1258–1266. https://doi.org/10.1158/1078-0432.CCR-19-1824.
1892 26. Petitprez, F., De Reyniès, A., Keung, E.Z., Chen, T.W.-W., Sun, C.-M., Calderaro, J.,
1893 Jeng, Y.-M., Hsiao, L.-P., Lacroix, L., Bougoüin, A., et al. (2020). B cells are associated
1894 with survival and immunotherapy response in sarcoma. Nature *577*, 556–560.
1895 https://doi.org/10.1038/s41586-019-1906-8.
1896 27. D'Angelo, S.P., Araujo, D.M., Abdul Razak, A.R., Agulnik, M., Attia, S., Blay, J.-Y.,
1897 Carrasco Garcia, I., Charlson, J.A., Choy, E., Demetri, G.D., et al. (2024). Afamitresgene
1898 autoleucel for advanced synovial sarcoma and myxoid round cell liposarcoma
1899 (SPEARHEAD-1): an international, open-label, phase 2 trial. The Lancet *403*, 1460–1471.
1900 https://doi.org/10.1016/S0140-6736(24)00319-2.
1901 28. Hong, D.S., Van Tine, B.A., Biswas, S., McAlpine, C., Johnson, M.L., Olszanski, A.J.,
1902 Clarke, J.M., Araujo, D., Blumenschein, G.R., Kebriaei, P., et al. (2023). Autologous T cell
1903 therapy for MAGE-A4+ solid cancers in HLA-A*02+ patients: a phase 1 trial. Nat. Med. *29*,
1904 104–114. https://doi.org/10.1038/s41591-022-02128-z.
1905 29. D'Angelo, S.P., Melchiori, L., Merchant, M.S., Bernstein, D., Glod, J., Kaplan, R.,
1906 Grupp, S., Tap, W.D., Chagin, K., Binder, G.K., et al. (2018). Antitumor Activity Associated
1907 with Prolonged Persistence of Adoptively Transferred NY-ESO-1 c259T Cells in Synovial
1908 Sarcoma. Cancer Discov. *8*, 944–957. https://doi.org/10.1158/2159-8290.CD-17-1417.
1909 30. D'Angelo, S.P., Druta, M., Van Tine, B.A., Liebner, D.A., Schuetze, S., Hasan, A.N.,
1910 Holmes, A.P., Huff, A., Kapoor, G.S., Zajic, S., et al. (2021). Safety and efficacy of
1911 letetresgene autoleucel (lete-cel; GSK3377794) in advanced myxoid/round cell

liposarcoma (MRCLS) following high lymphodepletion (Cohort 2): Interim analysis. J. Clin. Oncol. *39*, 11521–11521. https://doi.org/10.1200/JCO.2021.39.15_suppl.11521.

31. Robbins, P.F., Morgan, R.A., Feldman, S.A., Yang, J.C., Sherry, R.M., Dudley, M.E., Wunderlich, J.R., Nahvi, A.V., Helman, L.J., Mackall, C.L., et al. (2011). Tumor regression in patients with metastatic synovial cell sarcoma and melanoma using genetically engineered lymphocytes reactive with NY-ESO-1. J. Clin. Oncol. Off. J. Am. Soc. Clin. Oncol. *29*, 917–924. https://doi.org/10.1200/JCO.2010.32.2537.

32. Smithy, J.W., Blouin, A., Diamond, L.C., and Postow, M. (2022). Ensuring equity in the era of HLA-restricted cancer therapeutics. J. Immunother. Cancer *10*, e005600. https://doi.org/10.1136/jitc-2022-005600.

33. Jerby-Arnon, L., Neftel, C., Shore, M.E., Weisman, H.R., Mathewson, N.D., McBride, M.J., Haas, B., Izar, B., Volorio, A., Boulay, G., et al. (2021). Opposing immune and genetic mechanisms shape oncogenic programs in synovial sarcoma. Nat. Med. *27*, 289–300. https://doi.org/10.1038/s41591-020-01212-6.

34. Patel, A.P., Tirosh, I., Trombetta, J.J., Shalek, A.K., Gillespie, S.M., Wakimoto, H., Cahill, D.P., Nahed, B.V., Curry, W.T., Martuza, R.L., et al. (2014). Single-cell RNA-seq highlights intratumoral heterogeneity in primary glioblastoma. Science *344*, 1396–1401. https://doi.org/10.1126/science.1254257.

35. Timothy Tickle, Itay Tirosh, Christophe Georgescu, Maxwell Brown, Brian Haas inferCNV of the Trinity CTAT Project.. Klarman Cell Observatory, Broad Institute of MIT and Harvard, Cambridge, MA, USA. (Bioconductor).

https://doi.org/10.18129/B9.BIOC.INFERCNV

https://doi.org/10.18129/B9.BIOC.INFERCNV.

36. Abeshouse, A., Adebamowo, C., Adebamowo, S.N., Akbani, R., Akeredolu, T., Ally, A., Anderson, M.L., Anur, P., Appelbaum, E.L., Armenia, J., et al. (2017). Comprehensive and Integrated Genomic Characterization of Adult Soft Tissue Sarcomas. Cell *171*, 950-965.e28. https://doi.org/10.1016/j.cell.2017.10.014.

37. Ritchie, M.E., Phipson, B., Wu, D., Hu, Y., Law, C.W., Shi, W., and Smyth, G.K. (2015). limma powers differential expression analyses for RNA-sequencing and microarray studies. Nucleic Acids Res. *43*, e47. https://doi.org/10.1093/nar/gkv007.

38. Tiberi, S., Crowell, H.L., Samartsidis, P., Weber, L.M., and Robinson, M.D. distinct: a novel approach to differential distribution analyses.

39. Uhlén, M., Fagerberg, L., Hallström, B.M., Lindskog, C., Oksvold, P., Mardinoglu, A., Sivertsson, Å., Kampf, C., Sjöstedt, E., Asplund, A., et al. (2015). Proteomics. Tissue-based map of the human proteome. Science *347*, 1260419. https://doi.org/10.1126/science.1260419.

40. Pontén, F., Gry, M., Fagerberg, L., Lundberg, E., Asplund, A., Berglund, L., Oksvold, P., Björling, E., Hober, S., Kampf, C., et al. (2009). A global view of protein expression in human cells, tissues, and organs. Mol. Syst. Biol. *5*, 337. https://doi.org/10.1038/msb.2009.93.

41. The Tabula Sapiens Consortium*, Jones, R.C., Karkanias, J., Krasnow, M.A., Pisco, A.O., Quake, S.R., Salzman, J., Yosef, N., Bulthaup, B., Brown, P., et al. (2022). The Tabula

1954 Sapiens: A multiple-organ, single-cell transcriptomic atlas of humans. Science *376*,
1955 eabl4896. https://doi.org/10.1126/science.abl4896.
1956 42. Regev, A., Teichmann, S.A., Lander, E.S., Amit, I., Benoist, C., Birney, E.,
1957 Bodenmiller, B., Campbell, P., Carninci, P., Clatworthy, M., et al. (2017). The Human Cell
1958 Atlas. eLife *6*, e27041. https://doi.org/10.7554/eLife.27041.
1959 43. Bughda, R., Dimou, P., D'Souza, R.R., and Klampatsa, A. (2021). Fibroblast
1960 Activation Protein (FAP)-Targeted CAR-T Cells: Launching an Attack on Tumor Stroma.
1961 ImmunoTargets Ther. *Volume 10*, 313–323. https://doi.org/10.2147/ITT.S291767.
1962 44. June, C.H., and Sadelain, M. (2018). Chimeric Antigen Receptor Therapy. N. Engl. J.
1963 Med. *379*, 64–73. https://doi.org/10.1056/NEJMra1706169.
1964 45. MacKay, M., Afshinnekoo, E., Rub, J., Hassan, C., Khunte, M., Baskaran, N., Owens,
1965 B., Liu, L., Roboz, G.J., Guzman, M.L., et al. (2020). The therapeutic landscape for cells
1966 engineered with chimeric antigen receptors. Nat. Biotechnol. *38*, 233–244.
1967 https://doi.org/10.1038/s41587-019-0329-2.
1968 46. DuBois, S.G., Krailo, M.D., Glade-Bender, J., Buxton, A., Laack, N., Randall, R.L.,
1969 Chen, H.X., Seibel, N.L., Boron, M., Terezakis, S., et al. (2023). Randomized Phase III Trial
1970 of Ganitumab With Interval-Compressed Chemotherapy for Patients With Newly
1971 Diagnosed Metastatic Ewing Sarcoma: A Report From the Children's Oncology Group. J.
1972 Clin. Oncol. Off. J. Am. Soc. Clin. Oncol. *41*, 2098–2107.
1973 https://doi.org/10.1200/JCO.22.01815.
1974 47. Gounder, M.M., Rosenbaum, E., Wu, N., Dickson, M.A., Sheikh, T.N., D'Angelo, S.P.,
1975 Chi, P., Keohan, M.L., Erinjeri, J.P., Antonescu, C.R., et al. (2022). A Phase Ib/II

Randomized Study of RO4929097, a Gamma-Secretase or Notch Inhibitor with or without Vismodegib, a Hedgehog Inhibitor, in Advanced Sarcoma. Clin. Cancer Res. *28*, 1586–1594. https://doi.org/10.1158/1078-0432.CCR-21-3874.

48. Luke, J.J., Powderly, J.D., Merchan, J.R., Barve, M.A., Hotson, A.N., Mobasher, M., Kwei, L., Luciano, G., Buggy, J.J., Piccione, E., et al. (2019). Immunobiology, preliminary safety, and efficacy of CPI-006, an anti-CD73 antibody with immune modulating activity, in a phase 1 trial in advanced cancers. J. Clin. Oncol. *37*, 2505–2505. https://doi.org/10.1200/JCO.2019.37.15_suppl.2505.

49. Edwards, D., Handsley, M., and Pennington, C. (2008). The ADAM metalloproteinases. Mol. Aspects Med. *29*, 258–289. https://doi.org/10.1016/j.mam.2008.08.001.

50. Li, N., Spetz, M.R., and Ho, M. (2020). The Role of Glypicans in Cancer Progression and Therapy. J. Histochem. Cytochem. *68*, 841–862. https://doi.org/10.1369/0022155420933709.

51. Qin, S., Xu, L., Yi, M., Yu, S., Wu, K., and Luo, S. (2019). Novel immune checkpoint targets: moving beyond PD-1 and CTLA-4. Mol. Cancer *18*, 155. https://doi.org/10.1186/s12943-019-1091-2.

52. Du, Z., and Lovly, C.M. (2018). Mechanisms of receptor tyrosine kinase activation in cancer. Mol. Cancer *17*, 58. https://doi.org/10.1186/s12943-018-0782-4.

53. Zhou, B., Lin, W., Long, Y., Yang, Y., Zhang, H., Wu, K., and Chu, Q. (2022). Notch signaling pathway: architecture, disease, and therapeutics. Signal Transduct. Target. Ther. *7*, 95. https://doi.org/10.1038/s41392-022-00934-y.

54. Dorsam, R.T., and Gutkind, J.S. (2007). G-protein-coupled receptors and cancer. Nat. Rev. Cancer *7*, 79–94. https://doi.org/10.1038/nrc2069.

55. Neufeld, G., Mumblat, Y., Smolkin, T., Toledano, S., Nir-Zvi, I., Ziv, K., and Kessler, O. (2016). The role of the semaphorins in cancer. Cell Adhes. Migr. *10*, 652–674. https://doi.org/10.1080/19336918.2016.1197478.

56. Yan, H., Kamiya, T., Suabjakyong, P., and Tsuji, N.M. (2015). Targeting C-Type Lectin Receptors for Cancer Immunity. Front. Immunol. *6*. https://doi.org/10.3389/fimmu.2015.00408.

57. Pacini, C., Dempster, J.M., Boyle, I., Gonçalves, E., Najgebauer, H., Karakoc, E., Van Der Meer, D., Barthorpe, A., Lightfoot, H., Jaaks, P., et al. (2021). Integrated cross-study datasets of genetic dependencies in cancer. Nat. Commun. *12*, 1661. https://doi.org/10.1038/s41467-021-21898-7.

58. Nacev, B.A., Sanchez-Vega, F., Smith, S.A., Antonescu, C.R., Rosenbaum, E., Shi, H., Tang, C., Socci, N.D., Rana, S., Gularte-Mérida, R., et al. (2022). Clinical sequencing of soft tissue and bone sarcomas delineates diverse genomic landscapes and potential therapeutic targets. Nat. Commun. *13*, 3405. https://doi.org/10.1038/s41467-022-30453-x.

59. Woo, H.G., Park, E.S., Lee, J.-S., Lee, Y.-H., Ishikawa, T., Kim, Y.J., and Thorgeirsson, S.S. (2009). Identification of Potential Driver Genes in Human Liver Carcinoma by Genomewide Screening. Cancer Res. *69*, 4059–4066. https://doi.org/10.1158/0008-5472.CAN-09-0164.

60. Pollack, J.R., Sørlie, T., Perou, C.M., Rees, C.A., Jeffrey, S.S., Lonning, P.E., Tibshirani, R., Botstein, D., Børresen-Dale, A.-L., and Brown, P.O. (2002). Microarray analysis reveals a major direct role of DNA copy number alteration in the transcriptional program of human breast tumors. Proc. Natl. Acad. Sci. U. S. A. *99*, 12963–12968. https://doi.org/10.1073/pnas.162471999.

61. Wang, J., Zheng, J., Lee, E.E., Aguilar, B., Phan, J., Abdilleh, K., Taylor, R.C., Longabaugh, W., Johansson, B., Mertens, F., et al. (2023). A cloud-based resource for genome coordinate-based exploration and large-scale analysis of chromosome aberrations and gene fusions in cancer. Genes. Chromosomes Cancer *62*, 441–448. https://doi.org/10.1002/gcc.23128.

62. Kloss, C.C., Condomines, M., Cartellieri, M., Bachmann, M., and Sadelain, M. (2013). Combinatorial antigen recognition with balanced signaling promotes selective tumor eradication by engineered T cells. Nat. Biotechnol. *31*, 71–75. https://doi.org/10.1038/nbt.2459.

63. Roybal, K.T., Williams, J.Z., Morsut, L., Rupp, L.J., Kolinko, I., Choe, J.H., Walker, W.J., McNally, K.A., and Lim, W.A. (2016). Engineering T Cells with Customized Therapeutic Response Programs Using Synthetic Notch Receptors. Cell *167*, 419-432.e16. https://doi.org/10.1016/j.cell.2016.09.011.

64. Fedorov, V.D., Themeli, M., and Sadelain, M. (2013). PD-1- and CTLA-4-based inhibitory chimeric antigen receptors (iCARs) divert off-target immunotherapy responses. Sci. Transl. Med. *5*, 215ra172. https://doi.org/10.1126/scitranslmed.3006597.

2041 65. Su, C., Xu, Z., Shan, X., Cai, B., Zhao, H., and Zhang, J. (2023). Cell-type-specific co-
2042 expression inference from single cell RNA-sequencing data. Nat. Commun. *14*, 4846.
2043 https://doi.org/10.1038/s41467-023-40503-7.
2044 66. GTEx Consortium, Laboratory, Data Analysis &Coordinating Center (LDACC)—
2045 Analysis Working Group, Statistical Methods groups—Analysis Working Group,
2046 Enhancing GTEx (eGTEx) groups, NIH Common Fund, NIH/NCI, NIH/NHGRI, NIH/NIMH,
2047 NIH/NIDA, Biospecimen Collection Source Site—NDRI, et al. (2017). Genetic effects on
2048 gene expression across human tissues. Nature *550*, 204–213.
2049 https://doi.org/10.1038/nature24277.
2050 67. Kim, M.-S., Pinto, S.M., Getnet, D., Nirujogi, R.S., Manda, S.S., Chaerkady, R.,
2051 Madugundu, A.K., Kelkar, D.S., Isserlin, R., Jain, S., et al. (2014). A draft map of the
2052 human proteome. Nature *509*, 575–581. https://doi.org/10.1038/nature13302.
2053 68. Xiao, W., Mohseny, A.B., Hogendoorn, P.C.W., and Cleton-Jansen, A.-M. (2013).
2054 Mesenchymal stem cell transformation and sarcoma genesis. Clin. Sarcoma Res. *3*, 10.
2055 https://doi.org/10.1186/2045-3329-3-10.
2056 69. Ferretti, E., and Hadjantonakis, A.-K. (2019). Mesoderm specification and
2057 diversification: from single cells to emergent tissues. Curr. Opin. Cell Biol. *61*, 110–116.
2058 https://doi.org/10.1016/j.ceb.2019.07.012.
2059 70. Shekhani, M.T., Jayanthy, A.-S., Maddodi, N., and Setaluri, V. (2013). Cancer stem
2060 cells and tumor transdifferentiation: implications for novel therapeutic strategies. Am. J.
2061 Stem Cells *2*, 52–61.

2062 71. Tsherniak, A., Vazquez, F., Montgomery, P.G., Weir, B.A., Kryukov, G., Cowley, G.S.,
2063 Gill, S., Harrington, W.F., Pantel, S., Krill-Burger, J.M., et al. (2017). Defining a Cancer
2064 Dependency Map. Cell *170*, 564-576.e16. https://doi.org/10.1016/j.cell.2017.06.010.
2065 72. Yarmarkovich, M., Marshall, Q.F., Warrington, J.M., Premaratne, R., Farrel, A., Groff,
2066 D., Li, W., Di Marco, M., Runbeck, E., Truong, H., et al. (2023). Targeting of intracellular
2067 oncoproteins with peptide-centric CARs. Nature *623*, 820–827.
2068 https://doi.org/10.1038/s41586-023-06706-0.
2069 73. Gjerstorff, M.F., Andersen, M.H., and Ditzel, H.J. (2015). Oncogenic cancer/testis
2070 antigens: prime candidates for immunotherapy. Oncotarget *6*, 15772–15787.
2071 https://doi.org/10.18632/oncotarget.4694.
2072 74. Sarkizova, S., Klaeger, S., Le, P.M., Li, L.W., Oliveira, G., Keshishian, H., Hartigan,
2073 C.R., Zhang, W., Braun, D.A., Ligon, K.L., et al. (2020). A large peptidome dataset
2074 improves HLA class I epitope prediction across most of the human population. Nat.
2075 Biotechnol. *38*, 199–209. https://doi.org/10.1038/s41587-019-0322-9.
2076 75. Li, G., Iyer, B., Prasath, V.B.S., Ni, Y., and Salomonis, N. (2021). DeepImmuno: deep
2077 learning-empowered prediction and generation of immunogenic peptides for T-cell
2078 immunity. Brief. Bioinform. *22*, bbab160. https://doi.org/10.1093/bib/bbab160.
2079 76. Nielsen, M., Lundegaard, C., Blicher, T., Lamberth, K., Harndahl, M., Justesen, S.,
2080 Røder, G., Peters, B., Sette, A., Lund, O., et al. (2007). NetMHCpan, a method for
2081 quantitative predictions of peptide binding to any HLA-A and -B locus protein of known
2082 sequence. PloS One *2*, e796. https://doi.org/10.1371/journal.pone.0000796.

2083 77. Gonzalez-Galarza, F.F., McCabe, A., Santos, E.J.M.D., Jones, J., Takeshita, L., Ortega-
2084 Rivera, N.D., Cid-Pavon, G.M.D., Ramsbottom, K., Ghattaoraya, G., Alfirevic, A., et al.
2085 (2019). Allele frequency net database (AFND) 2020 update: gold-standard data
2086 classification, open access genotype data and new query tools. Nucleic Acids Res.,
2087 gkz1029. https://doi.org/10.1093/nar/gkz1029.
2088 78. Sewell, A.K. (2012). Why must T cells be cross-reactive? Nat. Rev. Immunol. *12*,
2089 669–677. https://doi.org/10.1038/nri3279.
2090 79. Kawashima, S., Pokarowski, P., Pokarowska, M., Kolinski, A., Katayama, T., and
2091 Kanehisa, M. (2007). AAindex: amino acid index database, progress report 2008. Nucleic
2092 Acids Res. *36*, D202–D205. https://doi.org/10.1093/nar/gkm998.
2093 80. Kim, Y., Sidney, J., Pinilla, C., Sette, A., and Peters, B. (2009). Derivation of an amino
2094 acid similarity matrix for peptide:MHC binding and its application as a Bayesian prior.
2095 BMC Bioinformatics *10*, 394. https://doi.org/10.1186/1471-2105-10-394.
2096 81. Antunes, D.A., Rigo, M.M., Freitas, M.V., Mendes, M.F.A., Sinigaglia, M., Lizée, G.,
2097 Kavraki, L.E., Selin, L.K., Cornberg, M., and Vieira, G.F. (2017). Interpreting T-Cell Cross-
2098 reactivity through Structure: Implications for TCR-Based Cancer Immunotherapy. Front.
2099 Immunol. *8*, 1210. https://doi.org/10.3389/fimmu.2017.01210.
2100 82. Bentzen, A.K., Such, L., Jensen, K.K., Marquard, A.M., Jessen, L.E., Miller, N.J.,
2101 Church, C.D., Lyngaa, R., Koelle, D.M., Becker, J.C., et al. (2018). T cell receptor
2102 fingerprinting enables in-depth characterization of the interactions governing recognition
2103 of peptide-MHC complexes. Nat. Biotechnol. https://doi.org/10.1038/nbt.4303.

83. Birnbaum, M.E., Mendoza, J.L., Sethi, D.K., Dong, S., Glanville, J., Dobbins, J., Ozkan, E., Davis, M.M., Wucherpfennig, K.W., and Garcia, K.C. (2014). Deconstructing the peptide-MHC specificity of T cell recognition. Cell *157*, 1073–1087. https://doi.org/10.1016/j.cell.2014.03.047.

84. Singh, N.K., Riley, T.P., Baker, S.C.B., Borrman, T., Weng, Z., and Baker, B.M. (2017). Emerging Concepts in TCR Specificity: Rationalizing and (Maybe) Predicting Outcomes. J. Immunol. *199*, 2203–2213. https://doi.org/10.4049/jimmunol.1700744.

85. Tagliamonte, M., Cavalluzzo, B., Mauriello, A., Ragone, C., Buonaguro, F.M., Tornesello, M.L., and Buonaguro, L. (2023). Molecular mimicry and cancer vaccine development. Mol. Cancer *22*, 75. https://doi.org/10.1186/s12943-023-01776-0.

86. Linette, G.P., Stadtmauer, E.A., Maus, M.V., Rapoport, A.P., Levine, B.L., Emery, L., Litzky, L., Bagg, A., Carreno, B.M., Cimino, P.J., et al. (2013). Cardiovascular toxicity and titin cross-reactivity of affinity-enhanced T cells in myeloma and melanoma. Blood *122*, 863–871. https://doi.org/10.1182/blood-2013-03-490565.

87. Morgan, R.A., Chinnasamy, N., Abate-Daga, D., Gros, A., Robbins, P.F., Zheng, Z., Dudley, M.E., Feldman, S.A., Yang, J.C., Sherry, R.M., et al. (2013). Cancer regression and neurological toxicity following anti-MAGE-A3 TCR gene therapy. J. Immunother. Hagerstown Md 1997 *36*, 133–151. https://doi.org/10.1097/CJI.0b013e3182829903.

88. Xie, N., Shen, G., Gao, W., Huang, Z., Huang, C., and Fu, L. (2023). Neoantigens: promising targets for cancer therapy. Signal Transduct. Target. Ther. *8*, 9. https://doi.org/10.1038/s41392-022-01270-x.

89. Jiang, W., and Boder, E.T. (2010). High-throughput engineering and analysis of peptide binding to class II MHC. Proc. Natl. Acad. Sci. U. S. A. *107*, 13258–13263. https://doi.org/10.1073/pnas.1006344107.

90. Liu, R., Jiang, W., and Mellins, E.D. (2021). Yeast display of MHC-II enables rapid identification of peptide ligands from protein antigens (RIPPA). Cell. Mol. Immunol. *18*, 1847–1860. https://doi.org/10.1038/s41423-021-00717-5.

91. Tang, S., Wang, Y., Luo, R., Fang, R., Liu, Y., Xiang, H., Ran, P., Tong, Y., Sun, M., Tan, S., et al. (2024). Proteomic characterization identifies clinically relevant subgroups of soft tissue sarcoma. Nat. Commun. *15*, 1381. https://doi.org/10.1038/s41467-024-45306-y.

92. Burns, J., Wilding, C.P., Krasny, L., Zhu, X., Chadha, M., Tam, Y.B., Ps, H., Mahalingam, A.H., Lee, A.T.J., Arthur, A., et al. (2023). The proteomic landscape of soft tissue sarcomas. Nat. Commun. *14*, 3834. https://doi.org/10.1038/s41467-023-39486-2.

93. Barretina, J., Caponigro, G., Stransky, N., Venkatesan, K., Margolin, A.A., Kim, S., Wilson, C.J., Lehár, J., Kryukov, G.V., Sonkin, D., et al. (2012). The Cancer Cell Line Encyclopedia enables predictive modelling of anticancer drug sensitivity. Nature *483*, 603–607. https://doi.org/10.1038/nature11003.

94. Gonçalves, E., Poulos, R.C., Cai, Z., Barthorpe, S., Manda, S.S., Lucas, N., Beck, A., Bucio-Noble, D., Dausmann, M., Hall, C., et al. (2022). Pan-cancer proteomic map of 949 human cell lines. Cancer Cell *40*, 835-849.e8. https://doi.org/10.1016/j.ccell.2022.06.010.

95. Majzner, R.G., Theruvath, J.L., Nellan, A., Heitzeneder, S., Cui, Y., Mount, C.W., Rietberg, S.P., Linde, M.H., Xu, P., Rota, C., et al. (2019). CAR T Cells Targeting B7-H3, a Pan-Cancer Antigen, Demonstrate Potent Preclinical Activity Against Pediatric Solid Tumors and Brain Tumors. Clin. Cancer Res. *25*, 2560–2574. https://doi.org/10.1158/1078-0432.CCR-18-0432.

96. Yoshida, K., Poon, V., Dash, A., Kunder, R., Chinn, L., and Kågedal, M. (2024). Simulation-based evaluation of personalized dosing approaches for ANTI-FGFR / KLB bispecific antibody fazpilodemab. CPT Pharmacomet. Syst. Pharmacol. *13*, 544–550. https://doi.org/10.1002/psp4.13111.

97. Vahdat, L.T., Schmid, P., Forero-Torres, A., Blackwell, K., Telli, M.L., Melisko, M., Möbus, V., Cortes, J., Montero, A.J., Ma, C., et al. (2021). Glembatumumab vedotin for patients with metastatic, gpNMB overexpressing, triple-negative breast cancer (“METRIC”): a randomized multicenter study. Npj Breast Cancer *7*, 57. https://doi.org/10.1038/s41523-021-00244-6.

98. Meininger, V., Genge, A., Van Den Berg, L.H., Robberecht, W., Ludolph, A., Chio, A., Kim, S.H., Leigh, P.N., Kiernan, M.C., Shefner, J.M., et al. (2017). Safety and efficacy of ozanezumab in patients with amyotrophic lateral sclerosis: a randomised, double-blind, placebo-controlled, phase 2 trial. Lancet Neurol. *16*, 208–216. https://doi.org/10.1016/S1474-4422(16)30399-4.

99. Wang, X., Qi, L., Chen, M., Zhang, Y., Gao, X., and Cai, Y. (2024). Feasibility study of ADCs targeting TROP-2, HER2, and CD46 in Ductal Adenocarcinoma and Intraductal

2167 Carcinoma of the prostate. World J. Urol. *42*, 404. https://doi.org/10.1007/s00345-024-
2168 05109-8.
2169 100. Rafiq, S., Hackett, C.S., and Brentjens, R.J. (2020). Engineering strategies to
2170 overcome the current roadblocks in CAR T cell therapy. Nat. Rev. Clin. Oncol. *17*, 147–
2171 167. https://doi.org/10.1038/s41571-019-0297-y.
2172 101. Rodriguez-Garcia, A., Palazon, A., Noguera-Ortega, E., Powell, D.J., and Guedan, S.
2173 (2020). CAR-T Cells Hit the Tumor Microenvironment: Strategies to Overcome Tumor
2174 Escape. Front. Immunol. *11*, 1109. https://doi.org/10.3389/fimmu.2020.01109.
2175 102. Parker, K.R., Migliorini, D., Perkey, E., Yost, K.E., Bhaduri, A., Bagga, P., Haris, M.,
2176 Wilson, N.E., Liu, F., Gabunia, K., et al. (2020). Single-Cell Analyses Identify Brain Mural
2177 Cells Expressing CD19 as Potential Off-Tumor Targets for CAR-T Immunotherapies. Cell
2178 *183*, 126-142.e17. https://doi.org/10.1016/j.cell.2020.08.022.
2179 103. Jing, Y., Liu, Y., Li, Q., Ye, Y., Diao, L., Huang, Y., Zhou, Y., Green, M.R., Mills, G.B., and
2180 Han, L. (2021). Expression of chimeric antigen receptor therapy targets detected by
2181 single-cell sequencing of normal cells may contribute to off-tumor toxicity. Cancer Cell
2182 *39*, 1558–1559. https://doi.org/10.1016/j.ccell.2021.09.016.
2183 104. Lee, A.T.J., Thway, K., Huang, P.H., and Jones, R.L. (2018). Clinical and Molecular
2184 Spectrum of Liposarcoma. J. Clin. Oncol. *36*, 151–159.
2185 https://doi.org/10.1200/JCO.2017.74.9598.
2186 105. Cassinelli, G., Zaffaroni, N., and Lanzi, C. (2016). The heparanase/heparan sulfate
2187 proteoglycan axis: A potential new therapeutic target in sarcomas. Cancer Lett. *382*,
2188 245–254. https://doi.org/10.1016/j.canlet.2016.09.004.

106. Wu, Z., Zhang, X., An, Y., Ma, K., Xue, R., Ye, G., Du, J., Chen, Z., Zhu, Z., Shi, G., et al. (2023). CLMP is a tumor suppressor that determines all-trans retinoic acid response in colorectal cancer. Dev. Cell *58*, 2684-2699.e6. https://doi.org/10.1016/j.devcel.2023.10.006.

107. Limoni, G., and Niquille, M. (2021). Semaphorins and Plexins in central nervous system patterning: the key to it all? Curr. Opin. Neurobiol. *66*, 224–232. https://doi.org/10.1016/j.conb.2020.12.014.

108. Worzfeld, T., and Offermanns, S. (2014). Semaphorins and plexins as therapeutic targets. Nat. Rev. Drug Discov. *13*, 603–621. https://doi.org/10.1038/nrd4337.

109. Gounder, M., Ratan, R., Alcindor, T., Schöffski, P., van der Graaf, W.T., Wilky, B.A., Riedel, R.F., Lim, A., Smith, L.M., Moody, S., et al. (2023). Nirogacestat, a γ-Secretase Inhibitor for Desmoid Tumors. N. Engl. J. Med. *388*, 898–912. https://doi.org/10.1056/NEJMoa2210140.

110. Mir, O., Azaro, A., Merchan, J., Chugh, R., Trent, J., Rodon, J., Ohnmacht, U., Diener, J.T., Smith, C., Yuen, E., et al. (2018). Notch pathway inhibition with LY3039478 in soft tissue sarcoma and gastrointestinal stromal tumours. Eur. J. Cancer Oxf. Engl. 1990 *103*, 88–97. https://doi.org/10.1016/j.ejca.2018.08.012.

111. Hadjimichael, A.C., Pergaris, A., Kaspiris, A., Foukas, A.F., Kokkali, S., Tsourouflis, G., and Theocharis, S. (2022). The EPH/Ephrin System in Bone and Soft Tissue Sarcomas' Pathogenesis and Therapy: New Advancements and a Literature Review. Int. J. Mol. Sci. *23*, 5171. https://doi.org/10.3390/ijms23095171.

2210 112. Kania, A., and Klein, R. (2016). Mechanisms of ephrin–Eph signalling in
2211 development, physiology and disease. Nat. Rev. Mol. Cell Biol. *17*, 240–256.
2212 https://doi.org/10.1038/nrm.2015.16.
2213 113. Martinez-Font, E., Pérez-Capó, M., Vögler, O., Martín-Broto, J., Alemany, R., and
2214 Obrador-Hevia, A. (2021). WNT/β-Catenin Pathway in Soft Tissue Sarcomas: New
2215 Therapeutic Opportunities? Cancers *13*, 5521.
2216 https://doi.org/10.3390/cancers13215521.
2217 114. Rodriguez-Garcia, A., Lynn, R.C., Poussin, M., Eiva, M.A., Shaw, L.C., O'Connor, R.S.,
2218 Minutolo, N.G., Casado-Medrano, V., Lopez, G., Matsuyama, T., et al. (2021). CAR-T cell-
2219 mediated depletion of immunosuppressive tumor-associated macrophages promotes
2220 endogenous antitumor immunity and augments adoptive immunotherapy. Nat.
2221 Commun. *12*, 877. https://doi.org/10.1038/s41467-021-20893-2.
2222 115. Ash, S.L., Orha, R., Mole, H., Dinesh-Kumar, M., Lee, S.P., Turrell, F.K., and Isacke,
2223 C.M. (2024). Targeting the activated microenvironment with endosialin (CD248)-directed
2224 CAR-T cells ablates perivascular cells to impair tumor growth and metastasis. J.
2225 Immunother. Cancer *12*, e008608. https://doi.org/10.1136/jitc-2023-008608.
2226 116. Wei, R., Dean, D.C., Thanindratarn, P., Hornicek, F.J., Guo, W., and Duan, Z. (2020).
2227 Cancer testis antigens in sarcoma: Expression, function and immunotherapeutic
2228 application. Cancer Lett. *479*, 54–60. https://doi.org/10.1016/j.canlet.2019.10.024.
2229 117. Fonseca, A.F., and Antunes, D.A. (2023). CrossDome: an interactive R package to
2230 predict cross-reactivity risk using immunopeptidomics databases. Front. Immunol. *14*,
2231 1142573. https://doi.org/10.3389/fimmu.2023.1142573.

118. Squair, J.W., Gautier, M., Kathe, C., Anderson, M.A., James, N.D., Hutson, T.H., Hudelle, R., Qaiser, T., Matson, K.J.E., Barraud, Q., et al. (2021). Confronting false discoveries in single-cell differential expression. Nat. Commun. *12*, 5692. https://doi.org/10.1038/s41467-021-25960-2.

119. R Core Team (2023). R: A Language and Environment for Statistical Computing. R Foundation for Statistical Computing, Vienna, Austria.

120. Hao, Y., Hao, S., Andersen-Nissen, E., Mauck, W.M., Zheng, S., Butler, A., Lee, M.J., Wilk, A.J., Darby, C., Zager, M., et al. (2021). Integrated analysis of multimodal single-cell data. Cell *184*, 3573-3587.e29. https://doi.org/10.1016/j.cell.2021.04.048.

121. McGinnis, C.S., Murrow, L.M., and Gartner, Z.J. (2019). DoubletFinder: Doublet Detection in Single-Cell RNA Sequencing Data Using Artificial Nearest Neighbors. Cell Syst. *8*, 329-337.e4. https://doi.org/10.1016/j.cels.2019.03.003.

122. Korsunsky, I., Millard, N., Fan, J., Slowikowski, K., Zhang, F., Wei, K., Baglaenko, Y., Brenner, M., Loh, P., and Raychaudhuri, S. (2019). Fast, sensitive and accurate integration of single-cell data with Harmony. Nat. Methods *16*, 1289–1296. https://doi.org/10.1038/s41592-019-0619-0.

123. Samuel Marsh, Maëlle Salmon, and Paul Hoffman (2024). samuel-marsh/scCustomize: Version 2.1.2. Version v2.1.2 (Zenodo). https://doi.org/10.5281/ZENODO.5706430 https://doi.org/10.5281/ZENODO.5706430.

124. Alquicira-Hernandez, J., and Powell, J.E. (2021). Nebulosa recovers single-cell gene expression signals by kernel density estimation. Bioinforma. Oxf. Engl. *37*, 2485–2487. https://doi.org/10.1093/bioinformatics/btab003.

125. Aran, D., Looney, A.P., Liu, L., Wu, E., Fong, V., Hsu, A., Chak, S., Naikawadi, R.P., Wolters, P.J., Abate, A.R., et al. (2019). Reference-based analysis of lung single-cell sequencing reveals a transitional profibrotic macrophage. Nat. Immunol. *20*, 163–172. https://doi.org/10.1038/s41590-018-0276-y.

126. The ENCODE Project Consortium (2012). An integrated encyclopedia of DNA elements in the human genome. Nature *489*, 57–74. https://doi.org/10.1038/nature11247.

127. Stunnenberg, H.G., International Human Epigenome Consortium, and Hirst, M. (2016). The International Human Epigenome Consortium: A Blueprint for Scientific Collaboration and Discovery. Cell *167*, 1145–1149. https://doi.org/10.1016/j.cell.2016.11.007.

128. Baron, M., Veres, A., Wolock, S.L., Faust, A.L., Gaujoux, R., Vetere, A., Ryu, J.H., Wagner, B.K., Shen-Orr, S.S., Klein, A.M., et al. (2016). A Single-Cell Transcriptomic Map of the Human and Mouse Pancreas Reveals Inter- and Intra-cell Population Structure. Cell Syst. *3*, 346-360.e4. https://doi.org/10.1016/j.cels.2016.08.011.

129. Robinson, M.D., McCarthy, D.J., and Smyth, G.K. (2010). edgeR : a Bioconductor package for differential expression analysis of digital gene expression data. Bioinformatics *26*, 139–140. https://doi.org/10.1093/bioinformatics/btp616.

130. Amezquita, R.A., Lun, A.T.L., Becht, E., Carey, V.J., Carpp, L.N., Geistlinger, L., Marini, F., Rue-Albrecht, K., Risso, D., Soneson, C., et al. (2020). Orchestrating single-cell analysis with Bioconductor. Nat. Methods *17*, 137–145. https://doi.org/10.1038/s41592-019-0654-x.

131. McCarthy, D.J., Campbell, K.R., Lun, A.T.L., and Wills, Q.F. (2017). Scater: pre-processing, quality control, normalization and visualization of single-cell RNA-seq data in R. Bioinformatics *33*, 1179–1186. https://doi.org/10.1093/bioinformatics/btw777.

132. Bausch-Fluck, D., Goldmann, U., Müller, S., Van Oostrum, M., Müller, M., Schubert, O.T., and Wollscheid, B. (2018). The in silico human surfaceome. Proc. Natl. Acad. Sci. *115*. https://doi.org/10.1073/pnas.1808790115.

133. Jiang, L., Wang, M., Lin, S., Jian, R., Li, X., Chan, J., Dong, G., Fang, H., Robinson, A.E., Snyder, M.P., et al. (2020). A Quantitative Proteome Map of the Human Body. Cell *183*, 269-283.e19. https://doi.org/10.1016/j.cell.2020.08.036.

134. Adam Mark, R.T. (2017). mygene. (Bioconductor). https://doi.org/10.18129/B9.BIOC.MYGENE https://doi.org/10.18129/B9.BIOC.MYGENE.

135. Wu, T., Hu, E., Xu, S., Chen, M., Guo, P., Dai, Z., Feng, T., Zhou, L., Tang, W., Zhan, L., et al. (2021). clusterProfiler 4.0: A universal enrichment tool for interpreting omics data. Innov. Camb. Mass *2*, 100141. https://doi.org/10.1016/j.xinn.2021.100141.

136. Yu, G., and He, Q.-Y. (2016). ReactomePA: an R/Bioconductor package for reactome pathway analysis and visualization. Mol. Biosyst. *12*, 477–479. https://doi.org/10.1039/C5MB00663E.

137. Yu, G., Wang, L.-G., Han, Y., and He, Q.-Y. (2012). clusterProfiler: an R Package for Comparing Biological Themes Among Gene Clusters. OMICS J. Integr. Biol. *16*, 284–287. https://doi.org/10.1089/omi.2011.0118.

138. Carlson M (2019). org.Hs.eg.db: Genome wide annotation for Human. R package version 3.8.2.

139. The Cancer Genome Atlas Research Network, Weinstein, J.N., Collisson, E.A., Mills, G.B., Shaw, K.R.M., Ozenberger, B.A., Ellrott, K., Shmulevich, I., Sander, C., and Stuart, J.M. (2013). The Cancer Genome Atlas Pan-Cancer analysis project. Nat. Genet. *45*, 1113–1120. https://doi.org/10.1038/ng.2764.

140. Cerami, E., Gao, J., Dogrusoz, U., Gross, B.E., Sumer, S.O., Aksoy, B.A., Jacobsen, A., Byrne, C.J., Heuer, M.L., Larsson, E., et al. (2012). The cBio cancer genomics portal: an open platform for exploring multidimensional cancer genomics data. Cancer Discov. *2*, 401–404. https://doi.org/10.1158/2159-8290.CD-12-0095.

141. Gao, J., Aksoy, B.A., Dogrusoz, U., Dresdner, G., Gross, B., Sumer, S.O., Sun, Y., Jacobsen, A., Sinha, R., Larsson, E., et al. (2013). Integrative analysis of complex cancer genomics and clinical profiles using the cBioPortal. Sci. Signal. *6*, pl1. https://doi.org/10.1126/scisignal.2004088.

142. Gao, Q., Liang, W.-W., Foltz, S.M., Mutharasu, G., Jayasinghe, R.G., Cao, S., Liao, W.-W., Reynolds, S.M., Wyczalkowski, M.A., Yao, L., et al. (2018). Driver Fusions and Their Implications in the Development and Treatment of Human Cancers. Cell Rep. *23*, 227-238.e3. https://doi.org/10.1016/j.celrep.2018.03.050.

143. Mertens F, Mitelman Database of Chromosome Aberrations and Gene Fusions in Cancer (2024). Mitelman F, Johansson B and Mertens F (Eds.), https://mitelmandatabase.isb-cgc.org.

144. Karlsson, M., Zhang, C., Méar, L., Zhong, W., Digre, A., Katona, B., Sjöstedt, E., Butler, L., Odeberg, J., Dusart, P., et al. (2021). A single–cell type transcriptomics map of human tissues. Sci. Adv. *7*, eabh2169. https://doi.org/10.1126/sciadv.abh2169.

145. Wells, D.A., and McAuley, M. (2023). HLAfreq: Download and combine HLA allele frequency data. Preprint, https://doi.org/10.1101/2023.09.15.557761 https://doi.org/10.1101/2023.09.15.557761.

146. The UniProt Consortium, Bateman, A., Martin, M.-J., Orchard, S., Magrane, M., Ahmad, S., Alpi, E., Bowler-Barnett, E.H., Britto, R., Bye-A-Jee, H., et al. (2023). UniProt: the Universal Protein Knowledgebase in 2023. Nucleic Acids Res. *51*, D523–D531. https://doi.org/10.1093/nar/gkac1052.

147. Vita, R., Mahajan, S., Overton, J.A., Dhanda, S.K., Martini, S., Cantrell, J.R., Wheeler, D.K., Sette, A., and Peters, B. (2019). The Immune Epitope Database (IEDB): 2018 update. Nucleic Acids Res. *47*, D339–D343. https://doi.org/10.1093/nar/gky1006.

148. Huang, X., Gan, Z., Cui, H., Lan, T., Liu, Y., Caron, E., and Shao, W. (2024). The SysteMHC Atlas v2.0, an updated resource for mass spectrometry-based immunopeptidomics. Nucleic Acids Res. *52*, D1062–D1071. https://doi.org/10.1093/nar/gkad1068.

149. Marcu, A., Bichmann, L., Kuchenbecker, L., Kowalewski, D.J., Freudenmann, L.K., Backert, L., Mühlenbruch, L., Szolek, A., Lübke, M., Wagner, P., et al. (2021). HLA Ligand Atlas: a benign reference of HLA-presented peptides to improve T-cell-based cancer immunotherapy. J. Immunother. Cancer *9*, e002071. https://doi.org/10.1136/jitc-2020-002071.

150. O'Donnell, T.J., Rubinsteyn, A., and Laserson, U. (2020). MHCflurry 2.0: Improved Pan-Allele Prediction of MHC Class I-Presented Peptides by Incorporating Antigen Processing. Cell Syst. *11*, 42-48.e7. https://doi.org/10.1016/j.cels.2020.06.010.

151. McFerrin L (2013). HDMD: Statistical Analysis Tools for High Dimension Molecular Data (HDMD).

152. Amerifar S (2021). ftrCOOL: Feature Extraction from Biological Sequences. Version version 2.0.0.

153. Liao, Y., Savage, S.R., Dou, Y., Shi, Z., Yi, X., Jiang, W., Lei, J.T., and Zhang, B. (2023). A proteogenomics data-driven knowledge base of human cancer. Cell Syst. *14*, 777-787.e5. https://doi.org/10.1016/j.cels.2023.07.007.

154. Thangudu, R.R., Rudnick, P.A., Holck, M., Singhal, D., MacCoss, M.J., Edwards, N.J., Ketchum, K.A., Kinsinger, C.R., Kim, E., and Basu, A. (2020). Abstract LB-242: Proteomic Data Commons: A resource for proteogenomic analysis. Cancer Res. *80*, LB-242-LB-242. https://doi.org/10.1158/1538-7445.AM2020-LB-242.

155. Sinha, A., Huang, V., Livingstone, J., Wang, J., Fox, N.S., Kurganovs, N., Ignatchenko, V., Fritsch, K., Donmez, N., Heisler, L.E., et al. (2019). The Proteogenomic Landscape of Curable Prostate Cancer. Cancer Cell *35*, 414-427.e6. https://doi.org/10.1016/j.ccell.2019.02.005.

156. Liu, W., Xie, L., He, Y.-H., Wu, Z.-Y., Liu, L.-X., Bai, X.-F., Deng, D.-X., Xu, X.-E., Liao, L.-D., Lin, W., et al. (2021). Large-scale and high-resolution mass spectrometry-based proteomics profiling defines molecular subtypes of esophageal cancer for therapeutic targeting. Nat. Commun. *12*, 4961. https://doi.org/10.1038/s41467-021-25202-5.

157. Beck, L., Harel, M., Yu, S., Markovits, E., Boursi, B., Markel, G., and Geiger, T. (2021). Clinical Proteomics of Metastatic Melanoma Reveals Profiles of Organ Specificity and

Treatment Resistance. Clin. Cancer Res. *27*, 2074–2086. https://doi.org/10.1158/1078-0432.CCR-20-3752.

158. Groeneveld, C.S., Sanchez-Quiles, V., Dufour, F., Shi, M., Dingli, F., Nicolle, R., Chapeaublanc, E., Poullet, P., Jeffery, D., Krucker, C., et al. (2024). Proteogenomic Characterization of Bladder Cancer Reveals Sensitivity to Apoptosis Induced by Tumor Necrosis Factor–related Apoptosis-inducing Ligand in FGFR3-mutated Tumors. Eur. Urol. *85*, 483–494. https://doi.org/10.1016/j.eururo.2023.05.037.

159. Boder, E.T., and Wittrup, K.D. (1997). Yeast surface display for screening combinatorial polypeptide libraries. Nat. Biotechnol. *15*, 553–557. https://doi.org/10.1038/nbt0697-553.

160. Raybould, M.I.J., Marks, C., Lewis, A.P., Shi, J., Bujotzek, A., Taddese, B., and Deane, C.M. (2020). Thera-SAbDab: the Therapeutic Structural Antibody Database. Nucleic Acids Res. *48*, D383–D388. https://doi.org/10.1093/nar/gkz827.

Figures

A

Single Cell Analysis Network for Adoptive Cellular therapy Targets (SCAN-ACT)

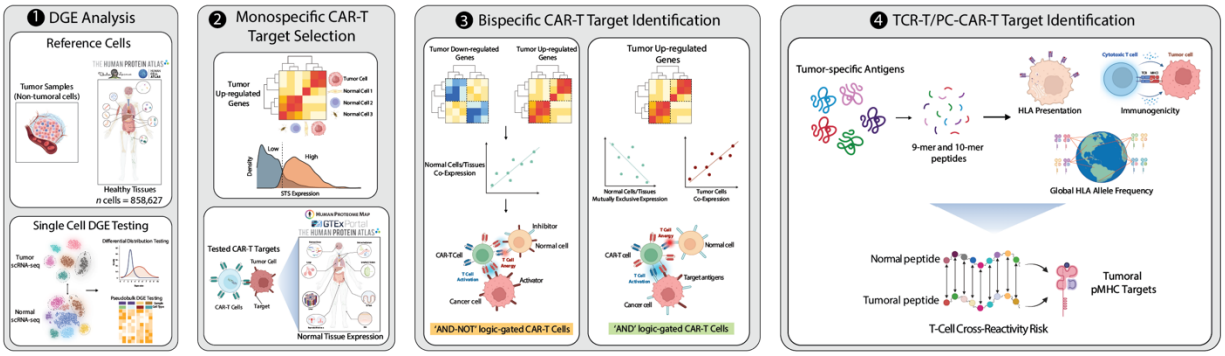

B

STS scRNA-seq Cohort Features

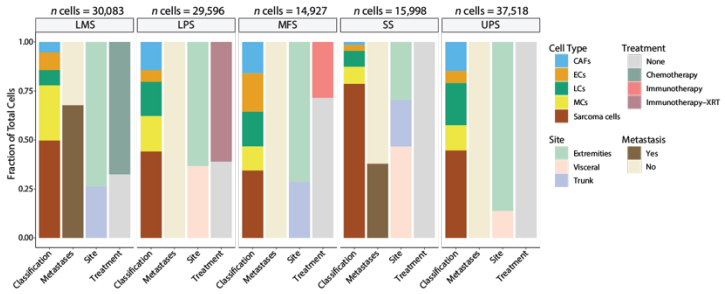

C

Differentially Expressed Genes in STS vs Other Cells in TME

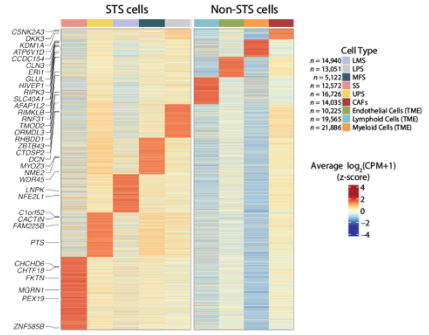

D

Differentially Expressed Genes in STS vs Normal Cells in HPA–TS–HCA

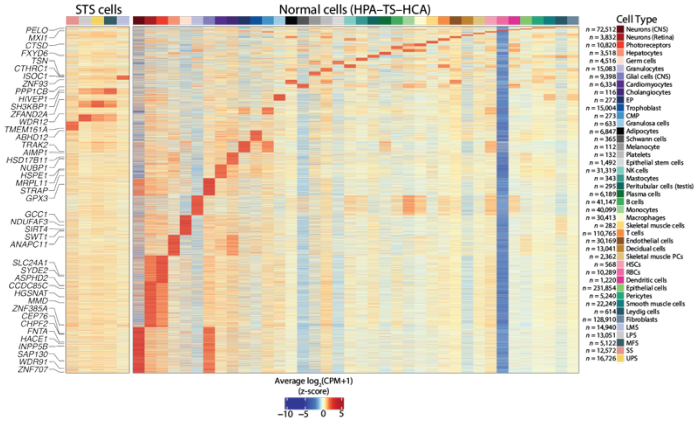

E

STS Up-regulated Genes (Total Genes)

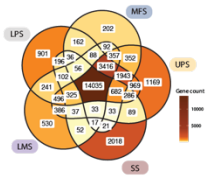

STS Down-regulated Genes (Total Genes)

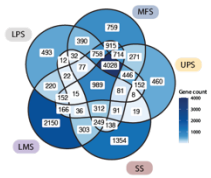

F

Differentially Expressed Genes (STS vs non-tumoral cells in TME)

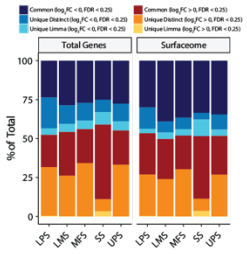

G

MMP14 – UPS vs Normal Cell Clusters in HPA-TS-HCA

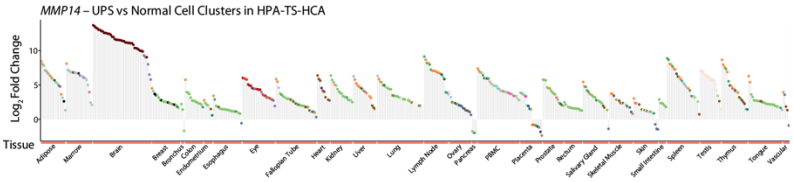

FAP – UPS vs Normal Cell Clusters in HPA-TS-HCA

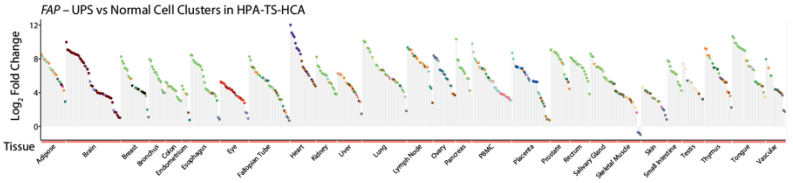

Cell type

- Adipocytes
- B cells
- Cardiomyocytes
- Cholangiocytes
- CMPs (marrow)
- Decidual cells
- Dendritic cells
- Endothelial cells
- Epithelial cells
- Epithelial stem cells
- EPCs (marrow)
- Fibroblasts
- Germ cells
- Glial cells
- Granulocytes
- Granulosa cells
- HSCs
- Hepatocytes
- Leydig cells
- Macrophages
- Mastocytes
- Melanocytes
- Monocytes
- Neurons (CNS)
- NK cells
- Pericytes
- Photoreceptors
- Plasma cells
- Platelets
- RBCs
- Retinal neurons
- Schwann cells
- Skeletal muscle cells
- Skeletal muscle PCs
- Smooth muscle cells
- T cells
- Trophoblast

H

FAP IHC - UPS

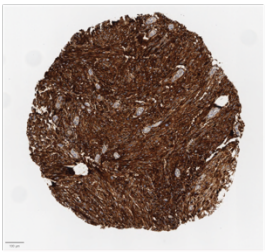

Figure 1. scRNA-seq for cellular therapy target identification.

(A). Flow diagram showing the full SCAN-ACT pipeline. Stacked bar charts showing the fraction of cells identified as tumoral, endothelial, myeloid, lymphoid, or CAFs, sample site of origin, prior treatment, and metastatic or primary tumors. (C, D) Heatmaps showing average RNA expression in STS versus non-tumoral cells in the TME (C) and normal cells in the HPA, TS, and HCA (D). RNA expression (log2(CPM+1)) was averaged and median-centered across cell types, and z-scored across genes. The number of cells analyzed is shown in the legend. Only genes differentially expressed in each STS and measured in all samples are shown. (E) Venn diagrams showing the number of STS up-regulated and down-regulated genes shared between histotypes. (F) Stacked bar chart showing the fraction of DEGs in STS versus non-tumoral cells in the TME, identified with Limma-voom, distinct, or both methods, considering surfaceome and total genes separately. (G) Lollipop plots showing the log2FC in expression for MMP14 and FAP between UPS cells and the normal cell clusters in the HPA, TS, and HCA using Limma-voom. Only statistically significant comparisons are shown (FDR < 0.25). (H) FAP IHC expression on tissue microarrays of UPS samples. CAFs: cancer associated fibroblasts; ECs: endothelial cells; LCs: lymphoid cells; MCs: myeloid cells; Mφ: Macrophages.

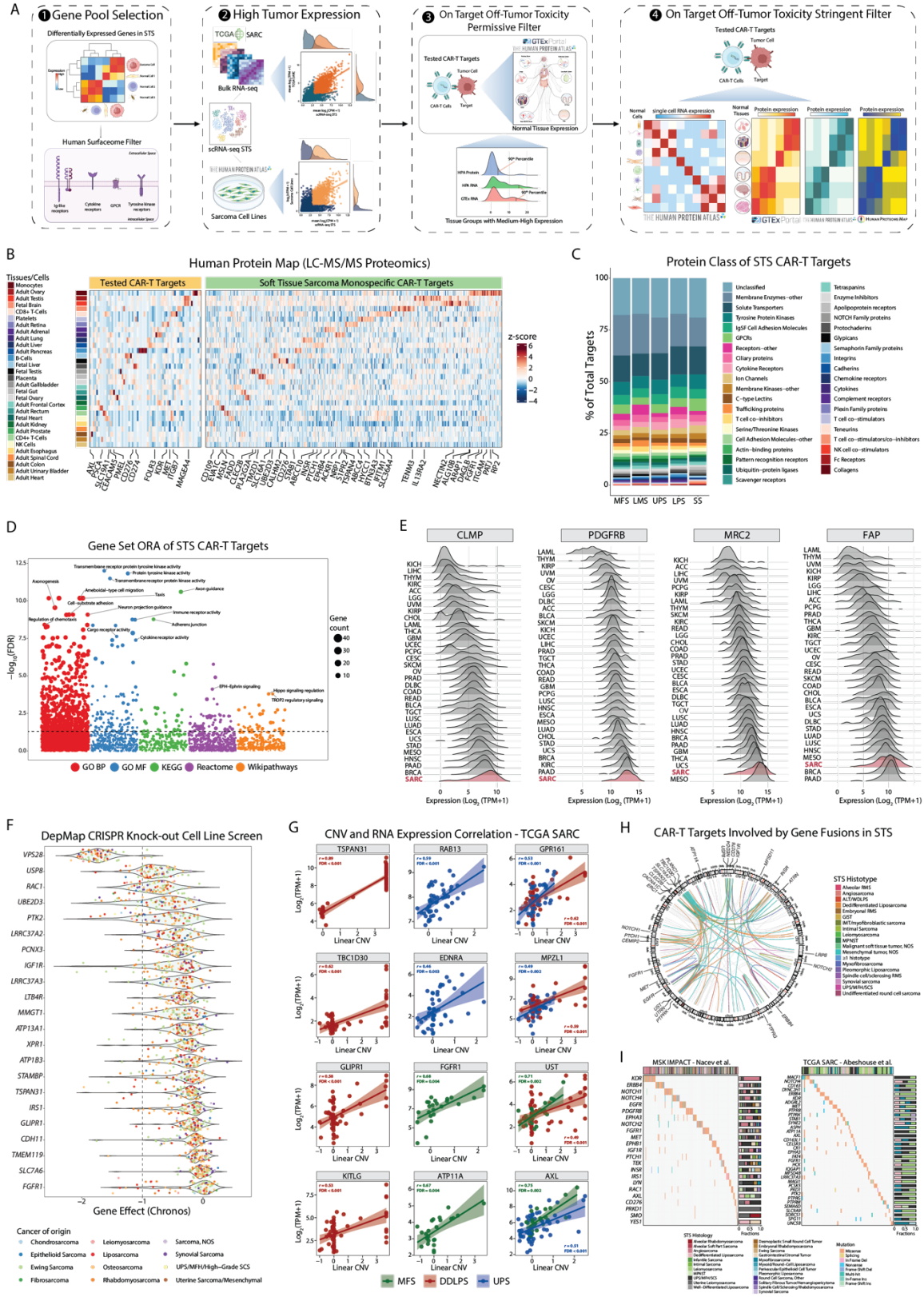
A
1 Gene Pool Selection
Differentially Expressed Genes in STS
Human Surfaceome Filter
2 High Tumor Expression
TCGA SARC
Bulk RNA-seq
scRNA-seq STS
Sarcoma Cell Lines
3 On Target Off-Tumor Toxicity Permissive Filter
Tested CAR-T Targets
Normal Tissue Expression
Tissue Groups with Medium-High Expression
4 On Target Off-Tumor Toxicity Stringent Filter
Tested CAR-T Targets
B
Human Protein Map (LC-MS/MS Proteomics)
Tissues/Cells
Tested CAR-T Targets
Soft Tissue Sarcoma Monospecific CAR-T Targets
z-score
C
Protein Class of STS CAR-T Targets
% of Total Targets
MFS LMS UPS LPS SS
D
Gene Set ORA of STS CAR-T Targets
GO BP GO MF KEGG Reactome Wikipathways
E
CLMP
PDGFRB
MRC2
FAP
Expression (Log2 (TPM+1))
F
DepMap CRISPR Knock-out Cell Line Screen
Gene Effect (Chronos)
Cancer of origin
G
CNV and RNA Expression Correlation - TCGA SARC
TSPAN31
RAB13
GPR161
TBC1D30
EDNRA
MPZL1
GLIPR1
FGFR1
UST
KITLG
ATP11A
AXL
Linear CNV
MFS DDLPS UPS
H
CAR-T Targets Involved by Gene Fusions in STS
STS Histotype
I
MSK IMPACT - Nacev et al.
TCGA SARC - Abeshouse et al.
STS Histology
Mutation

Figure 2. Monospecific CAR-T cell targets in STS.

(A) Diagram showing discovery pipeline for monospecific STS CAR-T targets. (B) Heatmap showing the protein expression in normal tissues and cells or tissue groups for CAR-T targets tested in humans (left panel) and for the STS targets (right panel) in the HPM dataset. (C) Bar chart showing the proportion of STS CAR-T targets for each protein class/family. (D) Scatter plot showing gene set ORA on the 449 CAR-T targets, using the gene ontology (GO) molecular function (MF) and biological process (BP), as well as the KEGG, Reactome, and WikiPathways terms. The x-axis shows the –log10(FDR) while the dots size indicates the number of targets per gene set. The horizontal line intersects at the significance threshold (FDR = 0.05). (E) Ridge plots showing RNA expression (log2(TPM+1)) in the Pan-Cancer TCGA Atlas for STS CAR-T targets. STS samples (SARC) are highlighted in bold red. (F) Violin plots showing the effect of CAR-T targets KO on sarcoma cell line growth from DepMap, quantified using the Chronos algorithm. Negative values indicate genes essential for cell growth. The vertical line indicates the median Chronos value for known essential genes (–1). Dots are colored based on the cell line cancer of origin. (G) Pearson correlation between linear CNV level and RNA expression in TCGA SARC for monospecific CAR-T targets. P-values were adjusted using the BH method setting significance to FDR < 0.01. (H) Circos plot showing gene fusions involving a CAR-T target in STS from the Mitelman database, MSK-IMPACT, and TCGA SARC. Colored links show fusions for the top 30 most recurrently fused genes, with link colors indicating the STS histotype. (I) Oncoplots showing recurring SNVs/Indels for monospecific CAR-T targets in MSK-IMPACT (left) and TCGA SARC (right). ALT: Atypical Lipomatous Tumor; GIST: Gastrointestinal Stromal Tumor; MPNST: Malignant Peripheral Nerve Sheath Tumor; IMT: Inflammatory Myofibroblastic Tumor; MFH: Malignant Fibrous Histiocytoma; SCS: High-grade Spindle Cell Sarcoma.

2395

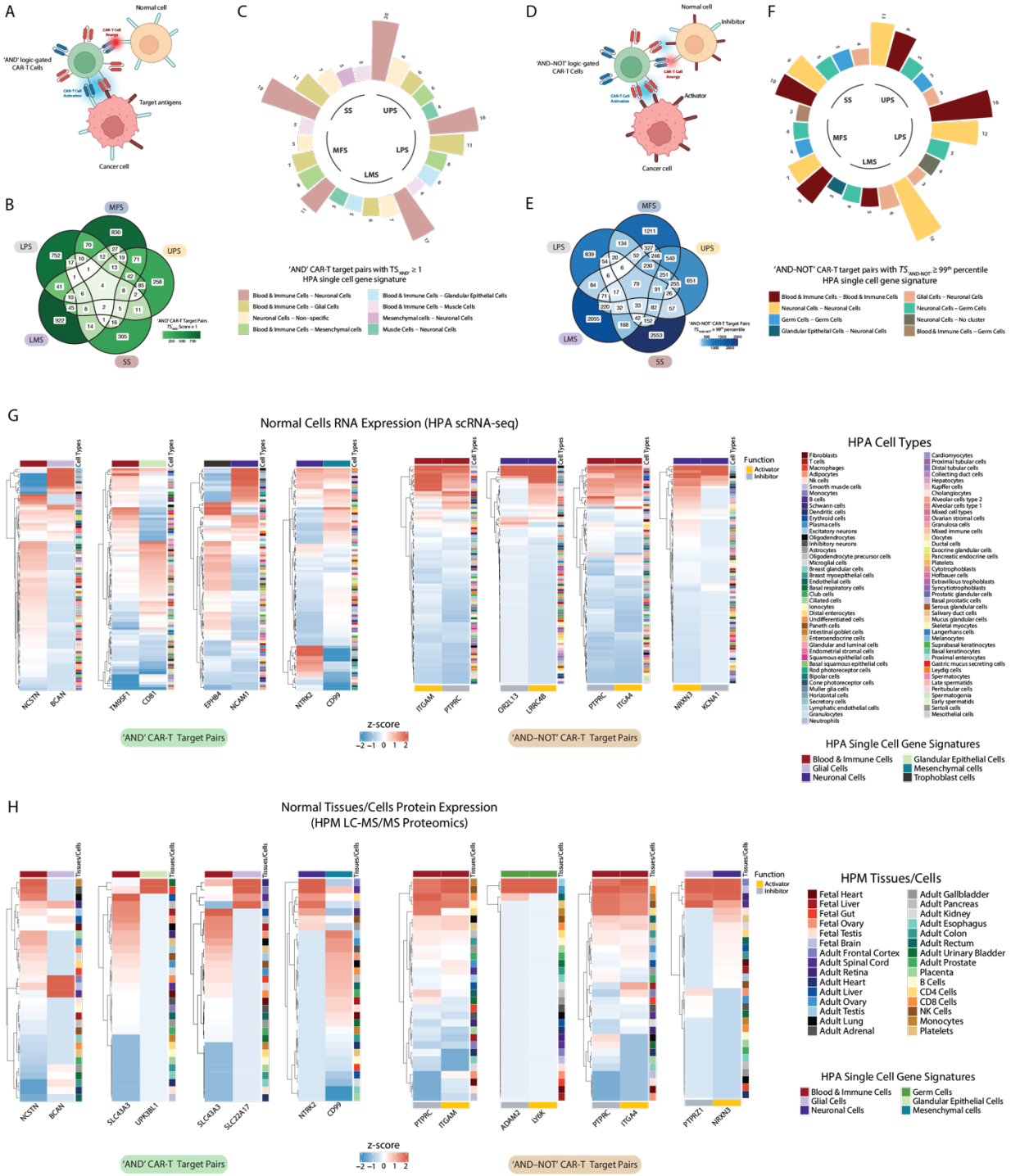
A
Normal cell
'AND' logic-gated CAR-T Cells
Target antigens
Cancer cell
B
MFS
UPS
LPS
LMS
SS
C
'AND' CAR-T target pairs with TS AND ≥ 1
HPA single cell gene signature
Blood & Immune Cells – Neuronal Cells
Blood & Immune Cells – Glial Cells
Neuronal Cells – Non-specific
Blood & Immune Cells – Mesenchymal cells
Blood & Immune Cells – Glandular Epithelial Cells
Blood & Immune Cells – Muscle Cells
Mesenchymal cells – Neuronal Cells
Muscle Cells – Neuronal Cells
D
Normal cell
Inhibitor
'AND–NOT' logic-gated CAR-T Cells
Activator
Cancer cell
E
F
'AND–NOT' CAR-T target pairs with TS AND–NOT ≥ 99th percentile
HPA single cell gene signature
Glial Cells – Neuronal Cells
Neuronal Cells – Neuronal Cells
Germ Cells – Germ Cells
Glandular Epithelial Cells – Neuronal Cells
Neuronal Cells – Germ Cells
Neuronal Cells – No cluster
Blood & Immune Cells – Germ Cells
G
Normal Cells RNA Expression (HPA scRNA-seq)
NCSTN
BCAN
TMPSF1
CD81
EPHB4
NCAM1
NTRK2
CD99
ITGAM
PTPRC
ORZL13
LRRC4B
PTPRC
ITGA4
NRXN3
KCNA1
'AND' CAR-T Target Pairs
z-score
'AND–NOT' CAR-T Target Pairs
Function
Activator
Inhibitor
HPA Cell Types
HPA Single Cell Gene Signatures
Blood & Immune Cells
Glial Cells
Neuronal Cells
Glandular Epithelial Cells
Mesenchymal cells
Trophoblast cells
H
Normal Tissues/Cells Protein Expression
(HPM LC-MS/MS Proteomics)
NCSTN
BCAN
SLC43A3
UPK3BL1
SLC43A3
SLC22A17
NTRK2
CD99
PTPRC
ITGAM
ADAM12
LY6K
PTPRC
ITGA4
PTPRZ1
NRXN3
'AND' CAR-T Target Pairs
z-score
'AND–NOT' CAR-T Target Pairs
Function
Activator
Inhibitor
HPM Tissues/Cells
Fetal Heart
Fetal Liver
Fetal Gut
Fetal Ovary
Fetal Testis
Fetal Brain
Adult Frontal Cortex
Adult Spinal Cord
Adult Retina
Adult Heart
Adult Liver
Adult Ovary
Adult Testis
Adult Lung
Adult Adrenal
Adult Gallbladder
Adult Pancreas
Adult Kidney
Adult Esophagus
Adult Colon
Adult Rectum
Adult Urinary Bladder
Adult Prostate
Placenta
B Cells
CD4 Cells
CD8 Cells
NK Cells
Monocytes
Platelets
HPA Single Cell Gene Signatures
Blood & Immune Cells
Glial Cells
Neuronal Cells
Germ Cells
Glandular Epithelial Cells
Mesenchymal cells

Figure 3. Bispecific CAR-T targets in STS: 'AND' and 'AND–NOT' logic-gated CARs. (A) Illustration of an 'AND' CAR-T cell activated by two different tumor antigens. (B) Venn diagram showing the number of 'AND' pairs in each STS. (C) Bar chart showing the top 5 most frequent 'AND' pairs by STS. Genes are classified based on their HPA single cell type signature. (D) Illustration of an 'AND-NOT' CAR-T cell activated by a tumor antigen, and inhibited by a normal cell antigen. (E) Venn diagram showing the number of shared and unique 'AND-NOT' pairs in each STS. (F) Bar chart showing the top 5 most frequent 'AND-NOT' pairs by STS. Genes are classified based on their HPA single cell signature, with the first indicating the activator and the second the inhibitor. (G, H) Heatmaps showing selected 'AND' and 'AND-NOT' pairs expression in the HPA scRNA-seq (G), and the HPM (H) datasets. Genes are annotated based on the HPA single-cell signature they belong to (top annotation), and their functional role as activators or inhibitors (bottom annotation, 'AND-NOT' pairs).

2396

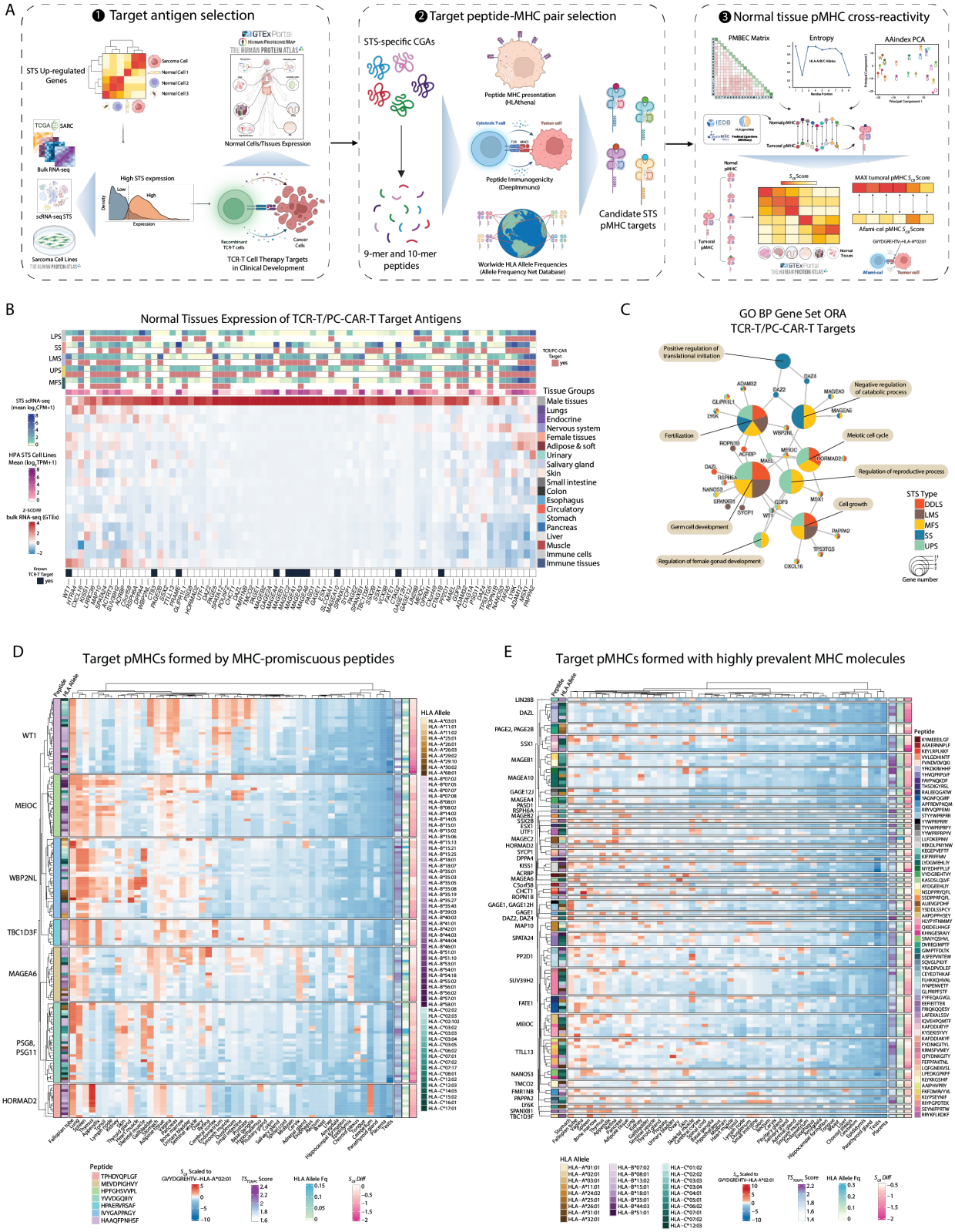
A
❶ Target antigen selection
STS Up-regulated Genes
Sarcoma Cell
Normal Cell 1
Normal Cell 2
Normal Cell 3
GTEx Portal
HUMAN PROTEOME MAP
THE HUMAN PROTEIN ATLAS
Normal Cells/Tissues Expression
TCGA SARC
Bulk RNA-seq
scRNA-seq STS
Sarcoma Cell Lines
High STS expression
Low
High
Diversity
Expression
Recombinant TCR-T cells
Cancer Cells
TCR-T Cell Therapy Targets in Clinical Development
❷ Target peptide-MHC pair selection
STS-specific CGAs
9-mer and 10-mer peptides
Peptide MHC presentation (HLAthena)
Cytotoxic T cell
Tumor cell
TCR
MHC
Peptide Immunogenicity (DeepImmuno)
Worlwide HLA Allele Frequencies (Allele Frequency Net Database)
Candidate STS pMHC targets
❸ Normal tissue pMHC cross-reactivity
PMBEC Matrix
Entropy
AAindex PCA
Relative Position
Principal Component 1
Principal Component 2
IEDB
HLA-peptide
Peptide-Spectrum Match
Normal pMHC
Tumoral pMHC
Normal pMHC
Tumoral pMHC
S_{cg} Score
MAX tumoral pMHC S_{cg} Score
Afami-cel pMHC S_{cg} Score
GVYDGREHTV-HLA-A*02:01
Normal Tissues
Afami-cel
Tumor cell
GTEx Portal
THE HUMAN PROTEIN ATLAS
B
Normal Tissues Expression of TCR-T/PC-CAR-T Target Antigens
LPS
SS
LMS
UPS
MFS
TCR/PC-CAR Target
yes
STS scRNA-seq (mean log2CPM+1)
HPA STS Cell Lines Mean (log2TPM+1)
Z-score bulk RNA-seq (GTEx)
Known TCR-T Target
yes
Tissue Groups
Male tissues
Lungs
Endocrine
Nervous system
Female tissues
Adipose & soft
Urinary
Salivary gland
Skin
Small intestine
Colon
Esophagus
Circulatory
Stomach
Pancreas
Liver
Muscle
Immune cells
Immune tissues
C
GO BP Gene Set ORA
TCR-T/PC-CAR-T Targets
Positive regulation of translational initiation
Negative regulation of catabolic process
Fertilization
Meiotic cell cycle
Regulation of reproductive process
Cell growth
Germ cell development
Regulation of female gonad development
STS Type
DDLS
LMS
MFS
SS
UPS
Gene number
D
Target pMHCs formed by MHC-promiscuous peptides
Peptide
HLA Allele
WT1
MEIOC
WBP2NL
TBC1D3F
MAGEA6
PSG8, PSG11
HORMAD2
HLA Allele
Peptide
TPHDYQPLGF
MEVDPIGHVY
HPFGHSVVPL
YVVDGQIIIY
HPAERVRSAF
IVYGAPPAGY
HAAQFPNHSF
S_{cg} Scaled to GVYDGREHTV-HLA-A*02:01
TS_{TCAPC} Score
HLA Allele Fq
S_{cg} Diff
E
Target pMHCs formed with highly prevalent MHC molecules
LIN28B
DAZL
PAGE2, PAGE2B
SSX1
MAGEB1
MAGEA10
GAGE12J
MAGEA4
PASD1
RSPH6A
MAGEB2
SSX2B
ESX1
UTF1
MAGEC2
HORMAD2
SYCP1
DPPA4
KISS1
ACBRP
MAGEA6
C5orf58
CHCT1
RQPN1B
GAGE1, GAGE12H
GAGE1
DAZ2, DAZ4
MAP10
SPATA24
PP2D1
SUV39H2
FATE1
MEIOC
TTLL13
NANOS3
TMCO2
FMR1NB
PAPPA2
LY6K
SPANXB1
TBC1D3F
Peptide
HLA Allele
S_{cg} Scaled to GVYDGREHTV-HLA-A*02:01
TS_{TCAPC} Score
HLA Allele Fq
S_{cg} Diff

Figure 4. Targeting intracellular antigens in STS: TCR-T and PC-CAR-T cells.

(A) TCR-T and PC-CAR-T pMHC target discovery pipeline. (B) Heatmap showing bulk RNA-seq GTEx expression for the 76 target antigens. Top annotation indicates predicted antigen in each STS, with average expression in STS scRNA-seq data and HPA STS cell lines. (C) Gene set ORA using GO BP terms for PC-CAR-T and TCR-T target antigens (FDR < 0.1, minimum and maximum gene set sizes of 2 and 500). (D, E) Heatmaps showing HPA/GTEx tissue-specific S_CR scores for target pMHCs scaled to the S_CR scores of afami-cel's target, GVYDGREHTV–HLA-A*02:01, obtained as follows: (((S_CR^j (target)-S_CR^j (reference)))/σ_j) ×2 if S_CR^j (target)>S_CR^j (reference), where σ_j is the standard deviation of the S_CR values for the 5,020 target pMHCs in the jth tissue. In (D), pMHCs with S_CR Diff ≤0, and formed by peptides that form pMHCs with ≥10 different HLA alleles in either locus are shown. In (E), only pMHCs with S_CR Diff ≤ 10th percentile and formed by one of the top 10 most prevalent HLA alleles at either locus are shown.

2397

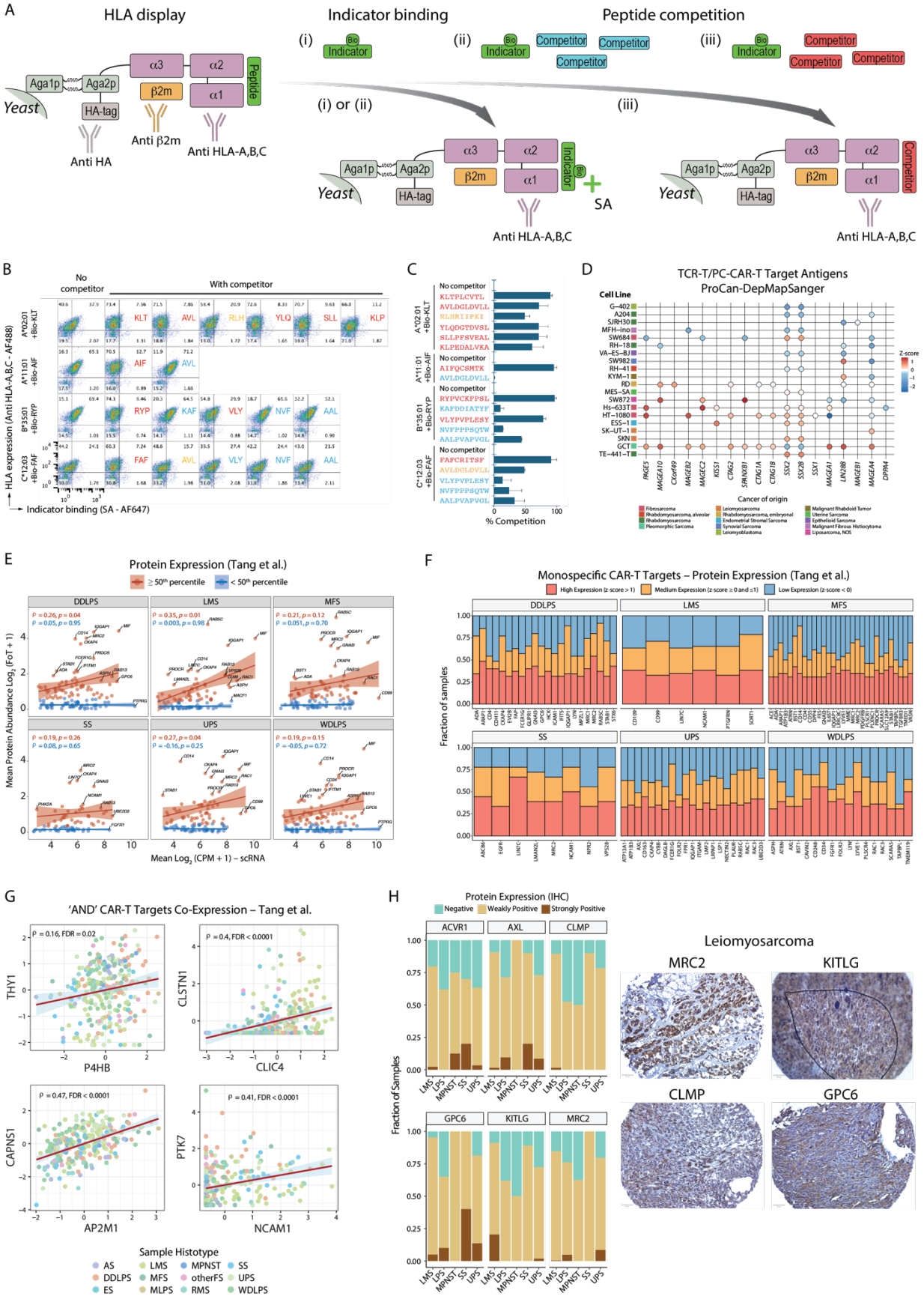
A
HLA display
Indicator binding
Peptide competition
Yeast
Aga1p
Aga2p
HA-tag
α3
α2
β2m
α1
Peptide
Anti HA
Anti β2m
Anti HLA-A,B,C
(i)
(ii)
(iii)
Bio
Indicator
Competitor
(i) or (ii)
SA
B
No competitor
With competitor
HLA expression (Anti HLA-A,B,C - AF488)
Indicator binding (SA - AF647)
C
% Competition
D
TCR-T/PC-CAR-T Target Antigens
ProCan-DepMapSanger
Cell Line
Z-score
Cancer of origin
E
Protein Expression (Tang et al.)
≥ 50th percentile
< 50th percentile
DDLPS
LMS
MFS
SS
UPS
WDLPS
Mean Protein Abundance Log2 (FoT + 1)
Mean Log2 (CPM + 1) – scRNA
F
Monospecific CAR-T Targets – Protein Expression (Tang et al.)
High Expression (z-score > 1)
Medium Expression (z-score ≥ 0 and ≤1)
Low Expression (z-score < 0)
Fraction of samples
G
'AND' CAR-T Targets Co-Expression – Tang et al.
THY1
P4HB
CLSTN1
CLIC4
CAPNS1
AP2M1
PTK7
NCAM1
Sample Histotype
AS
DDLPS
ES
LMS
MFS
MLPS
MPNST
otherFS
RMS
SS
UPS
WDLPS
H
Protein Expression (IHC)
Negative
Weakly Positive
Strongly Positive
ACVR1
AXL
CLMP
GPC6
KITLG
MRC2
Fraction of Samples
Leiomyosarcoma
MRC2
KITLG
CLMP
GPC6

Figure 5. Target validation.

(A) Vignette demonstrating the IMMUNE workflow for peptide-MHC binding assessment. (B) IMMUNE results for 14 pMHC targets identified through PS-TRACT, including KAFDDIATYF and RLHRIIPKI from SSXI, AVLDGLDVLL and VLYPVPLESY from PRAME, NVFPPPSQTW and YLQDGTDVSL from ADAM12, and SLLPFSVEAL, KLPEDALVKA and AALPVAPVGL from MSX1. The scatterplots report the mean fluorescence intensity (MFI) for the peptide-HLA binding indicator (x-axis) and for the HLA molecule tested (y-axis). Each peptide is identified by its first three amino acids. Strong binders are indicated in red, while moderate binders are shown in yellow, and weak binders in light blue. The KLT, AIF, RYP, and FAF peptides are used as positive controls for known strong binders for the HLA considered. (C) Bar chart showing the % Competition as measured with IMMUNE, for each tested pMHC target. Strong binders are indicated in red, moderate binders in yellow, and weak binders in light blue. (D) Dot plot showing protein expression in STS cell lines in ProCan-DepMapSanger. (E) Spearman correlation of scRNA-seq expression and protein abundance in the Tang et al. dataset. Only monospecific CAR-T targets for each histotype are plotted. LPS scRNA-seq samples were compared to DDLPS and WDLPS proteomics samples separately. (F) Bar charts showing the fraction of samples in each STS with high, medium, and low expression of selected monospecific CAR-T targets in the Tang et al. dataset. (G) Spearman correlation of protein expression in the Tang et al. dataset for 'AND' target pairs. (H) Protein expression by IHC in STS tissue micro-arrays. The bar chart shows the fraction of samples in each STS with negative, weakly positive, and strongly positive expression. Images show tissue sections of LMS samples scored as strongly positive for GPC6, MRC2, CLMP, and KITLG. MPNST: malignant peripheral nerve sheath tumor; MLPS: mucinous liposarcoma; others: other fibrosarcoma; ES: Ewing sarcoma; RMS: rhabdomyosarcoma; AS: angiosarcoma.

2398

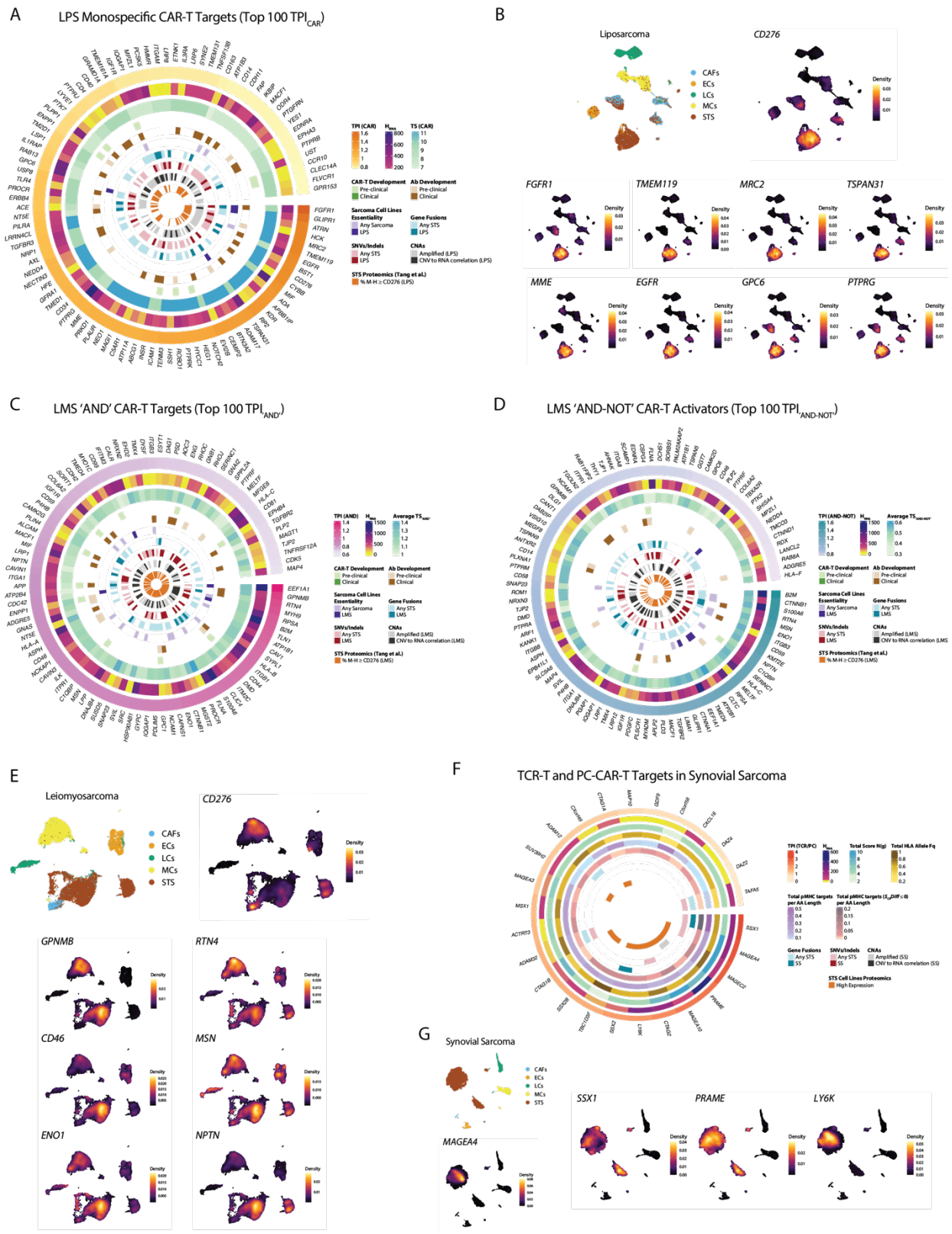
A
LPS Monospecific CAR-T Targets (Top 100 TPI$_{CAR}$)
B
Liposarcoma
CAFs
ECs
LCs
MCs
STS
CD276
FGFR1
TMEM119
MRC2
TSPAN31
MME
EGFR
GPC6
PTPRG
C
LMS 'AND' CAR-T Targets (Top 100 TPI$_{AND}$)
D
LMS 'AND-NOT' CAR-T Activators (Top 100 TPI$_{AND-NOT}$)
E
Leiomyosarcoma
CD276
GPNMB
RTN4
CD46
MSN
ENO1
NPTN
F
TCR-T and PC-CAR-T Targets in Synovial Sarcoma
G
Synovial Sarcoma
MAGEA4
SSX1
PRAME
LY6K

Figure 6. Integrated target prioritization.

(A, C, D) Circular heatmaps showing the top 100 CAR-T targets ranked by TPI for LPS (A, monospecific CAR-T targets), and LMS (C, D, bispecific CAR-T targets). (B, E, G) UMAP plots showing expression density of selected monospecific CAR-T targets in LPS (B), bispecific CAR-T targets in LMS (E), and TCR-T/PC-CAR-T target antigens in SS (G). In one UMAP plot per panel, cells are colored based on identity. (F) Circular heatmap showing TPI scoring for TCR-T and PC-CAR-T target antigens in SS.